THE UNIVERSITY OF MICHIGAN

COLLEGE OF ENGINEERING
Department of Chemical and Metallurgical Engineering

Technical Report No. 1

EXPERIMENTAL AND THEORETICAL INVESTIGATION OF CONTINUOUS FLOW COLUMN CRYSTALLIZATION

Joseph D. Henry, Jr.

ORA Project 01730

sponsored by:

NATIONAL SCIENCE FOUNDATION
GRANT NO. GK-1913
WASHINGTON, D.C.

administered through:

OFFICE OF RESEARCH ADMINISTRATION ANN ARBOR

October 1968

ACKNOWLEDGMENTS

I wish to express my appreciation to the following individuals and organizations for their contributions to this research:

Professor J. E. Powers, chairman of the doctoral committee, for his personal interest, guidance, and generous donation of time to the discussion of the problems which arose in the course of this investigation.

Professor J. D. Goddard, committee member, for his perceptive discussion of several aspects of the mathematical model developed in the dissertation.

Professor J. L. York and R. H. Kadlec, committee members, for their assistance, criticism, and helpful suggestions.

Professor E. A. Boettner, committee member, for his invaluable suggestions and help in confirming the results of the gas chromatographic analysis technique used in the course of this work; he willingly donated much of his time and the services of his staff.

Drs. R. Albertins and W. C. Gates, Jr. for their encouragement, assistance suggestions, and continued interest in this research.

Mr. M. D. Danyi for his assistance and suggestions in experimentally evaluating the effect of the feed position on column performance.

Mr. M. R. Player for his constructive criticism of several aspects of this work.

The personnel of the shops of the Department of Chemical and Metallurgical Engineering for their cooperation and assistance in constructing and maintaining the experimental equipment.

The National Science Foundation for traineeship support and sponsorship of this research through grant GK-1913.

Phillips Petroleum Company for donating the benzene and cyclohexane used in this investigation.

The Upjohn Company for the donation of the drive mechanism for the column crystallizer.

Mr. T. G. Smith for his careful proofreading of the manuscript.

The service units of the Office of Research Administration for their efficient and accurate production of this dissertation in its final form.

My wife, Ruth Ann, for her encouragement, support, and assistance in the preparation of this thesis.

TABLE OF CONTENTS

TABLE OF CONTENTS (Continued)

TABLE OF CONTENTS (Concluded)

LIST OF TABLES

LIST OF FIGURES

LIST OF FIGURES (Continued)

LIST OF FIGURES (Concluded)

NOMENCLATURE

A	Cross-section area of column measured perpendicularly to flow of crystal-liquid slurry, cm^2
a	Area available for interphase mass transfer per unit volume of column, cm^2/cm^3
b_1	Collection of terms defined by Eq. (75b)
b_2	Collection of terms defined by Eq. (75c)
b_3	Collection of terms defined by Eq. (75d)
C	Internal crystal rate, gm/min
C_1	Constant in general solution of differential equation for enriching section
C_2	Constant in general solution of differential equation for enriching section
$\bar{C}_1$	Constant in general solution of differential equation for stripping section
$\bar{C}_2$	Constant in general solution of differential equation for stripping section
C^*	Crystal rate corresponding to maximum value of the function defined by Eq. (24)
D	Coefficient of eddy diffusion, cm^2/min
e	2.71828
F	Response factor defined by Eq. (86)
K	Liquid phase mass transfer coefficient, cm/min
L	Mass flow rate of free liquid, gm/min
L'	Mass flow rate of adhering liquid, gm/min
L_E	Mass flow rate of enriching section product, gm/min

L_S	Mass flow rate of stripping section product, gm/min
$\mathcal{L}$	Length of purification section, cm
M_D	Mass transfer rate of impurity due to axial dispersion, gm/min
M_K	Mass transfer rate of impurity from the adhering liquid to free liquid, gm/min
	Summation index
Q_1	Collection of terms defined by Eq. (10a)
Q_2	Collection of terms defined by Eq. (10b)
$\bar{Q}_1$	Collection of terms defined by Eq. (20a)
$\bar{Q}_2$	Collection of terms defined by Eq. (20b)
r_1	Characteristic root of Eq. (13)
r_2	Characteristic root of Eq. (13)
$\bar{r}_1$	Characteristic root given by Eq. (22)
$\bar{r}_2$	Characteristic root given by Eq. (22)
R_E	Ratio of enriching section product rate to crystal rate, L_E/C
R_S	Ratio of stripping section product rate to crystal rate, L_S/C
X	Parameter in Eq. (55)
X_E	Value of X for enriching section defined by Eq. (51)
X_o	Value of X for total reflux operation, special case of Eq. (51)
X_S	Value of X for stripping section defined by Eq. (52)
Y	Free liquid impurity composition, ppm wt
Y'	Adhering liquid impurity composition, ppm wt
Y_E	Enriching section product composition, ppm wt

Y_F Feed composition, ppm wt

Y_P Collection of terms defined by Eq. (7)

$\bar{Y}_P$ Collection of terms defined by Eq. (18)

Y_S Stripping section product composition, ppm wt

Y_ϕ Free liquid composition inside the column at the feed point, ppm wt

Y_1 Free liquid composition at No. 1 sample tap, ppm wt

z Position in column measured from the freezing section, cm

z_F Feed position, cm

Greek Symbols

α Ratio of the adhering liquid to crystal rates

Δ Small increment

ϵ Impurity composition of crystal phase, ppm wt

η Volume fraction free liquid

Θ Function defined by Eq. (55)

ρ Free liquid density, gm/cm^3

$\sum$ Summation symbol

ψ_E Enriching section mass transfer factor defined by Eq. (41b), cm

ψ'_E Enriching section mass transfer factor defined by Eq. (46b), cm

ψ_S Stripping section mass transfer factor defined by Eq. (42b), cm

ψ'_S Stripping section mass transfer factor defined by Eq. (47b), cm

Subscripts

max	Denotes the maximum value of a function
min	Denotes the minimum value of a function

ABSTRACT

A theoretical and experimental investigation of the separation achieved in a column crystallizer which utilizes a spiral conveyor was conducted to determine the effect of variables associated with continuous flow operation. A system which exhibits negligible solid solubility was used. Several feed mixtures containing less than 31,000 ppm wt cyclohexane in benzene were employed. The principal variables evaluated in this study in a column of constant length were the feed position, internal crystal rate, and flow rates of terminal streams.

A mathematical model was developed which considers the transfer of impurity by axial dispersion in the reflux liquid, washing of impurity from the adhering liquid which is associated with the crystal phase, and the presence of impurity in the crystal phase due to either volumetric inclusion or slight solid solubility. The model was developed by employing a component material balance on an element of the reflux liquid and a balance embracing all streams. Two forms of the model were obtained. In the first case the axial dispersion term was included in both balances. The second form was obtained by including the axial dispersion term only in the material balance which includes all streams. This procedure is called the "transport equation approach" and has been applied previously by both Powers and Gates for column crystallizers operating with total reflux. This procedure considerably reduces the complexity of the final form of the model. A mathematical criterion is established which defines the conditions under which the form obtained by the transport equation

approach is applicable.

The experimental data are interpreted with the form of the model developed by the transport equation approach. This model satisfactorily predicts the influence of the variables associated with continuous flow operation on the terminal stream compositions and axial composition profiles.

The slope of the enriching section composition profile is a measure of the separation power of the column. The slope is determined by the internal crystal rate, pure end product rate, and the diffusional and mass transfer groups. The diffusional group is $D\rho A\eta$ where D is the axial diffusion coefficient, ρ is the liquid density, A is the column cross section area for flow, and η is the volume fraction of the free liquid. The mass transfer group is $\alpha(\alpha+1)/KaA\rho$ where K is the mass transfer coefficient between the adhering and free liquid, a is the specific surface area for mass transfer, and α is the adhering liquid-crystal rate ratio.

The diffusional and mass transfer groups are assumed to be constant for fixed spiral agitation conditions. The values of the two groups obtained from continuous flow data are compared with values obtained for the same agitation conditions from the total reflux data of Albertins.

Axial dispersion was found to be the dominant mechanism which limits the separation for continuous flow operation. This finding is consistent with the previous work of Albertins. In fact, the dominance of the diffusional term is more pronounced for the continuous flow case due to an additional dependence of the slope of the enriching section composition profile on the flow rate of the pure end product. The diffusional group obtained from the continuous flow

data is in reasonable agreement with the value determined from the total reflux data, i.e., for continuous flow operation $D\rho A\eta = 6.54 \pm 1.94$ gm-cm/min and for total reflux operation the same term is 6.86 ± 0.11 gm-cm/min.

Total reflux data provide a more severe test of the contribution of the mass transfer term because of the increased dominance of diffusion for the continuous flow case. The mass transfer groups and their standard errors obtained from continuous flow and total reflux data differ markedly, i.e., $\alpha(\alpha+1)/KA\rho = 0.410 \pm 0.44$ cm-min/gm and $0.910 \pm .08$ cm-min/gm, respectively.

The ultimate purity that can be achieved in a single column crystallizer is limited by the composition of the crystal phase, ϵ. It was reasoned that ϵ should be related to the mother liquor composition in the freezing section. The mother liquor composition is equal to the stripping section product composition if the freezing section is perfectly mixed. The values of ϵ calculated from the enriching section composition profile data are well correlated by a linear dependence on the stripping section product composition, Y_S, i.e., $\epsilon = 0.00142\ Y_S$. The values of ϵ ranged from 1 to 100 ppm wt C_6H_{12}. It is shown that Y_S is proportional to the feed composition when a very pure enriching section product is produced. Therefore the $\epsilon(Y_S)$ dependence implies that the purity which is attainable in a single pass is limited by the feed composition. There is no limit, however, to the purity that can be achieved if multiple pass operation is employed.

CHAPTER I

INTRODUCTION

The demand for ultrapure materials for both laboratory and commercial applications has led to the further development of many of the less common separation processes in recent years. Fractional solidification is an example of such a separation method. While fractional solidification has conventionally been carried out in staged crystallizer-solids recovery systems, the development of a crystallizer that can achieve several stages of separation in a single piece of equipment is relatively recent. This process which was patented by Arnold[6] in 1951 is called column crystallization.

Column crystallization is based on the countercurrent contacting of the crystals and crystal melt. Two column configurations have evolved. An end-fed column which utilizes an oscillatory flow of the liquid phase to transport the crystals has been developed for commercial application by Phillips Petroleum Company. A center-fed column which utilizes a spiral conveyor was developed by Schildknecht.[28] A variety of systems having phase diagrams of both the eutectic and solid solution type have been separated by column crystallization. Systems of the former type are of primary concern in this dissertation.

Most of the investigations of the Schildknecht column have been for total reflux operation. Powers[27] suggested a model for the purification of systems with negligible solid solubility which included consideration of impurity transfer by axial dispersion and washing of the adhering liquid associated with the crystal phase. He subjected this model to a preliminary check with a compositio

profile calculated from an experimental axial temperature profile. Powers assumed that the crystal phase was free from the impurity. Albertins[2] found in a later investigation where he measured the composition profile directly for the benzene-cyclohexane system that it was necessary to include the impurity associated with the crystal phase in his model. Both Powers' and Albertins' investigations were for total reflux operation.

Very little work has been done to evaluate the continuous flow operation of a center-fed column. Schildknecht and Mass[29] have separated solid solution systems by operating a column semicontinuously. Breiter[7] used a continuous flow column to separate components of both solid solution and eutectic systems. Most of his work was with systems which form solid solutions. Sea water was the only system with negligible solid solubility which he investigated. Only enough work was done with the sea water system to demonstrate the separation. Breiter did not propose a model to represent the separation of a eutectic system with continuous flow column crystallization.

In view of the minimal information available for the separation of systems which exhibit negligible solid solubility (eutectic systems) by continuous flow column crystallization such a study is the goal of this dissertation. The primary aim of the investigation is to explain the effects of the variables specifically associated with continuous flow operation of a center-fed column crystallizer, that is, feed position, terminal stream flow rates, etc. A mathematical model which includes the transfer of impurity by axial dispersion, washing of impurity from the adhering liquid and the impurity associated with the crystal phase is developed for the continuous flow case. Experimental data

obtained with continuous flow operation of a center-fed column are used to evaluate the model. The benzene-cyclohexane system was chosen so that comparisons could be made with the continuous flow data of this investigation and the total reflux data of Albertins.

CHAPTER II

REVIEW OF LITERATURE

Due to the relatively complex mechanical arrangement of a column crystallizer a process description is presented prior to the discussion of previous investigations of column crystallization. This will facilitate the understanding of the later sections of this chapter.

A. DESCRIPTION OF THE PROCESS

A column crystallizer is a device for carrying out countercurrent crystallization in a single piece of equipment. The process was patented by Arnold[6] in 1951. The major advantage of column crystallization is its capability to achieve separations equivalent to several stages in a single piece of equipment.

A column crystallizer consists of three distinct sections which are illustrated in Figure 1. Crystals are formed in the freezing section and pass through the purification section countercurrent to the liquid phase which is produced by melting the crystals in the melting section. The liquid phase is continuous while the crystal phase is the discontinuous or disperse phase. The column can be operated at total reflux or with continuous feed and product draw-off.

It is instructive to note the analogy of the process flows that occur in column crystallization and distillation. The freezing section which produces the crystal phase is analogous to the reboiler of a distillation column. The

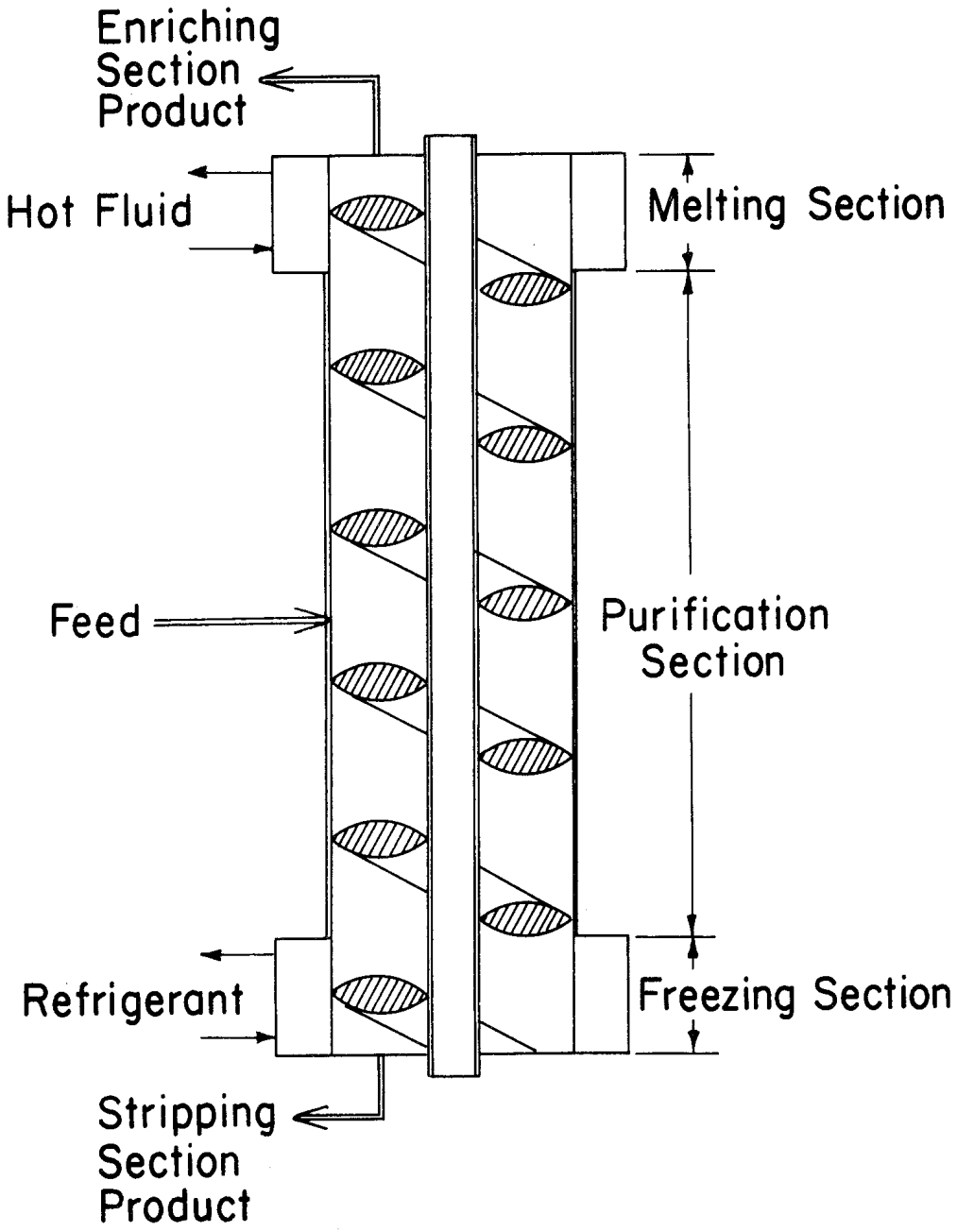

Figure 1. Sections used in a column crystallizer.

melting section is similar to a condenser; like the condenser it is the source of reflux liquid. Finally the purification section which includes an enriching and stripping section is similar to a packed tower distillation column. The hydrodynamics of the crystal slurry transport, however, are similar to the two phase flow that occurs in a pulsed liquid-liquid extraction column.

1. Column Configuration

Following Arnold's invention, both end-fed and center-fed column crystallizers evolved. The former has largely been developed by Phillips Petroleum Company. The end-fed column is primarily used for large scale applications such as the separation of p-xylene from its isomers. Figure 2 shows a typical process arrangement for the end-fed column. Findlay,[11] McKay,[19] Thomas,[32] and Weedman[34] have described the construction, operation and performance of the Phillips column. The crystal phase is conveyed by the action of a reciprocating piston.

The center-fed column shown in Figure 1 was developed by Schildknecht.[28] The crystals are conveyed in this column by a spiral which is both rotated and oscillated. Due to the fact that the Schildknecht column was used in this study a detailed discussion of its mechanical design is presented in Chapter IV.

2. Process Flow in the Schildknecht Column

As Figure 1 illustrates, the column consists of two concentric tubes with a spiral conveyor in the annular space between them. Crystals are formed in the freezing section and are transported through the column. In the case of a sys-

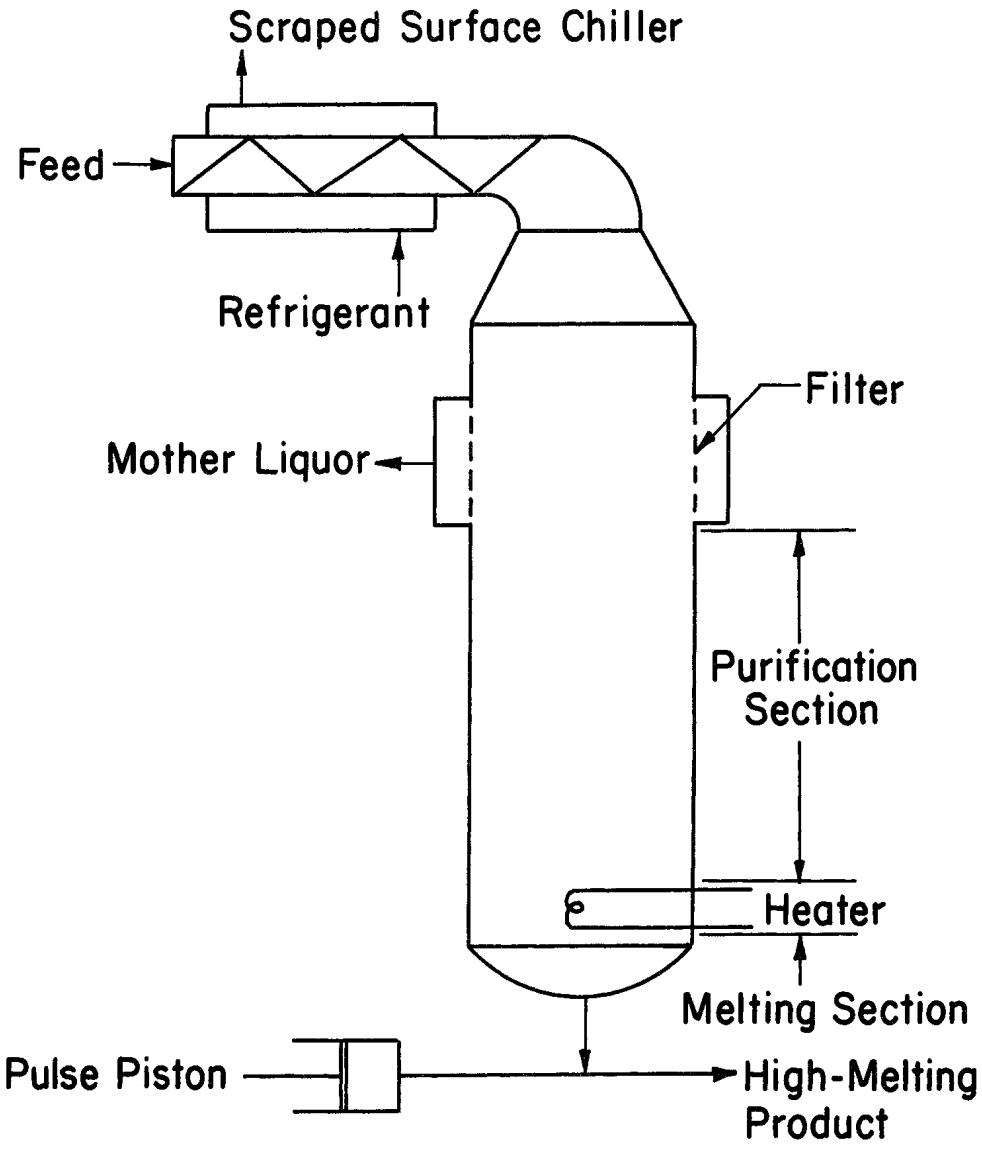

Figure 2. Phillips end-fed column crystallizer operated with feed and product draw-off.

tem of the eutectic type the crystals are below their melting point in the purification section, i.e., they are stable until they are melted.— The crystals are melted at the top of the column and a portion of the liquid is returned as countercurrent reflux. Most of the liquid movement is countercurrent to the rising crystals, but due to drag effects a small portion of the liquid stream rises with the crystals. This stream is called the adhering liquid and is continually contacted with countercurrent free liquid of lower impurity content. Rather than attempting to describe the complex hydrodynamic situation which occurs due to

the oscillation of the crystal-liquid slurry, the adhering liquid associated with the crystal phase is conceived as a distinct liquid phase. This is an idealization because the free and adhering liquids are in fact one phase. This approach facilitates visualization of the washing process and will be used in Chapter III to develop the model for the purification section. Figure 3 illustrates the movement of the phases in the purification section and shows the adhering liquid as an idealized distinct phase.

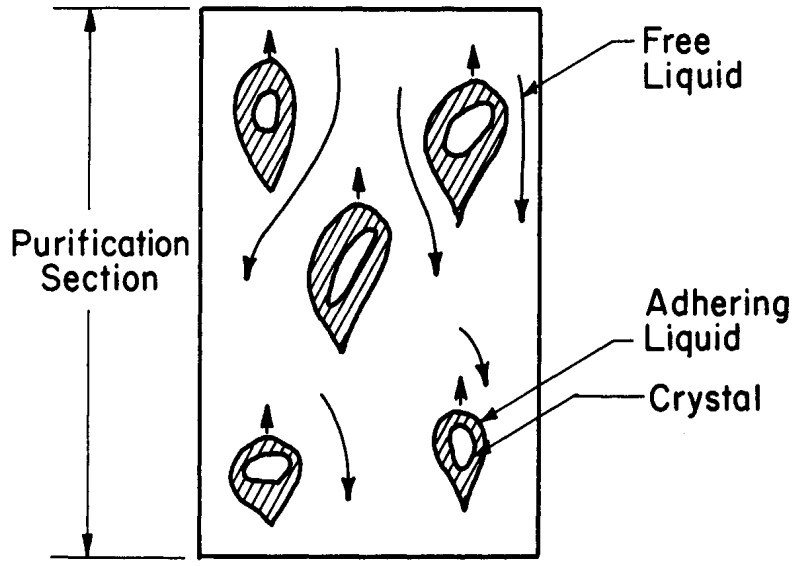

Figure 3. Crystals and melt in countercurrent contact.

The freezing section is an integral part of the column. The action of the spiral provides the advantage of scraped surface heat exchange. Refrigerant is pumped through the jacket of the freezing section. Crystals are transported to the purification section by the action of the spiral.

The purification section is immediately above the freezing section. Feed introduction divides the purification section into an enriching section above the feed point and a stripping section below. The crystals and adhering

liquid are transported countercurrent to liquid reflux of lower impurity content. The mass transfer between the countercurrent streams is enhanced by both rotation and oscillation of the spiral conveyor. The oscillation of the spiral conveyor also promotes axial dispersion of the impurity in a direction which opposes the separation. Consequently the conveyor agitation level must be chosen to strike a balance between increased mass transfer and axial dispersion. The melting section which is located directly above the purification section contains a heat source. The heater can be an electrical heater or a jacket around the column through which a heating fluid is circulated.

B. PUBLISHED REVIEWS

Several reviews of column crystallization which have appeared in the literature are summarized below. The yearly reviews of Palermo,[25] while they are comprehensive, contain little information specific to column crystallization and therefore they are not discussed here.

Albertins, Gates, and Powers[4] have reviewed the design, operation, and the effect of the variables in column crystallization. They compared the Schildknecht and Phillips columns. Their thorough review of the systems that have been purified by column crystallization includes a summary of feed and product compositions that resulted for the various terminal stream flow rates that have been reported. Binary and multicomponent mixtures of both the eutectic and solid solution type have been separated. These mixtures include aromatic and aliphatic hydrocarbons, aqueous systems, and fatty acids.

These authors also summarized the effect of variables on column performance.

Those variables affecting agitation of the crystal slurry have a critical effect on the performance of both the Schildknecht and Phillips columns. There appears to be an optimum level of agitation for both columns, that is, frequency and amplitude of oscillation of the spiral for the Schildknecht column and piston displacement and frequency for the Phillips column.

They also summarized several mathematical models for the Schildknecht column; however, with the exception of Powers' determination of the axial temperature profile and comparison with theory, the models were not subjected to a test with an experimental composition profile. Gates[14] has evaluated several possible models for total reflux operation of the Schildknecht column. The mathematical analysis of column crystallization by previous investigators will be discussed in more detail in later sections.

C. OTHER LITERATURE RELATED TO COLUMN CRYSTALLIZATION

Considerable work on crystallization has been reported by the Office of Saline Water. Sherwood and Brian[30] have investigated the washing of brine from a static bed of ice crystals. They found that their data could be explained by a plug flow-axial dispersion model. Moulton and Hendrickson[23] found that the salt associated with ice crystals was proportional to the initial salt concentration in the feed. Due to the fact that they also found that the final mother liquor composition was proportional to the feed composition, the impurity associated with the crystal phase was equivalently proportional to the final mother liquor composition.

There is also considerable information in the extraction literature that

is pertinent to column crystallization. No attempt is made to present a review here. Albertins[1] summarized the literature of pulsed liquid-liquid extraction and discussed the similarities with column crystallization. The hydrodynamics of a pulsed extraction column are similar to the pulsing action provided by the spiral in a column crystallizer. The effects of axial dispersion are similar in both processes.

D. EXPERIMENTAL AND THEORETICAL STUDIES FOR TOTAL REFLUX OPERATION

Most of the experimental results that have been compared with theoretical models were obtained at total reflux. This is particularly true of the Schildknecht column. Powers[27] and Yagi[35] have each postulated models for the column crystallizer.

Powers proposed a differential countercurrent contacting approach. He distinguished between the mechanism of purification for eutectic and solid solution systems. Only the model for the eutectic system is discussed here. The model which includes mass transfer between the adhering and free liquid and axial dispersion in the free liquid is based on the transport equation approach. This approach involves neglecting the axial dispersion term in the component material balance on an element of free liquid in the purification section. The diffusion term is retained, however, in the material balance which includes all streams in the purification section. The words "transport equation approach" as used in the remainder of this dissertation imply the assumption described above. The crystal phase was assumed to be pure, i.e., any inclusion or occlusion of impurity was neglected. The model was in

qualitative agreement with data obtained for the purification of azobenzene with a Schildknecht column. The purification section temperature profile that was used for this comparison did not provide a basis for checking the assumption that the crystal phase was pure. Powers neglected all heat transfer effects, i.e., he assumed that all internal stream flow rates were independent of position in the purification section. This is a reasonable assumption for a nearly adiabatic column where refreezing of liquid on the subcooled crystals leaving the freezing section is not significant. Refreezing is not an important consideration in the Schildknecht column due to the small axial temperature gradients that are common to production of ultrapure materials.

Yagi developed a model for the end-fed column that applies for purification of eutectic systems with batch operation. He neglected impurity in the crystal phase as well as axial dispersion in the liquid phase. He apparently recognized the importance of refreezing of the reflux liquid in the Phillips column due to the large axial temperature gradient that exists. Although he included an energy balance in his analysis, he did not include the term corresponding to the refreezing effect.

Albertins[2] studied the separation of the eutectic system benzene-cyclohexane in a Schildknecht column crystallizer operated at total reflux. His investigation included both theoretical and experimental considerations. In fact, his results obtained at total reflux are extended to the continuous draw-off case in this thesis.

Albertins' experimental data are based on the measurement of the axial composition profile in the column. These data provided the first test of the

assumption that the crystal phase is pure for the separation of a eutectic system. This was achieved by sampling the composition profile and analyzing the samples with a calibrated gas chromatograph. The original theory of Powers predicted that the free liquid composition profile should be exponential if the crystal phase were pure. Figure 4 shows a typical composition profile obtained by Albertins. It is readily apparent that the profile is not exponential in the upper half of the purification section. Albertins explained this deviation from the exponential profile by the existence of a constant impurity level in the crystal phase.

Albertins also evaluated the influence of the major operating variables. He found that it is necessary to provide sufficient agitation to keep the phases well fluidized. This condition is necessary to obtain a good separation. Oscillation frequencies of 140 to 290 osc/min were required at an amplitude of 1 mm and a spiral rotation rate of 59 RPM. At these levels of agitation the column plugged at a crystal rate of 5.4 gm/min. The column operated smoothly at crystal rates below 5.4 gm/min. The charge composition had no effect on the separation other than that explained by material balance considerations.

Albertins used a plug flow-axial dispersion model to explain his data. This model also included a constant impurity level in the crystal phase. Although he considered mass transfer between the adhering and free liquid, he concluded that only axial dispersion played a role in the mass transfer mechanism. As pointed out by Gates,[13] Albertins neglected the impurity in the crystal phase when he considered the axial dispersion—mass transfer model

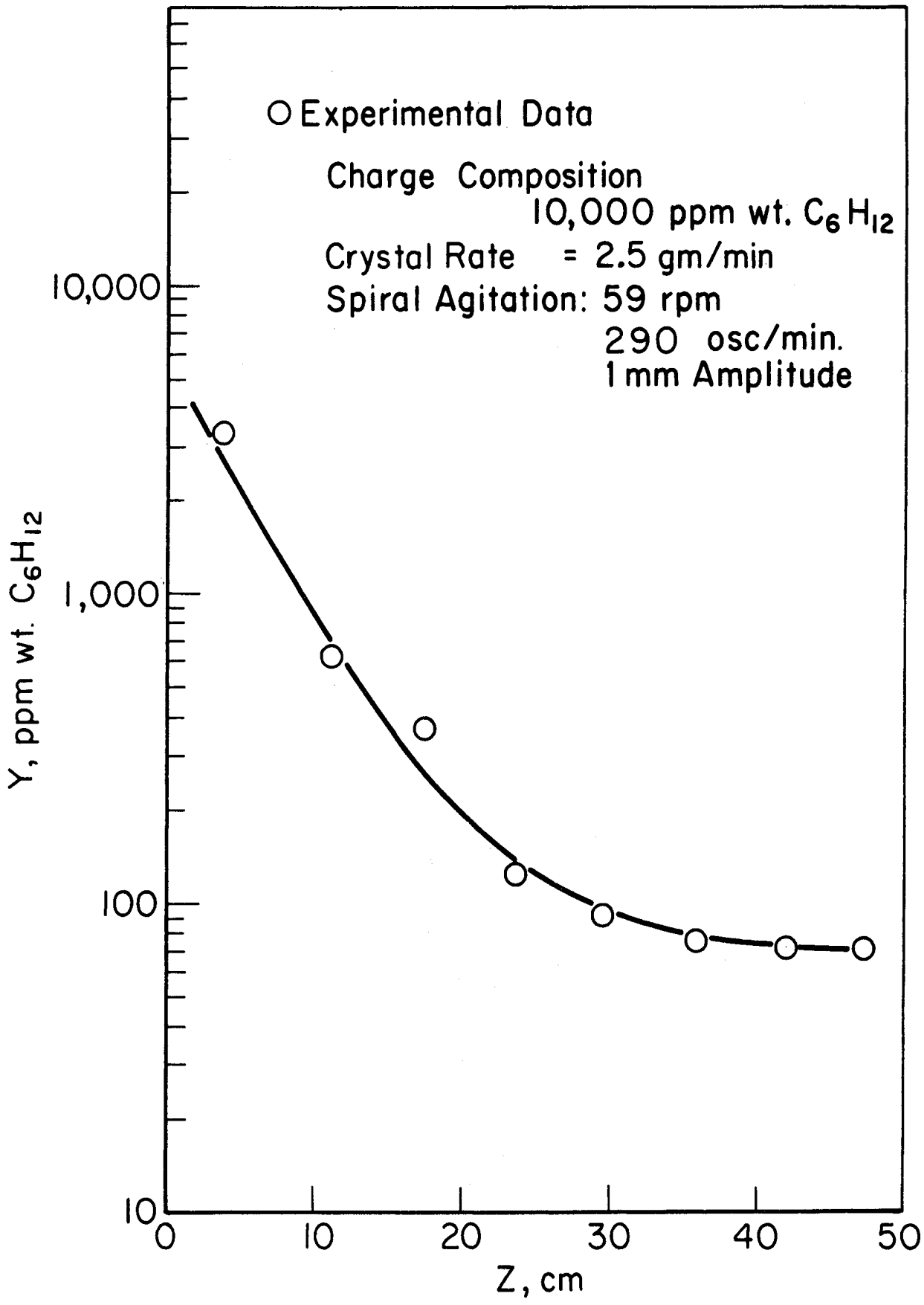

Figure 4. Typical free liquid composition profile obtained by Albertins[1] for total reflux operation.

(which he included in his axial dispersion-plug flow model) in order to reach this conclusion.

Gates[14] performed a thorough study of the models for the separation of both solid solutions and eutectic systems at total reflux. In both cases he compared his models with experimental data. He found for the case of eutectic systems that when the mass transfer mechanism is considered simultaneously with effects of a constant impurity level in the crystal phase, both the axial dispersion and the mass transfer between the adhering and free liquid are significant effects, but that axial dispersion is the larger effect. The detailed mathematics of Gates' model for eutectic systems are not presented here; his model is a special case of the model that is developed in Chapter III for the continuous draw-off case.

E. PREVIOUS INVESTIGATIONS WITH CONTINUOUS FEED AND PRODUCT DRAW-OFF

Both the end-fed and center-fed column crystallizers have been operated continuously. Most of the studies were experimental, and little effort was made to compare the experimental data with a mathematical model. These investigations are summarized in this section together with theoretical models that have been presented for continuous flow operation.

1. End-Fed Column

The basis for the commercial application of the end-fed column is the ability to operate it continuously. The major commercial application has been the purification of xylenes.[20] Most of the investigations of the end-fed column have been pilot plant studies, e.g., McKay and Goard[21] described

the separation of xylenes, methyl-vinyl-pyridine, methyl-ethyl-pyridine, organic esters, and food stuffs such as beer.

One major difference between the performance of the end-fed and center-fed columns is the fact that there appears to be a composition discontinuity in the end-fed column when eutectic systems are purified. McKay and his co-workers[22] measured the axial composition profile for the separation of xylenes and found that the p-xylene composition was constant throughout most of the purification section and increased sharply in the vicinity of the crystal melter. All of the enrichment occurred in a 2 in. region near the melting section. The fraction of solids also increased sharply in this region. These results confirm the occurrence of significant refreezing of the reflux liquid on the crystal phase. No attempt was made in these investigations to incorporate the refreezing concept into a mathematical model that could be used to predict the performance of an end-fed column crystallizer.

Player[26] recently developed a mathematical model that included refreezing considerations. While there are no experimental data in the public domain which could be used to check his model (McKay's profile data mentioned above did not include the internal flow rates), it did predict qualitatively the existence of a discontinuity in the region near the melting section.

2. Center-Fed Column

In order to obtain quantities of material larger than could be obtained with total reflux operation, Schildknecht and Mass[29] operated a center-fed column semicontinuously. They fed and removed products at periodic intervals.

Diphenyl, azobenzene, and sea water have been purified by this technique. Typical feed and product quantities are 10 ml and 5 ml respectively, added and withdrawn at 20 minute intervals.

In a later investigation Breiter[7] purified azobenzene-stilbene, caprolactam, and sea water with fully continuous operation. The bulk of the work was done on the former two systems which form solid solutions with their impurities. Only enough work was done with the sea water system (the only eutectic system investigated) to demonstrate the separation.

A typical separation for a solid solution system is described below. A 50:50 mixture of azobenzene-stilbene was fed to a column 70 cm long at a rate of 132 gm/hr. The melting section product was 96.2 mol % azobenzene and the freezing section product was 1.3 mol % azobenzene. The product recovery was 49% and the column was operated with a reflux ratio of 15.

Breiter used a model completely analogous to the McCabe-Thiele procedure for binary distillation to interpret his data. The above separation required 13.5 ideal stages which corresponds to a HETP of 4.7 cm. Schildknecht and Breiter have made no attempt to use the differential countercurrent contacting approach that was suggested earlier by Powers.[27] It is interesting to note that Breiter has found that he can obtain purer products with fully continuous operation than with periodic operation. Thus even for laboratory separations continuous draw-off is the most desirable mode of operation if more than a few milliliters of product are required.

Anikin[5] suggested using the mathematical model already developed for packed fractionating columns[8] because the physiocochemical processes which

occur in both processes are similar. Axial dispersion in the liquid phase was neglected. It is this author's opinion that this is the chief deficiency of Anikin's model. He did not evaluate his model experimentally.

The Benzole Producers[16,17] have operated a bench scale Schildknecht column for purification of benzene. They are currently designing a pilot plant that will have a capacity of 30 gal/hr. They hope to apply the center-fed column to the large scale production of benzene. They are not currently interested in producing ultrapure benzene, thus, they are using very low reflux rates. In fact, in some cases quantities of enriching section product were withdrawn that exceeded the internal crystal rate. Such operating conditions correspond to cocurrent flow of the free liquid and crystal phases in the enriching section as opposed to conventional countercurrent operation of the column crystallizer. They have demonstrated with countercurrent operation that benzene with as little as 10 ppm impurities can be produced from a 10,000 ppm feed. They made no attempt to model the system nor did they obtain axial composition profile data that are essential to the thorough evaluation of a model.

The Benzole Producers have indicated that the Schildknecht column may find application for large scale production of benzene. Recently Newton Chambers Engineering Ltd. have announced that a crystallization process based on the Schildknecht column is being developed.[24]

Powers[4] presented a model for the purification of eutectic systems with continuous feed and product draw-off that is similar to his model for total reflux operation. He assumed that the mass transfer factor (defined later) is the same for both total reflux and continuous operation. As will be

shown in Chapter III this is not the case. Powers did not subject his model to an experimental check.

Danyi, Henry, and Powers[10] have recently reported the production of ultra-pure benzene (< 10 ppm impurities) with a center-fed column operating continuously. They found that for such operations the length of the stripping section should be minimized and that it is sometimes desirable to use multipass operation. Further details of this work are presented in Chapter VI.

F. SUMMARY

There is a need to develop a model for the continuous draw-off case. While center-fed columns have been operated continuously, data do not exist for the purification of eutectic systems that could be used to evaluate a model for such an operation. In view of the potential large scale application of the center-fed column, an experimental and theoretical study of the continuous flow case would be especially timely. It is also apparent that the continuous mode of operation will find increased application in the laboratory.

CHAPTER III

THEORETICAL DEVELOPMENTS

A mathematical model is developed for a center-fed column crystallizer operating with continuous feed and product draw-off. Considerations are limited to the purification of simple eutectic systems in regions below the eutectic composition. Various mechanisms that might influence the separation are discussed. A model is developed which includes those parameters which are believed to be important. The implementation of the model by a numerical technique is also summarized. The implications of the model are discussed, i.e., predictions are made concerning various aspects of the performance of a continuous flow column.

A. POSSIBLE MECHANISMS

In the case of purification of systems with negligible solid solubility a high degree of separation occurs in the freezing section. The crystals formed in the freezing section are relatively pure, but the adhering liquid associated with them is impure due to the rejection of impurities from the crystal phase during the freezing process. The purification section provides a means of reducing the impurity content of the adhering liquid. This is accomplished by washing the adhering liquid with purer reflux liquid (henceforth called free liquid) that is formed in the melting section. Figure 3 of Chapter II illustrates the movement of the phases in the purification section with the adhering liquid idealized as a distinct phase.

It is convenient to think of the adhering liquid as a distinct phase and

consider the washing as an interfacial mass transfer process. The driving force for mass transfer is the difference in composition between the adhering and free liquid. This continual washing establishes an axial composition gradient in the purification section.

Axial dispersion in the free liquid acts to oppose the separation. The axial dispersion is driven by the axial composition gradient and is sensitive to hydrodynamic conditions in the column.

It is possible for impurities to be associated with the crystals. This can be caused by either volumetric liquid inclusions or by the trapping of impurities on the irregular surface of the crystals. Also solid solubility may occur in the ppm range. The washing process mentioned above very likely has little or no effect on the level of impurity associated with the crystal phase. Consequently the crystal composition is essentially constant in the purification section.

An axial temperature gradient is established in the purification section as a result of the progressive concentration of the impurity toward the freezing section. The crystals entering the purification section are at a temperature below their melting point. In an adiabatic column the crystals would exchange this sensible heat with the liquid by refreezing an appropriate quantity of the liquid. The axial temperature gradients are sufficiently small, so that refreezing of this type is negligible, for example, the largest axial temperature drop between the top and bottom of the purification section encountered in this study was 8°C which would correspond to a 10% increase in the crystal rate in the purification section. Most of the axial temperature gradient occurs in the region near the freezing section below the first sample

tap. Hence any small increase in the crystal rate due to refreezing occurs below the region where the composition profile is sampled. Therefore any heat transfer effects can be neglected, i.e., the internal crystal and liquid flow rates can be considered constant in both the enriching and stripping sections. Both Albertins[2] and Gates[14] concluded that heat effects could be neglected for columns operated at total reflux.

The mathematical model that is developed below includes the following considerations:

- Mass transfer of the impurity from the adhering to free liquid.
- Mass transfer of impurity in the free liquid by axial dispersion.
- A constant level of impurity in the crystal phase resulting from volumetric inclusion or other phenomena.
- Constant internal flow rates.

B. FORMULATION OF MODEL

Mathematical models for both the enriching and stripping sections are presented below. A separate derivation is not presented for the total reflux case, because it is a special case of the continuous flow model. Much of the development that follows is based on the earlier work of Albertins[2] and Gates.[14] The model that Gates employed to analyze Albertins' data is the total reflux analog of the model that is developed by the transport equation approach for the continuous flow case in a later section of this chapter.

It is possible to operate the enriching section of a column crystallizer with either countercurrent or cocurrent flow. Countercurrent flow is the

normal case where free liquid is generated in the melting section which is used to wash the adhering liquid. The model is developed here specifically for the countercurrent case, but the differential equations that result are equally applicable to cocurrent flow. The application of this model to the cocurrent case will be discussed in a later section of this chapter.

The process flows illustrated in Figure 3 are further idealized in Figure 5 which shows the internal flows in relation to a differential element of the purification section. The flows are denoted by L, L', and C which represent the mass flow rates of the free liquid, adhering liquid, and crystals respectively. The compositions Y, Y', ϵ represent the weight fraction of impurity (cyclohexane in this study) of the free liquid, adhering liquid and crystal phase respectively.

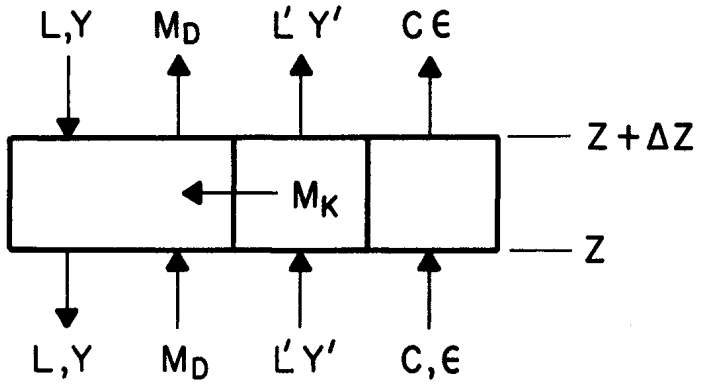

$$M_D = -D\,\rho A \eta \frac{dY}{dZ}$$

$$M_K = K_a A \rho (Y' - Y) \Delta Z$$

Figure 5. Elemental description of column crystallizer.

The impurity is transported by bulk flow, axial dispersion and mass transfer. The bulk flow is represented by LY, L'Y', and Cϵ. The expression repre-

senting the rate of axial dispersion, M_D, is assumed to be of the form of Fick's Law as presented in Eq. (1).

$$M_D = - D\rho A\eta \frac{dY}{dz} \tag{1}$$

D is the effective diffusivity which includes the contributions of molecular diffusion, Taylor diffusion and backmixing; ρ is the free liquid density; A is the area through which liquid and crystals flow; and η is the volume fraction of free liquid in the purification section. The rate of mass transfer between the adhering and free liquid, M_K, is assumed to be proportional to the difference in composition of the adhering and free liquid as shown in Eq. (2).

$$M_K = KaA\rho(Y'-Y)\Delta z \tag{2}$$

K is the mass transfer coefficient; a is the interfacial area between the adhering and free liquid per unit volume; and z is the axial position in the column measured from the freezing section. The internal flow rates L, L', C; and the factors A, K, a, ρ, D, η are assumed to be independent of the position in the column.

A material balance on a differential element of the free liquid yields Eq. (3).

$$L \frac{dY}{dz} + KaA\rho(Y'-Y) + D\rho A\eta \frac{d^2Y}{dz^2} = 0 \tag{3}$$

This expression is general for both the enriching and stripping section. Another relation between Y and Y' is needed before Eq. (3) can be solved.

1. Enriching Section, $(z>z_F)$

A material balance on the enriching section as shown in envelope I in

Figure 6 yields a second relation between Y and Y' which is given in Eq. (4).

$$C\epsilon + L'Y' - LY - D\rho A\eta \frac{dY}{dz} = L_E Y_E \tag{4}$$

where L_E and Y_E are the pure end product rate and composition. An overall balance about envelope I gives Eq. (5).

$$L = L' + C - L_E \tag{5}$$

Equations (3), (4), and (5) can be combined to give the following differential equation which relates the impurity content of the free liquid to the position in the enriching section:

$$\frac{D\eta L'}{Ka}\frac{d^2Y}{dz^2} + \left(\frac{LL'}{KaA\rho} + D\rho A\eta\right)\frac{dY}{dz} + (C-L_E)Y = C\epsilon - L_E Y_E \tag{6}$$

Equation (6) is a linear second order ordinary differential equation. Inspection of this equation shows that its particular solution is given by Eq. (7).

$$Y_P = (C\epsilon - L_E Y_E)/(C-L_E) \tag{7}$$

It was assumed throughout the course of this investigation that the flow rate of adhering liquid is proportional to the crystal rate as described by Eq. (8).

$$L' = \alpha C \tag{8}$$

Using this expression the homogeneous part of Eq. (6) becomes,

$$\frac{d^2Y}{dz^2} + \left[\frac{KaA\rho}{\alpha C} + \frac{(\alpha+1-R_E)C}{D\rho A\eta}\right]\frac{dY}{dz} + \frac{(1-R_E)Ka}{D\eta\alpha}Y = 0 \tag{9}$$

where $R_E = L_E/C$. The definitions (10a) and (10b) are introduced to simplify further manipulations.

$$Q_1 = \frac{KaA\rho}{\alpha C} + \frac{(\alpha+1-R_E)C}{D\rho A\eta} \tag{10a}$$

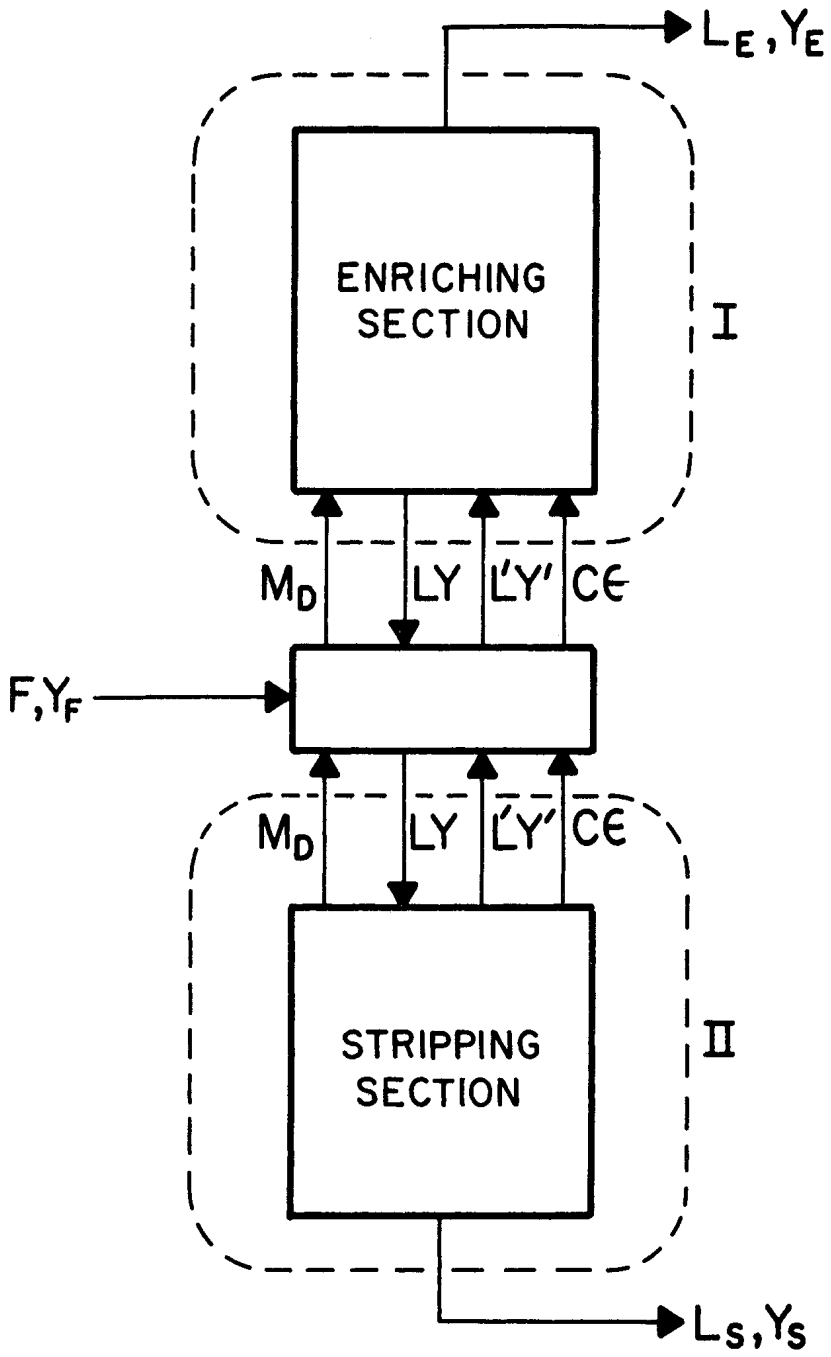

Figure 6. Relationship between internal and external streams.

$$Q_2 = \frac{Ka(1-R_E)}{D\eta\alpha} \tag{10b}$$

Equation (9) then becomes Eq. (11).

$$\frac{d^2Y}{dz^2} + Q_1 \frac{dY}{dz} + Q_2 Y = 0 \tag{11}$$

The complete solution of Eq. (6) is given by Eq. (12).

$$Y = Y_P + C_1 e^{r_1 z} + C_2 e^{r_2 z} \tag{12}$$

The roots r_1 and r_2 must satisfy the following characteristic equation:

$$r^2 + Q_1 r + Q_2 = 0 \tag{13}$$

The roots of this quadratic equation are given by Eq. (14).

$$r_1, r_2 = Q_1 \left[-1 \pm (1 - 4Q_2/Q_1^2)^{1/2} \right] \Big/ 2 \tag{14}$$

2. Stripping Section, ($z<z_F$)

The development of a relation between Y and Y' for the stripping section and its combination with Eq. (3) is completely analogous to the preceding development for the enriching section. A component material balance around envelope II of Figure 6 yields Eq. (15).

$$C\epsilon + L'Y' - LY - D\rho A\eta \frac{dY}{dz} = - L_S Y_S \tag{15}$$

An overall balance around the envelope gives Eq. (16).

$$L = L' + C + L_S \tag{16}$$

The differential equation describing the stripping section that results from combining Eqs. (3), (15), and (16) is given in Eq. (17).

$$\frac{D\eta L'}{Ka}\frac{d^2Y}{dz^2}+\left(\frac{LL'}{KaA\rho}+D\rho A\eta\right)\frac{dY}{dz}+(C+L_S)Y = C\epsilon + L_SY_S \tag{17}$$

The particular solution of this equation is given by Eq. (18).

$$\overline{Y}_P = (C\epsilon+L_SY_S)/(C+L_S) \tag{18}$$

The homogeneous part of Eq. (17) can be simplified to:

$$\frac{d^2Y}{dz^2}+\overline{Q}_1\frac{dY}{dz}+\overline{Q}_2Y = 0 \tag{19}$$

where,

$$\overline{Q}_1 = \frac{KaA\rho}{\alpha C}+\frac{(\alpha+1+R_S)C}{D\rho A\eta} \tag{20a}$$

$$\overline{Q}_2 = \frac{Ka(1+R_S)}{D\eta\alpha} \tag{20b}$$

$$R_S = L_S/C \tag{20c}$$

The complete solution of Eq. (17) is presented in Eq. (21).

$$Y = \overline{Y}_P + \overline{C}_1e^{\overline{r}_1z} + \overline{C}_2e^{\overline{r}_2z} \tag{21}$$

The roots $\overline{r}_1$ and $\overline{r}_2$ are the characteristic roots given by Eq. (22).

$$\overline{r}_1,\overline{r}_2 = \overline{Q}_1\left[-1\pm(1-4\,\overline{Q}_2/\overline{Q}_1^2)^{1/2}\right]\Big/2 \tag{22}$$

3. Boundary Conditions

A boundary condition for both Eqs. (12) and (21) can be obtained from the fact that the free liquid composition is continuous across the feed point. This boundary condition is given in Eq. (23).

$$z = z_F, \quad Y = Y_\phi \tag{23}$$

where Y_ϕ is the composition of free liquid inside the column at the feed point (Y_ϕ in general is not equal to Y_F). This condition applies to both the enriching and stripping section composition profiles. In fact it is this relation that couples Eqs. (12) and (21).

In addition to the above boundary condition the restriction that Y must be between zero and one if compositions are expressed in weight fractions or between 0 and 10^6 if compositions are expressed in ppm wt must be satisfied. This condition also applies to both Eqs. (12) and (21).

4. Summary of Assumptions

Prior to further discussion of the model, all of the assumptions included in its development are listed below:

- The column is assumed to be at steady state.
- All internal flow rates are constant; this is equivalent to neglecting all heat transfer effects.
- The impurity level associated with the crystal phase, ϵ, is constant.
- Radial variations in each phase are negligible.
- All transport properties are assumed to be constant.
- The flow rate of adhering liquid is assumed to be proportional to the crystal rate.

C. SIMPLIFICATION OF THE MODEL

The model presented in the previous section can be simplified. Examina-

tion of the roots of the characteristic equations leads to the elimination of one of the characteristic roots. The resulting first order model has a form that can be compared with the model that is developed by the transport equation approach in a later section of this chapter. This comparison will facilitate the interpretation of experimental data presented in Chapter V.

1. Enriching Section

The nature of the roots of Eq. (14) is governed by the magnitude and sign of Q_2/Q_1^2 defined by Eq. (24).

$$\frac{Q_2}{Q_1^2} = (Ka/D\eta\alpha)(1-R_E)\Bigg/\left[\frac{KaA\rho}{\alpha C} + \frac{(\alpha+1-R_E)C}{D\rho A\eta}\right]^2 \tag{24}$$

It can be shown that Q_2/Q_1^2 has a maximum with respect to crystal rate. Differentiating Eq. (24) with respect to C at constant R_E and setting the result equal to zero yields:

$$\left(\frac{Q_2}{Q_1^2}\right)_{max} = \frac{(1-R_E)}{4(\alpha+1-R_E)} \tag{25}$$

The maximum occurs at a crystal rate of:

$$C^* = \left[\frac{KaD\eta A^2\rho^2}{\alpha(\alpha+1-R_E)}\right]^{1/2} \tag{26}$$

If one further examines Eq. (24) it is apparent that there is a family of curves (Q_2/Q_1^2 versus C) corresponding to different values of R_E. Each curve has a maximum described by Eq. (25). It is clear that the largest value of $(Q_2/Q_1^2)_{max} < 1/4$, because α is greater than zero. Consequently both roots of

Eq. (14) are real and negative for continuous flow and total reflux operation.

The relative importance of the two roots r_1, r_2 (given by Eq. (14)) depend on their relative magnitudes. The roots are given by Eqs. (27a) and (27b).

$$r_1 = \frac{Q_1}{2}\left[-1+(1-4\ Q_2/Q_1^2)^{1/2}\right] \tag{27a}$$

$$r_2 = \frac{Q_1}{2}\left[-1-(1-4\ Q_2/Q_1^2)^{1/2}\right] \tag{27b}$$

The ratio of the magnitude of the two roots, r_2/r_1 is a minimum when Q_2/Q_1^2 is a maximum. Therefore $(r_2/r_1)_{min}$ corresponds to total reflux operation (R_E = 0). When this ratio is a minimum the contribution of $C_2e^{r_2z}$ relative to $C_1e^{r_1z}$ is maximized.

It is necessary to obtain numerical values of r_1 and r_2 in order to examine the relative contributions of the terms $C_1e^{r_1z}$ and $C_2e^{r_2z}$ in Eq. (12). The terms involving the axial diffusion coefficient, $D\rho A\eta$, and the mass transfer coefficient, $KaA\rho$, must be known before the values of r_1 and r_2 corresponding to $(r_2/r_1)_{min}$ can be calculated. The empirical results derived from the total reflux data of Albertins[1] are used to determine the diffusional and mass transfer terms. The values of r_1 and r_2 that correspond to the minimum ratio of r_2/r_1 are -0.284 cm^{-1} and -0.676 cm^{-1}, respectively. The details of these calculations are presented in Appendix F. Consequently e^{r_2z} decays more rapidly than e^{r_1z}.

The term involving r_2 cannot be neglected in Eq. (12) until the relative magnitudes of C_1 and C_2 are established. At this point the following boundary condition is applied to the expression for the enriching section composition

profile (Eq. (12)):

$$z = z_F, \quad Y = Y_\phi \tag{23}$$

Utilizing the values of r_1, r_2 and the above boundary condition for a feed position of 4.0 cm above the freezing section, Eq. (12) becomes:

$$Y_\phi - Y_P = 0.321\ C_1 + 0.0669\ C_2 \tag{28}$$

The argument now proceeds by making the hypothesis that the relative magnitudes of C_1 and C_2 are such that the term $C_2e^{r_2z}$ is significant to the degree that its effect could be observed experimentally. It will be shown that such a hypothesis leads to a physically intractable result.

In order to experimentally detect the presence of $C_2e^{r_2z}$, this term must be at least 10% of $C_1e^{r_1z}$ at a position two sample taps above the feed point, consequently, it is assumed that

$$\frac{C_2e^{r_2z_6}}{C_1e^{r_1z_6}} = 0.1 \tag{29}$$

where z_6 (the subscript denotes the sample tap number) is the position of the second sample tap above the feed point (17.75 cm in this case). The values of r_1 and r_2 presented above can now be used to calculate the value of C_2/C_1 corresponding to the original hypothesis (Eq. (29)). The calculation yields $C_2/C_1 = 103$.

Equation (12) must also account for the level of impurity in the free liquid in the upper portion of the enriching section, for example at the top sample tap, z_1, whose position is 47.5 cm above the freezing section. Equa-

tion (12) reduces to Eq. (30) when the values of z_1, r_1, r_2 and $C_2 = 103\ C_1$ are substituted.

$$Y_1 - Y_P = C_1/722{,}000 \tag{30}$$

It is convenient to establish the minimum value of C_1 in order to check if the original hypothesis of the magnitude of the term involving C_2 is consistent with the expression for the enriching section profile evaluated at Z_F (Eq. (28)). The magnitude of C_1 is 722,000 (Y_1-Y_P). Examination of the experimental composition profile data (Appendix C) in view of Eq. (30) indicates that for many cases

$$Y_\phi < 722{,}000\ (Y_1-Y_P) \tag{31}$$

This is an empirical observation. Consequently Y_ϕ is a conservative estimate of the minimum value of C_1.

The validity of the original hypothesis of Eq. (29) can now be checked. Using the value of $C_1 = Y_\phi$ and the identity $C_2 = C_2/C_1\ Y_\phi$ Eq. (28) becomes:

$$Y_\phi - Y_P = 0.321\ Y_\phi + 0.0669\ \frac{C_2}{C_1}\ Y_\phi \tag{32}$$

Substituting $C_2/C_1 = 103$ into Eq. (32) and rearranging gives $Y_\phi = -Y_P/6.21$. Inspection of the defining relation for Y_P shows that it is positive in many cases. Consequently the above relation predicts that Y_ϕ is negative which contradicts the restriction stated earlier that $0 \leq Y \leq 10^6$. Therefore the original hypothesis of Eq. (29) concerning the relative magnitude of $C_2e^{r_2z}$ and $C_1e^{r_1z}$ is not valid. The condition that Y must be greater than zero requires that

$$\frac{C_2 e^{r_2 z_e}}{C_1 e^{r_1 z}} < 0.1 \qquad (33)$$

Thus neglecting the term in Eq. (12) involving $C_2 e^{r_2 z}$ is justified in view of the fact that its presence cannot be detected experimentally.

It is recognized that the validity of neglecting this term is based on consideration of a special case, i.e., particular values of r_1 and r_2 were used. It is pointed out, however, that the values of r_1 and r_2 were chosen to maximize the contribution of the term involving r_2, i.e., the values of r_1 and r_2 corresponding to $(r_2/r_1)_{min}$ were used. Therefore it is valid to reduce the expression for the enriching section composition profile (Eq. (12)) as follows:

$$Y = Y_P + C_1 e^{r_1 z} \qquad (34)$$

The constant C_1 can be evaluated by using the boundary condition presented in Eq. (23). Finally, the free liquid composition profile in the enriching section can be represented by Eq. (35).

$$\frac{Y - Y_P}{Y_\phi - Y_P} = e^{r_1 (z - z_F)} \qquad (35)$$

2. Stripping Section

The simplification of Eq. (21) to a form similar to Eq. (34) can be justified by arguments similar to those presented above. In this case the group $\bar{Q}_2 | \bar{Q}_1^2$ governs the nature of the characteristic roots $\bar{r}_1$ and $\bar{r}_2$. Like the corresponding group for the enriching section $(\bar{Q}_2 | \bar{Q}_1^2)_{max}$ is less than 1/4. Therefore $\bar{r}_1$ and $\bar{r}_2$ are real and negative. Also, arguments similar to those used in the enriching section case justify neglecting $\bar{C}_2 e^{\bar{r}_2 z}$ relative to $\bar{C}_1 e^{\bar{r}_1 z}$.

Equation (21) therefore reduces to Eq. (36).

$$Y = \bar{Y}_P + \bar{C}_1 e^{\bar{r}_1 z} \tag{36}$$

$$\bar{r}_1 = \frac{\bar{Q}_1}{2}\left[-1+(1-4\,\bar{Q}_2/\bar{Q}_1^2)^{1/2}\right] \tag{37}$$

Applying the boundary condition described by Eq. (23), Eq. (36) becomes:

$$\frac{Y_\phi-\bar{Y}_P}{Y-\bar{Y}_P} = e^{\bar{r}_1(z_F-z)} \tag{38}$$

3. Summary of the Resulting Model

The final expressions for the composition profiles in the enriching and stripping section are now obtained by introducing the definitions of Q_1, Q_2, $\bar{Q}_1$, $\bar{Q}_2$, Y_P and $\bar{Y}_P$. It is convenient to introduce two additional definitions:

$$\psi_E = -1/r_1 \tag{39}$$

$$\psi_S = -1/\bar{r}_1 \tag{40}$$

The expressions for the two composition profiles now become:

Enriching Section

$$\frac{Y-(C\epsilon-L_E Y_E)/(C-L_E)}{Y_\phi-(C\epsilon-L_E Y_E)/(C-L_E)} = e^{-(z-z_F)/\psi_E} \tag{41a}$$

where,

$$\psi_E = \frac{2}{\left[\frac{KaA\rho}{\alpha C}+\frac{(\alpha+1-R_E)C}{D\rho A\eta}\right]\left\{1-\sqrt{1-\frac{4(Ka/D\eta\alpha)(1-R_E)}{\left[\frac{KaA\rho}{\alpha C}+\frac{(\alpha+1-R_E)C}{D\rho A\eta}\right]^2}}\right\}} \tag{41b}$$

Stripping Section

$$\frac{Y_\phi-(C\epsilon+L_SY_S)/(C+L_S)}{Y-(C\epsilon+L_SY_S)/(C+L_S)} = e^{-(z_F-z)/\psi_S} \qquad (42a)$$

where,

$$\psi_S = \frac{2}{\left[\frac{KaA\rho}{\alpha C}+\frac{(\alpha+1+R_S)C}{D\rho A\eta}\right]\left\{1-\sqrt{1-\frac{4(Ka/D\eta\alpha)(1+R_S)}{\left[\frac{KaA\rho}{\alpha C}+\frac{(\alpha+1+R_S)C}{D\rho A\eta}\right]^2}}\right\}} \qquad (42b)$$

It can be seen that the parameters ψ_E and ψ_S determine the separation power of a continuous flow column crystallizer operating at specified conditions. Henceforth these parameters will be referred to as mass transfer factors. Equations (41a) and (42a) show that as the mass transfer factors ψ_E and ψ_S increase the slope of the axial composition decreases, i.e., the separation decreases. Therefore the mass transfer factors are inverse measures of the separation power of the enriching and stripping section respectively.

D. TRANSPORT EQUATION APPROACH

Expressions for the enriching and stripping section composition profiles can also be obtained by employing the transport equation approach. This method utilizes the same mechanisms previously discussed, but involves a mathematical simplification of the material balance on an element of free liquid, Eq. (3), in the purification section. Impurity transfer by axial diffusion is neglected in this balance. The diffusion term $D\rho A\eta \frac{dY}{dz}$ is retained, however, in the material balances, Eqs. (4) and (15). The transport equation approach was first used by Furry, Jones and Onsager[12] to model thermal diffusion columns and later applied by Powers[27] to column crystallization.

Neglecting the diffusional term Eq. (3) becomes:

$$L \frac{dY}{dz} + KaA\rho(Y'-Y) = 0 \tag{43}$$

This relation can be combined with Eqs. (4) and (15) to obtain a first order, ordinary differential equation describing the enriching and stripping sections.

Enriching Section

$$\left(\frac{LL'}{KaA\rho} + D\rho A\eta\right)\frac{dY}{dz} + (C-L_E)Y = C\epsilon - L_E Y_E \tag{44}$$

Stripping Section

$$\left(\frac{LL'}{KaA\rho} + D\rho A\eta\right)\frac{dY}{dz} + (C+L_S)Y = C\epsilon + L_S Y_S \tag{45}$$

These equations are readily solved by applying the following boundary condition to each.

$$z = z_F, \quad Y = Y_\phi \tag{23}$$

Enriching Section

$$\frac{Y-(C\epsilon-L_E Y_E)/(C-L_E)}{Y_\phi-(C\epsilon-L_E Y_E)/(C-L_E)} = e^{-(z-z_F)/\psi'_E} \tag{46a}$$

$$\psi'_E = \frac{1}{C-L_E}\left[D\rho A\eta + \frac{\alpha(\alpha+1)C^2}{KaA\rho} - \frac{\alpha L_E C}{KaA\rho}\right] \tag{46b}$$

Stripping Section

$$\frac{Y_\phi-(C\epsilon+L_S Y_S)/(C+L_S)}{Y-(C\epsilon+L_S Y_S)/(C+L_S)} = e^{-(z_F-z)/\psi'_S} \tag{47a}$$

$$\psi_S' = \frac{1}{C+L_S}\left[D\rho A\eta + \frac{\alpha(\alpha+1)C^2}{KaA\rho} + \frac{\alpha L_S C}{KaA\rho}\right] \tag{47b}$$

It is instructive to compare the expressions for the composition profiles listed above that were developed by the transport equation approach with the corresponding relations that were developed in the previous section without neglecting the diffusional term in Eq. (3) as subsequently simplified by consideration of limiting cases. Comparison of Eqs. (46) and (47) with Eqs. (41) and (42) developed earlier show that both procedures result in enriching and stripping section profiles of the same form. The mass transfer factors for the enriching and stripping section profiles are different, however, i.e.,

$$\psi_E \neq \psi_E' \tag{48}$$

and

$$\psi_S \neq \psi_S' \tag{49}$$

These parameters can be related by further manipulation. The square root terms in Eqs. (41b) and (42b) are expanded in a Taylor series as follows:

$$\sqrt{1-4X} = 1 - 2\sum_{n=1}^{\infty}\frac{(2n-2)!}{n!(n-1)!}X^n \tag{50}$$

where,

$$X_E = (Ka/D\eta\alpha)(1-R_E)\Big/\left[\frac{KaA\rho}{\alpha C} + \frac{(\alpha+1-R_E)C}{D\rho A\eta}\right]^2 \tag{51}$$

$$X_S = (Ka/D\eta\alpha)(1+R_S)\Big/\left[\frac{KaA\rho}{\alpha C} + \frac{(\alpha+1+R_S)C}{D\rho A\eta}\right]^2 \tag{52}$$

Rearrangement of Eqs. (41b) and (42b) using the above relations yields:

$$\psi_E = \psi_E'/\theta(X_E) \tag{53}$$

$$\psi_S = \psi_S'/\theta(X_S) \tag{54}$$

where,

$$\theta(X) = 1 + X + 2X^2 + 5X^3 + \ldots = \sum_{n=1}^{\infty} \frac{(2n-2)!}{n!\,(n-1)!} X^{n-1} \tag{55}$$

The mass transfer factors, ψ_E and ψ_S, predicted by the original model are related to those predicted by the transport equation approach by the correction factors $\theta(X_E)$ and $\theta(X_S)$.

The mass transfer factors obtained by the transport equation approach become the same as those predicted by the original model when X_E and X_S are small, for example,

$$\begin{aligned} &X_E < 0.1, \quad X_S < 0.1 \\ &\theta(X_E) = \theta(X_S) \cong 1 \end{aligned} \tag{56}$$

therefore,

$$\psi_E = \psi_E' \tag{57}$$

$$\psi_S = \psi_S' \tag{58}$$

A demonstration that X_E and X_S are less than 0.1 requires calculation of these parameters from their defining expressions (Eqs. (51) and (52)). The validity of the approximation of Eq. (56) and the limitations involved with calculating X_E and X_S are discussed in Chapter V. Gates[14] assumed that $X_0 < 0.1$ (the subscript 0 refers to total reflux operation) when he analyzed the total reflux data of Albertins.[1] As shown above this is equivalent to using the transport

equation approach.

Finally, one mathematical peculiarity of the expression for the enriching section profile (Eqs. (46)) is noted. When $R_E = 1$ ($L_E = C$) Eqs. (46a) and (46b) reduce to 1 = 1 which prevents its application. If Eqs. (46) are re-derived setting $L_E = C$ the following relation results:

$$Y = Y_\phi - (z-z_F)\left[\frac{(L_E Y_E - C\epsilon)}{\left(\frac{\alpha^2 C^2}{KaA\rho} + D\rho A\eta\right)}\right] \tag{59}$$

It can be seen that in this special case the free liquid composition is linear with position z.

E. IMPLEMENTATION OF THE MODEL

Models have been developed for the enriching and stripping sections, but before they can be utilized for column calculations the free liquid compositions at both ends of the purification section ($z = \mathcal{L}$ and $z = 0$) must be related to the terminal compositions Y_E and Y_S. Once this is achieved an iterative procedure is presented that can be used to perform column calculations.

1. End Compositions for the Purification Section

The relationships between the compositions at the ends of the purification section and the terminal compositions are established by modeling the melting and freezing sections. Both sections are assumed to be perfectly mixed as illustrated in Figure 7.

The enriching section can be operated either countercurrently or cocurrently. The direction of the free liquid flow is determined by the

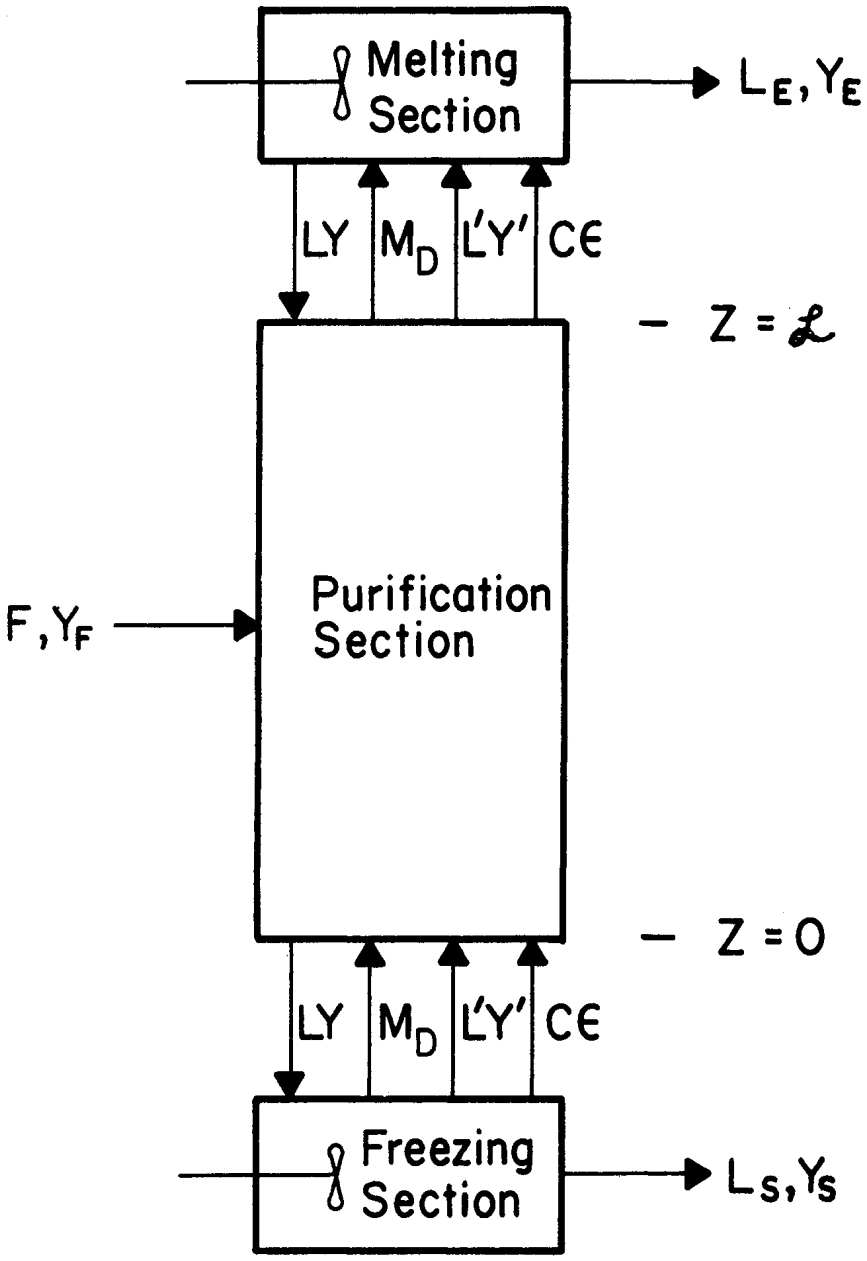

Figure 7. Melting and Freezing section models.

relative magnitudes of overhead product draw-off rate and the mass flow rates of the crystal phase and adhering liquid. The following two relations determine whether the flow in the enriching section is countercurrent or cocurrent:

Countercurrent Flow

$$L_E < L' + C \tag{60}$$

Cocurrent Flow

$$L_E > L' + C \tag{61}$$

Countercurrent operation is the normal mode, i.e., the purpose of the enriching section is to wash impurities from the adhering liquid which requires generation of a countercurrent free liquid stream, L, in the melting section. For countercurrent operation the composition at the top of the enriching section, $z = \mathcal{L}$, is the same as the terminal composition Y_E because both streams are outputs from a perfect mixer; therefore for conventional countercurrent operation:

$$z = \mathcal{L}, \quad Y = Y_E \tag{62}$$

The cocurrent case is more complicated. With this type of operation the direction of free liquid is the opposite of that shown in Figure 7. This stream is now an input to the perfectly mixed melting section, and in general $Y \neq Y_E$ at the top of the purification section. It is noted that there is minimal separation occurring in the enriching section with cocurrent operation, because a portion of the feed stream passes cocurrently up the column with the crystals and adhering liquid. It is therefore reasonable to assume $\frac{dY}{dz} = 0$ at $z = \mathcal{L}$. This condition can be combined with Eqs. (4) and (43) to obtain the following relation for cocurrent operation:

$$z = \mathcal{L}, \quad Y = \frac{L_E Y_E - C\epsilon}{L_E - C} \tag{63}$$

The composition of the free liquid at the bottom of the stripping section, Y_0, can be related to the bottoms product composition Y_S. Due to the perfect mixing conditions that are assumed in the freezing section $Y' = Y_S$. Also it is reasonable to neglect impurity transfer by the crystal phase at the bottom of the purification section, i.e., $L_S Y_S \gg C\epsilon$. Equations (15), (18), (36), and (40) can be combined utilizing the above conditions that prevail at the bottom of the stripping section to obtain the following relation between Y_0 and Y_S:

$$\frac{Y_0}{Y_S} = \frac{L' + L_S - D\rho A\eta \; L_S/\psi_S'(L_S + C)}{L' + L_S + C - D\rho A\eta/\psi_S'} \tag{64}$$

The dependence of Y_0 on Y_S therefore depends on the ratio $\rho DA\eta/\psi_S'$. It can be shown that when axial diffusion is the dominant mechanism determining ψ_S' that Eq. (64) reduces to $Y_0/Y_S \cong 1$. Consequently the following relation will be used to facilitate column calculations:

$$z = 0, \quad Y = Y_S \tag{65}$$

It is shown in Chapter V that column calculations using this relation are in good agreement with experimental data.

2. Column Calculations

The following parameters are specified before calculations are started: F, Y_F, L_S, C, $\mathcal{L}$ and z_F. Also ψ_E, ψ_S and ϵ are specified either from experimental data or from correlations obtained from the appropriate experimental

data. The terminal compositions Y_E, Y_S, and the composition profile $Y(z)$ can then be calculated by the following iterative procedure

- Assume Y_E.
- Calculate Y_S from the overall material balance,

$$FY_F = L_E Y_E + L_S Y_S \tag{66}$$

- Calculate $Y_{\phi 1}$ from the mathematical model for the enriching section.
- Calculate $Y_{\phi 2}$ from the stripping section model.
- Increment Y_E and repeat the calculations until $Y_{\phi 1} \cong Y_{\phi 2}$ i.e., until a convergence criterion is satisfied. This matching procedure satisfies the requirement that Y be continuous across the feed point.
- Calculate the composition profile $Y(z)$ from the converged values of Y_ϕ and Y_S.

A Fortran IV program has been written which implements the above procedure. The program listing, definition of symbols and typical output are presented in Appendix D.

F. IMPLICATIONS OF THE MODEL

The mathematical model developed earlier for the enriching and stripping section (see Eqs. (41a) and (42a)) can be used to predict the performance of a center-fed column crystallizer. Equations (41a) and (42a) when solved simultaneously will predict the influence of product draw-off rates (L_E and L_S), feed position (z_F), and the internal crystal rate on the purity of the overhead product (Y_E). Such predictions require a knowledge of ψ_E, ψ_S, and ϵ or

equivalently Ka, $D\eta$, α, and ϵ from experimental data on the particular system of interest. The results of Albertins'[1] study for total reflux operation were used to estimate the above parameters. The iterative column calculation procedure can then be used to make the predictive calculations.

Examination of Eq. (41a) indicates that the $\ln(Y-Y_P)$ should decrease linearly with the position z in the enriching section. Recalling Eq. (7), Y_P is defined as follows:

$$Y_P = \frac{C\epsilon - L_E Y_E}{C - L_E} \tag{7}$$

The important property of Y_P is that it can change sign depending on the relative magnitudes of the amount of impurity transported by the crystal phase, $C\epsilon$, and the amount of impurity in the overhead product $L_E Y_E$. When Y_P is positive, zero, and negative the enriching section composition profile (lnY vs z) is respectively concave upward, linear, and concave downward. Figure 8a illustrates these three distinct enriching section profile shapes.

Similarly Eq. (42a) shows that $\ln(Y-\bar{Y}_P)$ should also decrease linearly with the position in the stripping section. In this case however $\bar{Y}_P$ is always positive as indicated by Eq. (18).

$$\bar{Y}_P = (C\epsilon + L_S Y_S)/(C + L_S) \tag{18}$$

Due to the relative large magnitude of $\bar{Y}_P$ the free liquid composition in the stripping section can decay rapidly to $\bar{Y}_P$ and then remain essentially constant until the feed position is reached. This effect is particularly noticeable when the feed position, z_F, is well above the freezing section. Figure 8b qualitatively illustrates the flat portion of the stripping section profile

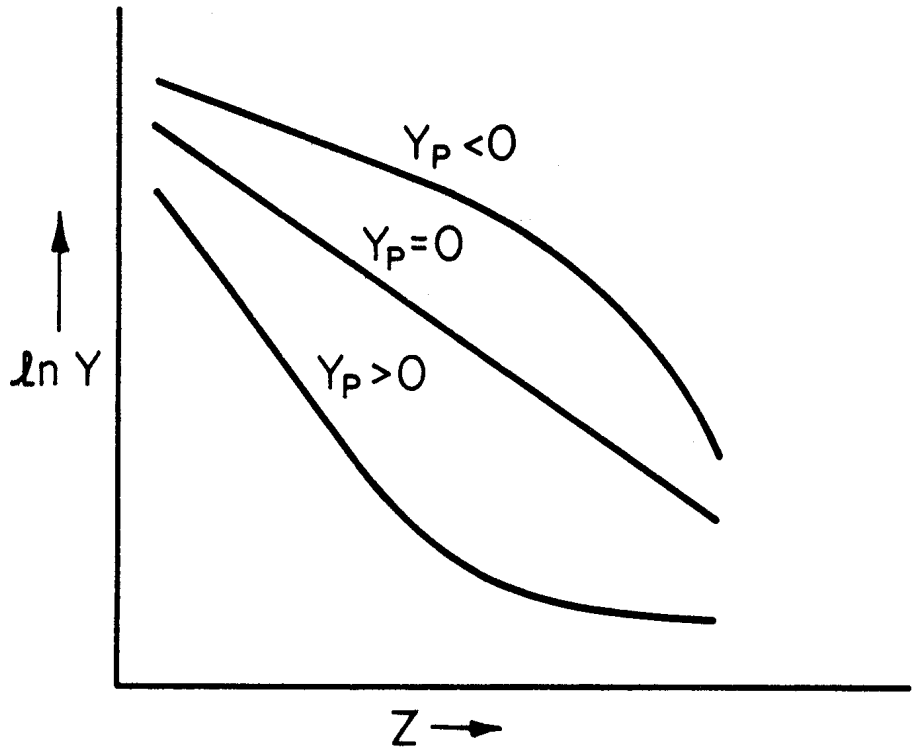

(a) Enriching Section Composition Profiles

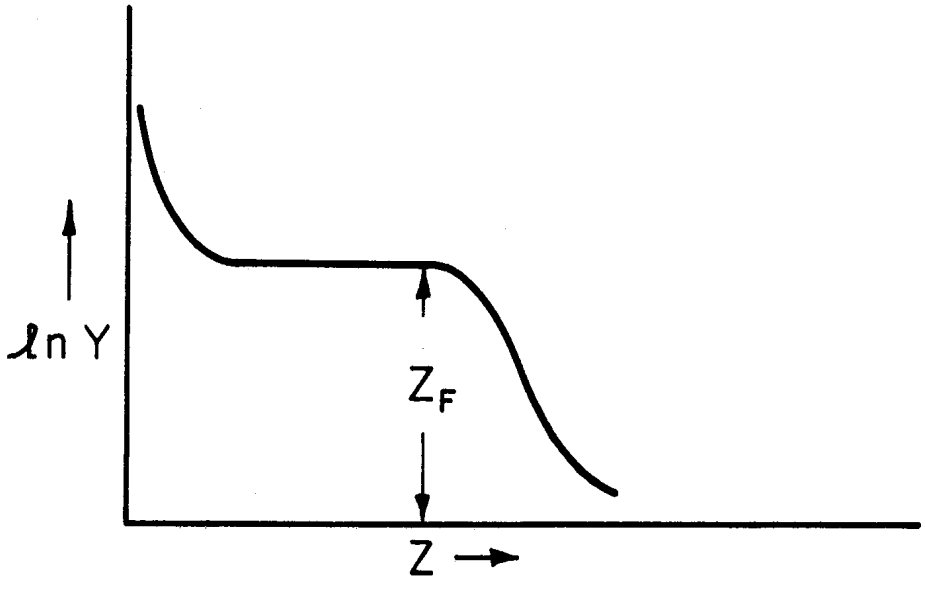

(b) Comparison of Stripping and Enriching Section Composition Profiles

Figure 8. Composition profile shapes predicted by the model.

relative to the profile in the enriching section. Both Figures 8a and 8b represent profile shapes that were obtained by applying theory via the column calculation procedure presented earlier. It is desirable to avoid such a flat region in the stripping section profile, because this type of profile indicates that a portion of the column does not contribute to the separation. Column calculations show that the flat portion of the stripping profile can be eliminated by moving the feed point closer to the freezing section, that is, by decreasing the length of the stripping section.

A closer inspection of the mass transfer factor in the enriching section (ψ_E) shows a strong dependence on the ratio of the overproduct draw-off rate to internal crystal rate (R_E). The mass transfer factor is a minimum (which corresponds to a maximum separation power) at total reflux and increases as R_E is increased. Due to the exponential dependence of the free liquid composition on ψ_E, the separation that can be achieved in a column is extremely sensitive to R_E, i.e., as R_E increases Y_E increases.

G. APPROXIMATIONS

Finally, several approximations are introduced that result from the relative magnitudes of the various parameters that are determined from the experimental data. These relations will be applied in Chapter V to facilitate analysis of the data.

The terminal stream material balance (Eq. (66)) can be simplified when the column is operated such that a very pure overhead product is obtained. In this case the amount of impurity leaving the column in the overhead stream is

negligible compared to that contained in the feed and bottoms streams, that is, $L_E Y_E \ll L_S Y_S$ and FY_F. Under these conditions Eq. (66) reduces to Eq. (67).

$$Y_S \cong \frac{F}{L_S} Y_F \tag{67}$$

The expression for $\bar{Y}_P$ (Eq. (18)) which determines the shape of the stripping section composition profile can be obtained in a form that facilitates the calculation of $\bar{Y}_P$ from experimental parameters. The amount of impurity in the crystal phase is much smaller than that in the bottoms stream, i.e., $C\epsilon \ll L_S Y_S$. The relation for $\bar{Y}_P$ becomes:

$$\bar{Y}_P = \frac{L_S Y_S}{C+L_S} \tag{68}$$

If L_S, C, and Y_S are known from experiments, $\bar{Y}_P$ can be calculated, but Eq. (68) is very sensitive to errors in L_S. Equation (68) and the modified terminal stream balance (Eq. (67)) can be combined to give:

$$\bar{Y}_P = \frac{FY_F}{C+L_S} \tag{69}$$

which is less sensitive to experimental errors in L_S.

The equations developed earlier which relate the mass transfer factors ψ_E' and ψ_S' to the operating parameters (see Eqs. (46b) and (47b)) can be combined to yield an expression for ψ_E' in terms of ψ_S'. Considerable simplification results from neglecting the mass transfer terms in relation to the diffusional term.

$$\psi_S' = \psi_E' \frac{(C-L_E)}{(C-L_S)} \tag{70}$$

This relation is only valid when axial diffusion is the dominant mechanism

determining the mass transfer factors. It can be used to calculate ψ_S' from experimental values of ψ_E' when experimental values of ψ_S' are not available.

CHAPTER IV

EXPERIMENTAL INVESTIGATION

The details of equipment construction, operating procedures, variables studied and experimental data are discussed in this chapter. Much of the experimental equipment and procedure are common to the previous study of Albertins. His equipment was modified for use in this investigation. While the description of equipment presented below is intended to be complete, many aspects of the fabrication, etc. are presented in more detail in Albertins' thesis.[1]

A. DESCRIPTION OF EQUIPMENT

1. The Column Proper

A center-fed column crystallizer of the Schildknecht type was used in this study. A sketch of the column and pertinent dimensions are given in Figure 9. Figure 10 is a photograph of the column. The column was constructed from a 32 mm O.D. pyrex tube 70 cm long. A 1.1 cm O.D. stainless steel tube was placed inside the glass tube to define the annulus which contained the stainless steel spiral. The spiral of lenticular cross section and 1 cm pitch was provided by Speciality Design Company.[31] The area normal to the flow of the crystal slurry defined by two spiral turns, the stainless steel tube, and the glass tube was 0.6 cm^2. Six copper-constantan thermocouples were mounted in 1/16 in. holes in the wall of the steel tube with epoxy resin. The seventh thermocouple is located in the freezing section. Eight sample taps were fused

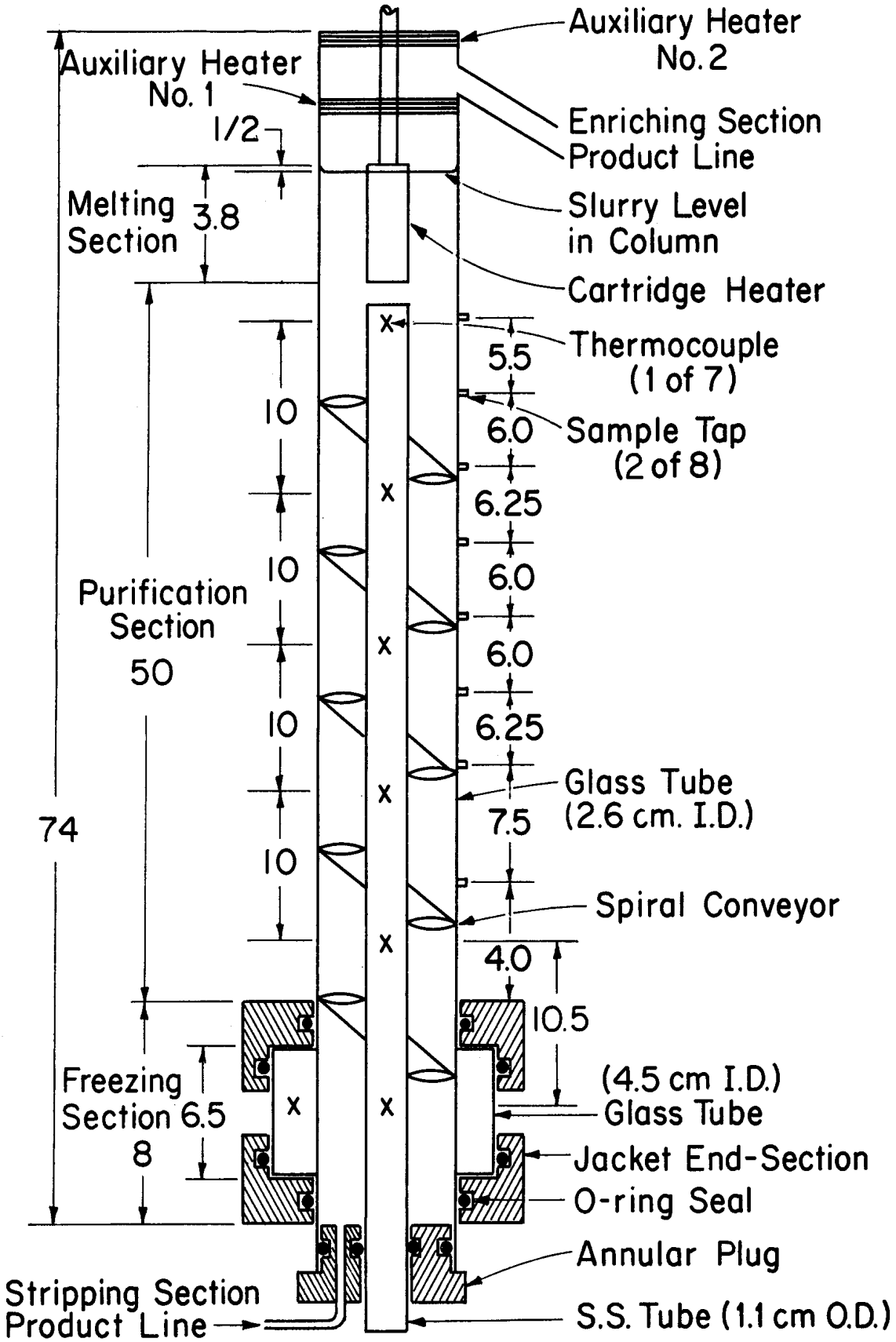

Figure 9. Schematic diagram of the column crystallizer used in this investigation.

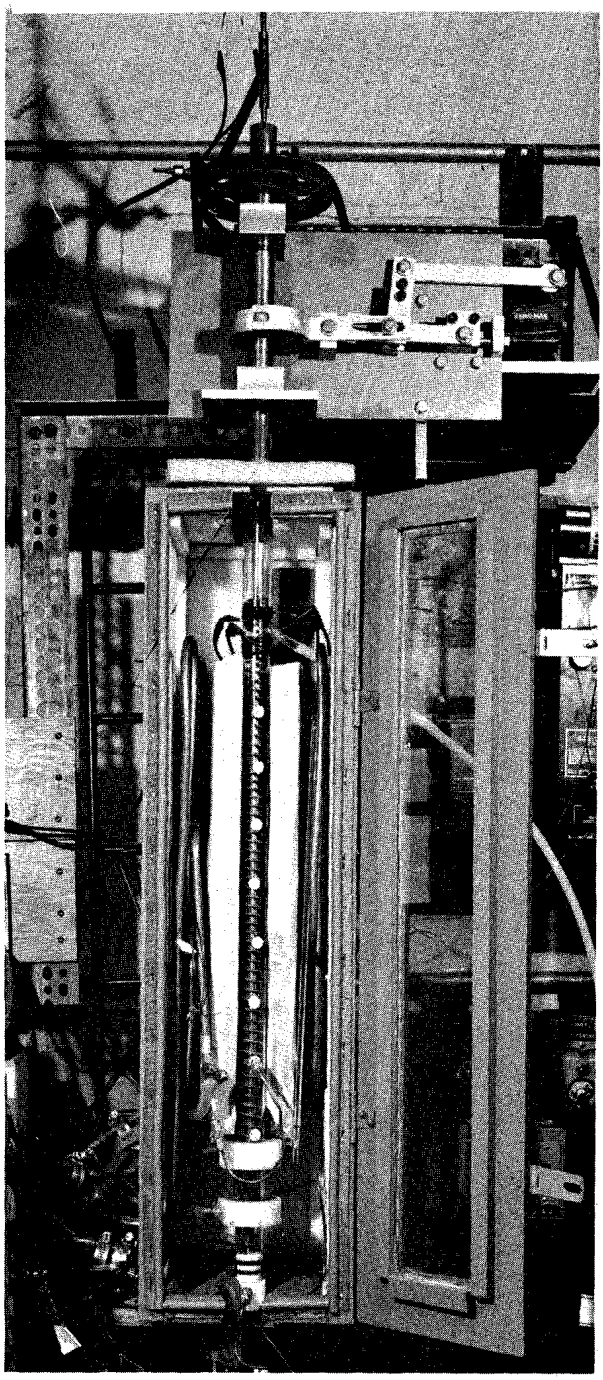

Figure 10. Photograph of the column crystallizer used in this investigation.

in the glass column. The taps consisted of a 1/4 in. glass sleeve which could hold a rubber septum; interior to the glass sleeve was a 1/32 in. pinhole that minimized communication of the column contents with the tap area.

The freezing section was at the lower end of the glass column as shown in Figure 9. It consisted of a glass jacket mounted in two nylon rings. Methanol coolant was circulated through the jacket. All nylon-glass seals were formed by neoprene O-rings.

The annulus between the glass and steel tubes at the bottom of the column was closed with a nylon plug. In this case Viton O-rings, which are resistant to benzene, were used for the glass-nylon and nylon-steel seals.

The melting section was defined as that portion of the column occupied by the internal heater. The melting section heater was a G.E. Calrod cartridge heater (240 ohms) mounted with its lower end 2.5 cm above the top sample tap as shown in Figure 9.

In addition to the internal melting section heater, two auxiliary heaters were placed above and external to the melting section. Each consisted of several turns of resistance wire wrapped around the glass column. Auxiliary heater No. 1 was used to flush the gap between the melting section and the overhead draw-off line. This procedure is described more fully in a later section of this chapter. The second auxiliary heater was used to melt back any crystals that inadvertently got past the melting section and draw-off line in the case that insufficient power was supplied to the melting section heater or auxiliary heater No. 1.

2. Feed and Product Draw-Off System

The installation of a feed and product draw-off system represented the most significant modification of Albertins' equipment. Both the feed and bottoms product were transported and controlled by proportioning pumps. Both pumps were coupled to the same drive. The stroke of each side of the pump could be adjusted for a flow rate range of 0.6 - 7.0 ml/min. The pump specification was Hills-McCanna UM2 Feed size 2(MLE)33 catalog No. 117147. The feed and product streams were pumped through 1/8 in. copper lines equipped with Swagelok fittings. It was necessary to place the pump above the liquid level in the column to prevent benzene from flowing through the pump on the open stroke due to the liquid head driving force. The pump stroke-flow relationship was linear. A calibration curve is presented in Appendix B.

The feed material was cooled prior to introduction into the column. The feed cooler was a hairpin double pipe exchanger. The shell side was a 3/8 in. copper tube and the tube side was constructed of 15 ga stainless steel hypodermic tubing. Benzene was cooled on the tube side and methanol coolant was circulated on the shell side. The exchanger was 3.8 ft long which provided sufficient area to allow the temperature of the benzene effluent to approach that of the coolant within 0.5°C. A thermocouple was installed in the benzene effluent line to measure the feed temperature. This was accomplished by soldering the thermocouple bead in the wall of the hypodermic tubing.

It was possible to introduce the feed at any of the sample taps. This was accomplished by terminating the 1/8 in. copper line from the feed cooler with a Swagelok plug. The plug was drilled and fitted with a 25 ga hypodermic

needle. This arrangement made it possible to simply plug in the feed through any of the rubber septums in the various sample taps. Figure 11 shows the feed introduction assembly.

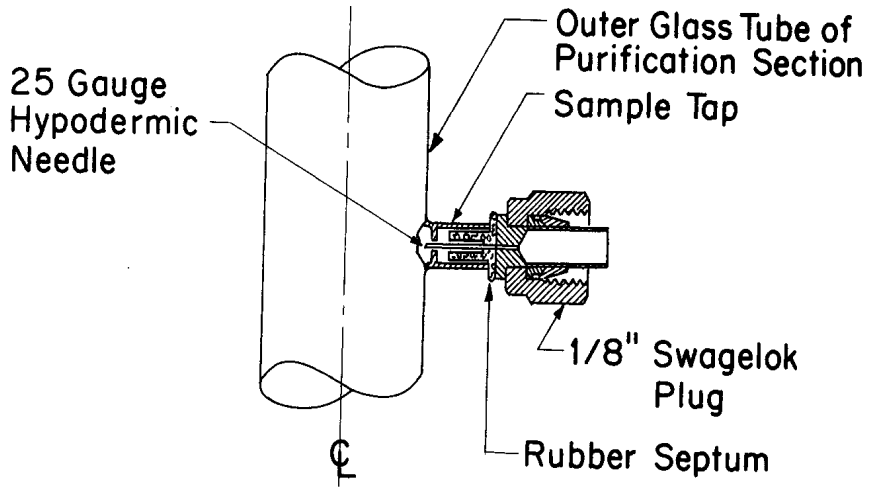

Figure 11. Feed introduction assembly.

The bottoms product was withdrawn through a drain in the plug at the bottom of the column. As mentioned previously both the feed and bottoms streams were transported by the proportioning pump. Consequently the overhead product was allowed to trickle through the overhead line. The overhead product was removed through a 3/8 in. glass tube that was fused into the wall of the column. It was inclined at 45° to prevent build up of liquid above the draw-off point. The overhead product flowed to a receiver through 3/8 in. I.D. teflon tubing. The bottoms product was collected in a receiver at the level of the pump outlet.

3. Spiral Drive Mechanism

The spiral was both rotated and oscillated by the drive mechanism shown in Figure 10. The power was provided by two 1/3 H.P. motors. It was possible

to vary the oscillation and rotational speed independently from 0-440 cycles/min using two ZERO-MAX variable speed reducers. The spiral was connected to the drive by a 2-1/2 in. long nylon coupling.

4. Column Environment

The column itself was insulated on three sides with 1 in. thick styrofoam. The front was left open so the interior of the column could be observed. The entire column was placed in a constant temperature air bath shown in Figure 10. The temperature was controlled at 5.5°C, the melting point of benzene. The air bath was an insulated plywood box equipped with a cooling coil. The front door of the box had a window that permitted inspection of the column.

5. Refrigeration System

Three levels of coolant were required to operate the column crystallizer. These include the coolant to the freezing jacket, feed cooler, and the constant temperature air bath. The system consisted of a primary refrigerant bath that provided methanol coolant at -30°C and three secondary baths which were used to control the secondary refrigerant (also methanol) by on-off control of the primary refrigerant pumps. The coolant temperatures to the freezing jacket and feed cooler were controlled by Foxboro model 5041-15 on-off controllers. Since these were originally designed for high temperature service, thermopiles were used to obtain the necessary signals. The coolant to the air bath was controlled by an American Instrument Company bimetallic thermoregulator.

B. OPERATING PROCEDURES

1. Start-Up

The column was charged with 300 ml of the feed material prior to beginning each run. When the feed composition was changed from run to run, the column, pump and lines were flushed with the new feed material. The desired terminal flow rates were established by adjusting the stroke of each side of the proportioning pump, i.e., the feed and stripping section product rates were set. The terminal flow rates were determined by collecting and weighing the various streams. The remaining steps of the start-up procedure are listed below in the order in which they were performed:

- The coolant flow to the coil in the air bath that surrounds the column was turned on. The air bath temperature was maintained at 5.5°C.
- The spiral rotation and oscillation were started.
- The coolant to the freezing section was turned on. The coolant temperature was decreased from 2°C to the desired temperature at a rate of approximately 20°C/hr. This was done to avoid plugging of the freezing section.
- The feed and bottoms product pump was started.
- Coolant flow to the feed cooler was initiated. In most cases the feed temperature was controlled at a level 1-2°C above the freezing point of the feed.

The crystals were allowed to rise through the purification section to the melting section. At this point sufficient power was applied to the melting

section heater to cause the crystal slurry-liquid interface to equilibrate at a position near the top of the melting section heater.

The column was operated with the crystal interface in this position for approximately an hour prior to flushing the region above the melting section. As Figure 9 illustrates there is a 2.5 cm gap of liquid between the melting section and overhead draw-off line. Note that crystals do not normally enter this region. Prior to start-up this gap contains liquid of feed composition. In order to accelerate the rate at which the composition of this region approached the melting section composition, this gap was flushed in the manner described below. The melting section heater was turned off and the crystal slurry was allowed to rise to a position just below the overhead draw-off line. The interface was controlled at this point for 15 min by adjusting the power to auxiliary heater No. 1. The No. 1 auxiliary heater was then turned off and the melting resumed with the melting section heater to reestablish the position of the crystal-liquid interface in the melting section. This procedure was employed twice in the first few hours of each run.

2. Operation

Once the crystal slurry position was reestablished after the flushing procedure, adjustments were made in the coolant temperature to the freezing section to achieve the desired crystal rate. Except during the first hour after start-up, it was not difficult to determine the power necessary to just melt the crystals entering the melting section.

The temperatures of the coolants to the freezing section and feed cooler

were controlled at set points established by calibrated thermometers in the secondary refrigerant baths. The cold bath temperature was controlled at a set point established by a thermometer in the bath itself. No difficulty was experienced in controlling the various temperatures or the position crystal slurry interface as the column approached steady state.

3. Flow Measurements

As mentioned earlier the terminal stream flow rates were determined by collecting and weighing the overhead and bottoms products. These rates were constant within ±10% during a run in the range 0.6 to 4 gm/min. An experiment was designed to check the overall material balance. The feed material was placed in a 100 ml graduated cylinder and the two product streams were returned to the cylinder. If there are no leaks in the system, i.e., if the overall material balance closes, the liquid level in the graduated cylinder should remain constant. At an overhead rate of 2.15 gm/min and a bottoms rate of 3.01 gm/min the interface remained constant for 1 hr 15 min. Consequently, it is concluded that there were no leaks in the system and that the overall material balance closed. The constant interface also implies that there was no appreciable moisture pickup by the products.

The crystal rate was calculated from the power required to melt the crystals entering the melting section. The voltmeter used for the crystal rate measurement was calibrated by Mr. C. H. Eichhorn at the Electrical Measurements Laboratory of The University of Michigan. This procedure involves the assumption that the overhead product is at its melting point. An experiment

was performed to check the validity of the assumption. It was not readily possible to install a permanent thermocouple in the column in the vicinity of the overhead draw-off line, consequently, the following scheme was used. The spiral and the melting section heater were turned off and a thermocouple was pushed into position through the overhead line. The temperature was measured in this manner several times. The overhead product temperature was 7.5°C (2.0°C above its melting point) for a run where the crystal rate was 5.7 gm/min, and the overhead product rate 1.01 gm/min. Therefore the sensible heat provided by the melting section heater to the product stream is negligible (0.5%) compared to latent heat required to melt the crystals.

4. Temperature Measurements

All thermocouple potentials were measured with a digital voltmeter (United Systems Corp., 40 m.v. full scale, 0.1% accuracy). The primary reference temperature was that of a vigorously stirred eight gallon bath. As recommended by Albertins[1] the temperature of the benzene at the top sample tap which was at least 0.999 pure was used as a secondary reference. This was also the case for this investigation for all runs where the temperature profiles were measured. Copper constantan thermocouples were used in all cases.

5. Sampling Technique

The overhead and bottoms products were sampled periodically throughout each run. Since these samples were obtained external to the column, its operation was not disturbed. As will be described in the next section these samples were used to verify the existence of steady state prior to taking the

composition profile samples.

Albertins developed a reliable profile sampling technique which was used in this study. After steady state was achieved the spiral was stopped and the power to all heaters was turned off. The coolant to the freezing section was left on. The air bath door was opened and a 0.5 ml sample was withdrawn from each sample tap with a separate syringe. The feed introduction assembly was removed from the septum (see Figure 11) before the free liquid at the feed position was sampled. The order of sampling was from the top of the purification section to the bottom. Typically 90-100 sec were required to withdraw the eight samples.

6. Approach to Steady State

Due to the fact that the mathematical model of the column crystallizer was restricted to steady state, it is essential to show that the column was at steady state. The overhead composition decreases with time until steady state is achieved. The column was considered to be at steady state when the overhead product composition did not change with time. Figure 12 shows typical data of this type.

This hypothesis was checked by duplicate Runs 11 and 13. In both runs the overhead product composition became constant after 7 hrs. The internal composition profile was obtained after 7 hrs in Run 11 and 9.5 hrs in Run 13. No disturbances occurred during this 2.5 hr period. As Figure 13 illustrates both experimental profiles can be represented satisfactorily by the one smoothed line.

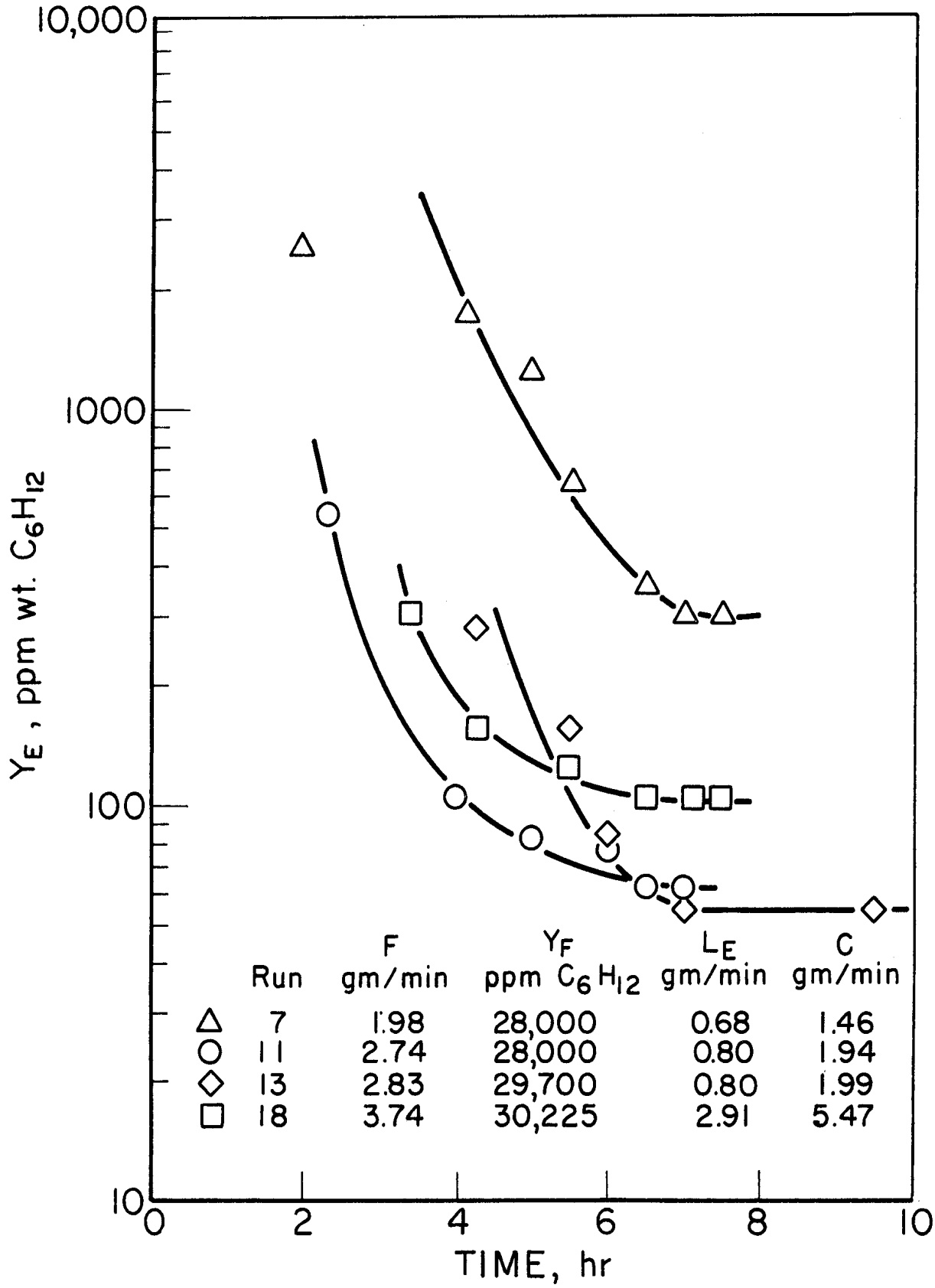

Figure 12. Approach to steady state indicated by the enriching section product composition.

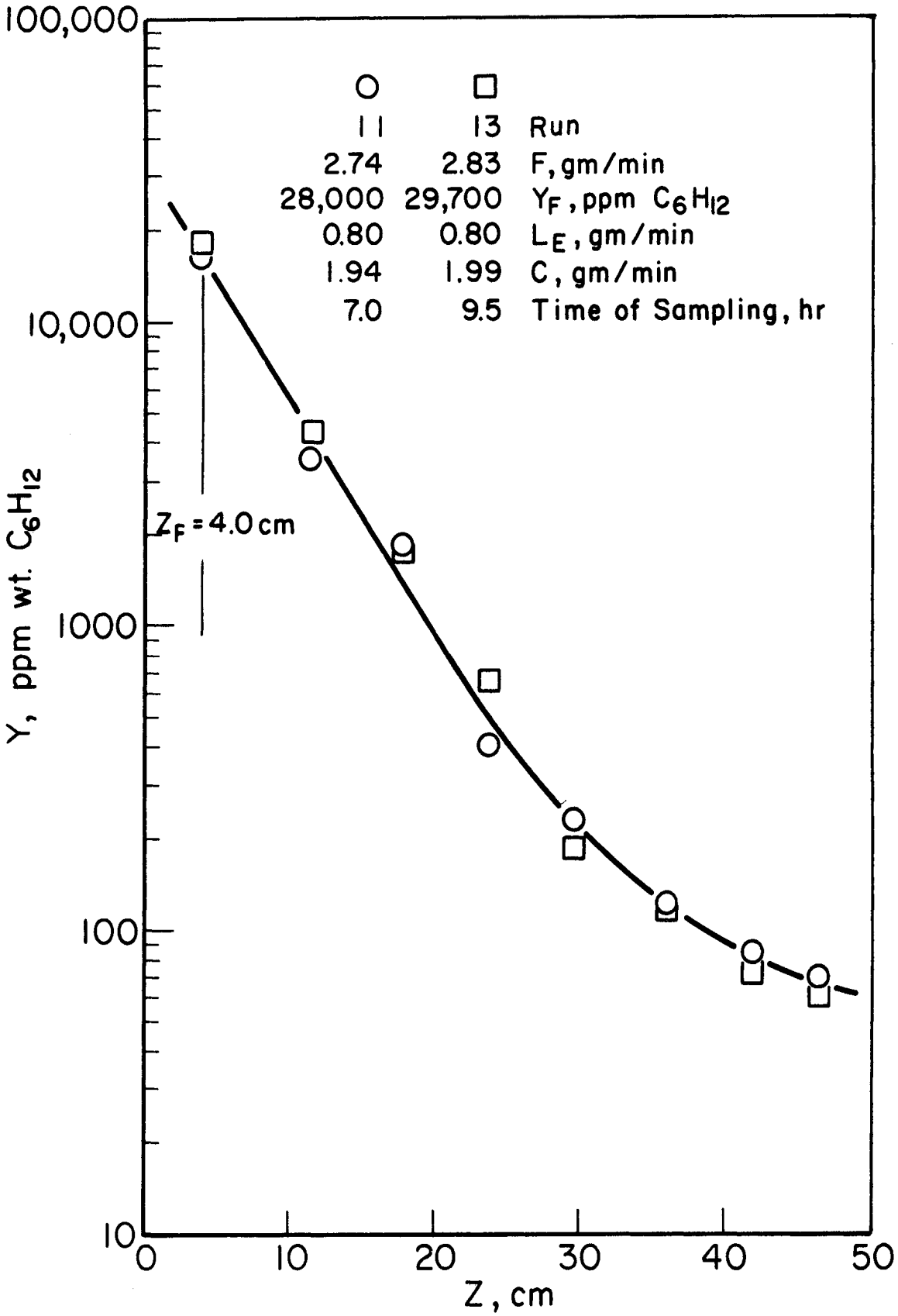

Figure 13. Approach to steady state indicated by the enriching section composition profile.

7. Analytical Method

Analyses were made using an F & M Model 5750 gas chromatograph with flame ionization detectors. The analyses were reproducible within ±3%. The analytical method for cyclohexane in benzene was confirmed independently by gas chromatographic and mass spectrographic techniques by Prof. E. A. Boettner of the School of Public Health at The University of Michigan. Further details of the analytical method are presented in Appendix A.

C. VARIABLES INVESTIGATED

The following variables associated with continuous draw-off operation were studied in this investigation:

- Terminal stream flow rates
  - —Feed rate: 2.0 - 5.6 gm/min
  - —Bottoms product: 0.48 - 3.6 gm/min
  - —Overhead product: 0.30 - 3.3 gm/min
- Internal crystal rate: 1.46 - 6.95 gm/min
- Feed composition: 1500, 10,000, 28,000 ppm wt C_6H_{12}
- Feed position: 4.0, 23.75, 29.75 cm above the freezing section

The only variable associated with the continuous flow problem that was not studied was the state of the feed entering the column. In all cases a liquid feed 1-2°C above its melting point was fed to the column.

The primary goal of this study was to determine the effect of parameters associated with continuous flow operation, consequently many possible variables were not studied. The following variables were held constant:

- Length of the purification section of the column: 50 cm.
- Rate of rotation, frequency and amplitude of oscillation of the spiral: 59 rpm, 290 min^{-1}, 1 mm, respectively.
- Configuration and length of the freezing section.
- Coolant circulation rate to freezing section.
- Amount and configuration of insulation.
- The temperature of the air bath: 5.5°C.

The size and nature of the individual crystals in the slurry inside the purification section were not investigated. Attempts to measure the size of the crystals in the purification section were not successful. Crystals were withdrawn from one of the sample taps but sufficient melting occurred in transferring them to the cold stage of a microscope (in a chilled container) to render the observations meaningless. Photographs were taken of the crystal liquid slurry in the column by Mr. G. G. Davenport of the Office of Research Administration of The University of Michigan. The lighting conditions were such that high speed (plus-X) film had to be used. The grain in the resulting enlarged photographs was so coarse that individual crystals could not be distinguished. No further attempts were made to photograph the crystals.

D. SYSTEM TO BE INVESTIGATED

The benzene-cyclohexane system was chosen for this investigation because it affords many advantages. Chief among these is the fact that Albertins used this system; therefore it was possible to make comparisons with his results obtained at total reflux. Benzene-cyclohexane has a phase diagram of the simple

eutectic type.[33] The system is also amenable to straightforward analyses by gas chromatographic techniques. Lastly, as mentioned earlier, there is evidence that commercial incentives to purify benzene by column crystallization may exist.

The starting material for preparing all feed materials was Phillips pure grade benzene. This material contained several impurities. An analysis is presented in Table I. The details of the identification and determination of the composition of the various impurities are discussed in Appendix A. Phillips 99.5 wt% cyclohexane was added to the benzene to obtain the 10,000 and 28,000 ppm wt feed stocks. In all runs the cyclohexane content of the feed was determined by the gas chromatograph.

TABLE I

IMPURITIES IN PHILLIPS PURE GRADE BENZENE

Component	ppm wt
Cyclohexane	1500
Methylcyclopentane	1081
Toluene	475
Hexane	267
2-Methylpentane	215
3-Methylpentane	218
Cyclopentane	151
Unidentified materials	139
Total impurity	4046

E. EXPERIMENTAL RESULTS

The experimental data are tabulated in Appendix C. The operating conditions, terminal compositions and composition profiles are shown for each run. The overhead product-crystal rate ratio was varied from 0.1 to 1.69. Crystal rates ranging from 1.4 to 6.95 gm/min were employed. The column was inoperable due to plugging at crystal rates higher than 6.95 gm/min.

F. REPRODUCIBILITY OF THE DATA

The reproducibility of the composition profile data is demonstrated by Figures 13 and 20. The profiles for duplicate Runs 11 and 13 given in Figure 13 can be represented by one smoothed line. A similar pair of runs (14 and 15) are shown in Figure 20 of Chapter V. An error analysis of the various experimental parameters is presented in Chapter V.

CHAPTER V

INTERPRETATION OF RESULTS

Both the theory of column crystallization and the experimental investigation have been discussed in previous chapters. Two forms of the mathematical model based on the same mechanisms were developed in Chapter III. One form was obtained by simplification of the second order model, and the other form was obtained by employing the transport equation approach. The details of the experimental investigation were presented in Chapter IV and tables of data for each experimental run appear in Appendix C.

The purposes of this chapter are threefold. First, the experimental results are used to test the model. Second, the limits of operation of the center-fed crystallizer are discussed. Third, an error analysis of the experimental parameters is presented.

A. EVALUATION OF THE MODEL

The mathematical model is subjected to eight tests in this section. The first seven tests treat the data that were obtained with the enriching section operating countercurrently. The eighth test considers the enriching section product-crystal rate ratio, R_E, and includes a discussion of the cocurrent mode of operation.

It was shown in Chapter III that the two forms of the model that were obtained differ only in the expressions used for the mass transfer factors (ψ and ψ', see Eqs. (53) and (54)). The first five tests presented below are concerned

with the parameters other than the mass transfer factors. Hence these tests do not distinguish between the two forms of the model, but rather illustrate other quantitative aspects of the theory. The discussion of the mass transfer factors, the sixth test, treats the two forms of the model. The seventh test considers the application of the correlations obtained from earlier tests to predictive column calculations. Finally, the eight test discusses the effects of the parameter, R_E.

1. Enriching Section Composition Profile Shape

The first test compares the enriching section profile shapes that were predicted by the theory with the experimental profiles. It was shown in Chapter III that the enriching section composition profiles could have three characteristic shapes. As shown in Figure 8a, Eq. (35) which describes the enriching section profile predicts that plots of the natural log of the free liquid composition (Y) versus the position in the column (z) can give profiles that are concave upward or downward or a straight line. The shape determining group, Y_P, is the particular solution of the differential equation which describes the enriching section profile (Eq. (6)). The enriching section profile shape depends on the sign and magnitude of Y_P (see discussion in Chapter III) which is governed by the relative magnitudes of $C\epsilon$ and $L_E Y_E$ as shown in Eq. (7).

The results from three experimental runs which were designed to test this prediction are presented in Figure 14. Comparison of these profiles with Figure 8a demonstrates that the theoretical development is qualitatively consistent with the shapes of the experimentally determined profiles.

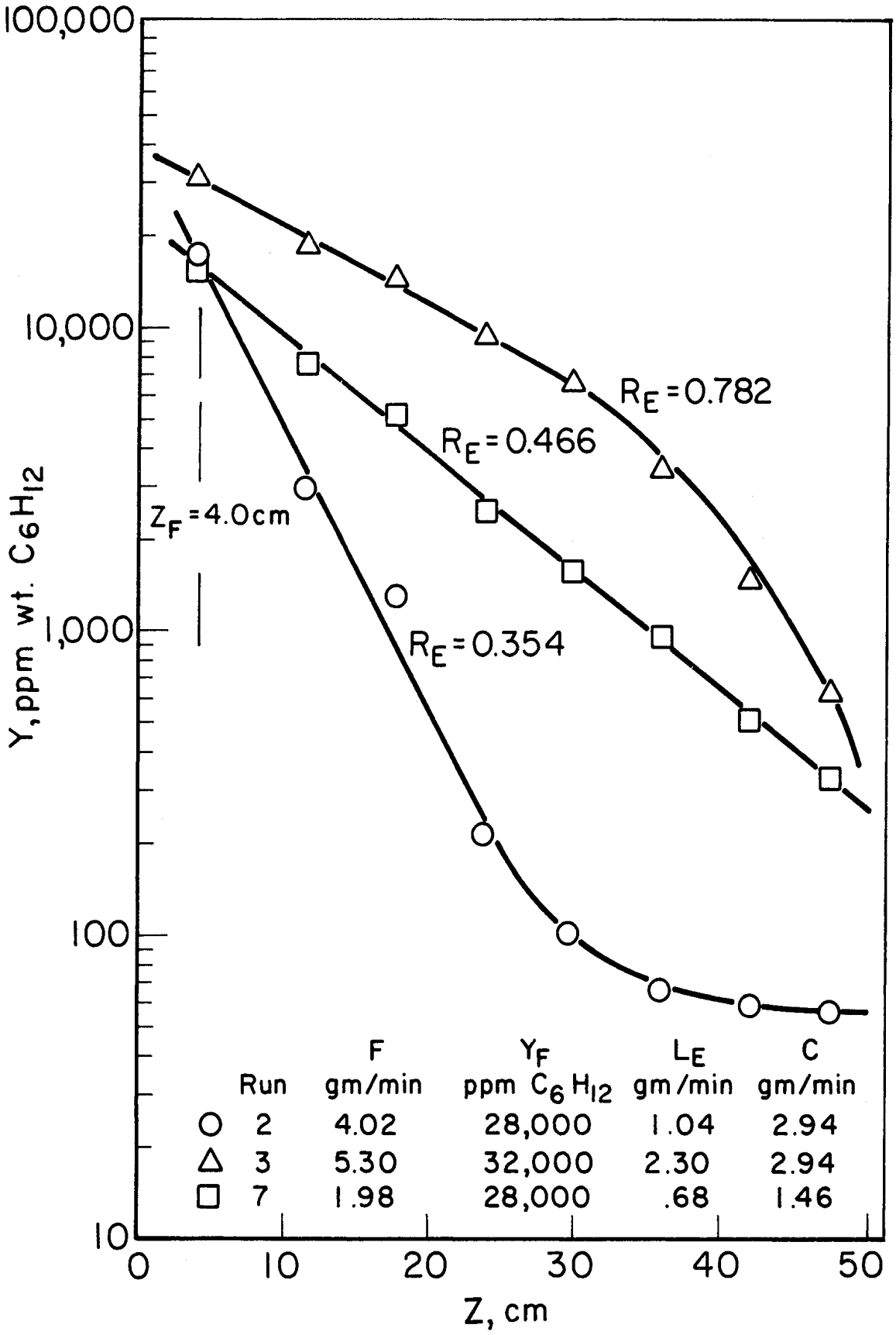

Figure 14. Experimental confirmation of the three enriching section composition profile shapes.

Equation (35) also predicts that a semi-logarithmic plot of $Y - Y_p$ vs z should be linear. The modified composition profiles for Runs 2, 3, and 7 are presented in Figure 15. The profiles are linear for all three cases as predicted by the theory. The values of Y_p were chosen such that the modified profiles were linear. In Run 7 the raw data Y vs z (Figure 14) was linear indicating that $Y_p = 0$.

The values of Y_p were chosen by assuming values and inspecting the resulting modified profile for linearity. This procedure was checked for Run 5 by performing a linear regression analysis for various assumed values of Y_p on the $\ln(Y-Y_p)$ vs z data. The composition profile for Run 5 is shown in Figure 21 and is of the convave downward type. The value of Y_p (-82 ppm) which corresponded to the minimum sum squared deviation was chosen (see Figure 16). The value obtained by inspection as described above was -80 ppm. Therefore the more tedious regression analysis method was not used for the other runs. The values of Y_p for each run are given in Table X in Appendix C.

2. Stripping Section Profile Shape

This test considers the stripping section profile shape. It was also shown in Chapter III that the stripping section composition profile has a characteristic shape. The expression for the stripping section profile (Eq. (38)) predicted that the composition profile would be flat as illustrated by Figure 8b. The results of experiments designed to test this prediction are presented in Figures 17 and 18. These data confirm the existence of the flat or inactive region in the stripping section profile. Danyi[9] participated in

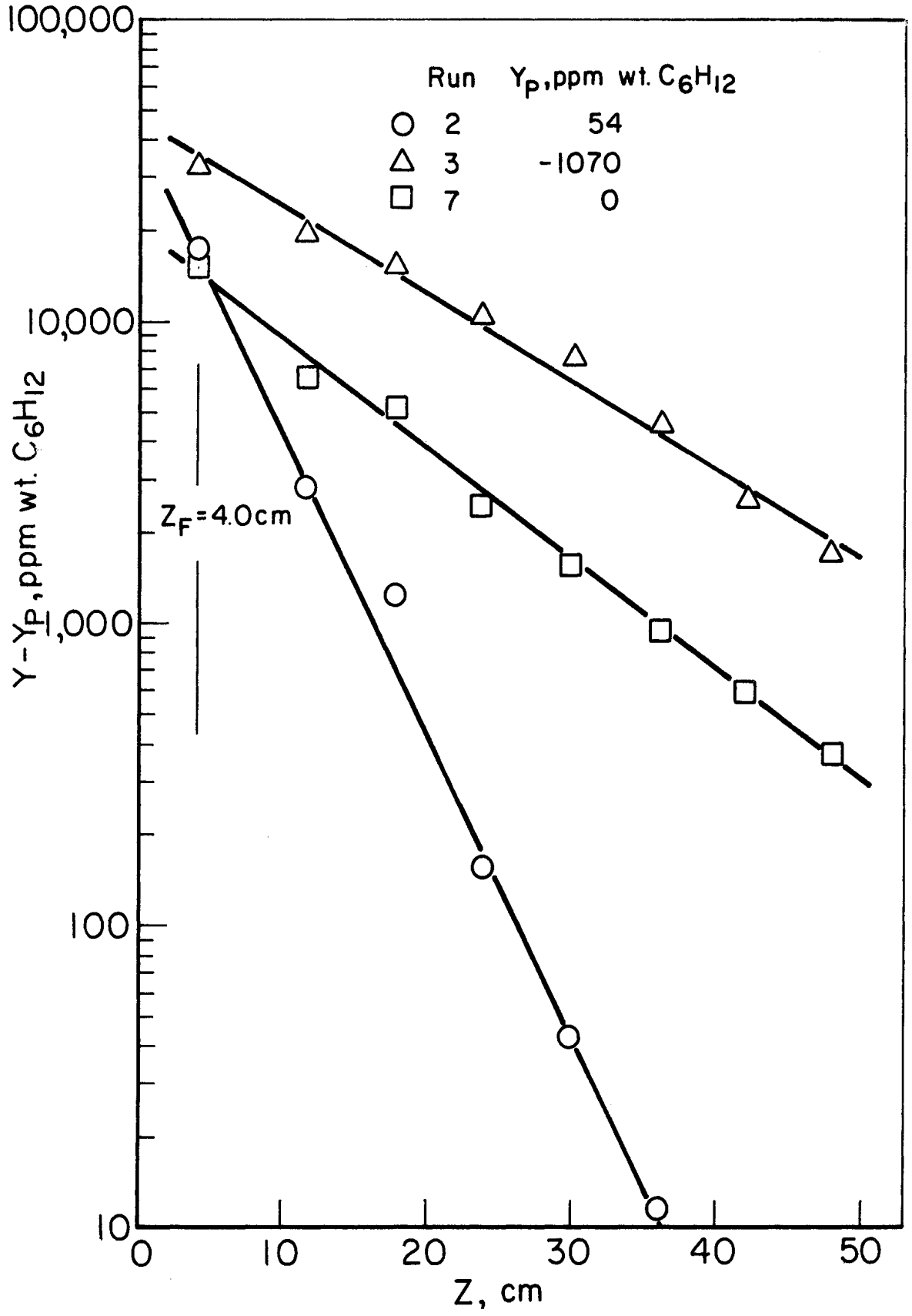

Figure 15. Modified enriching section composition profiles.

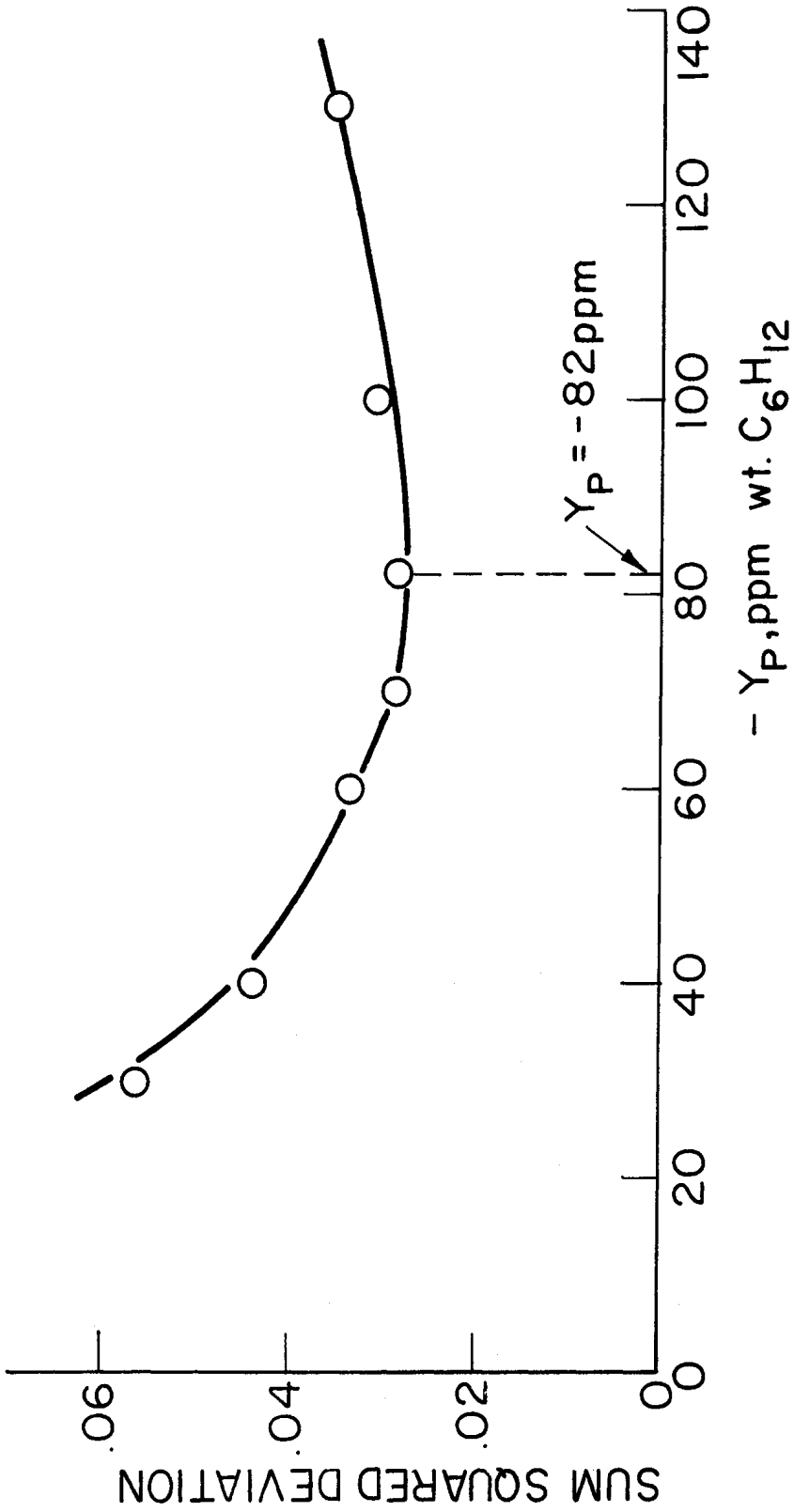

Figure 16. Determination of Y_P for Run 5.

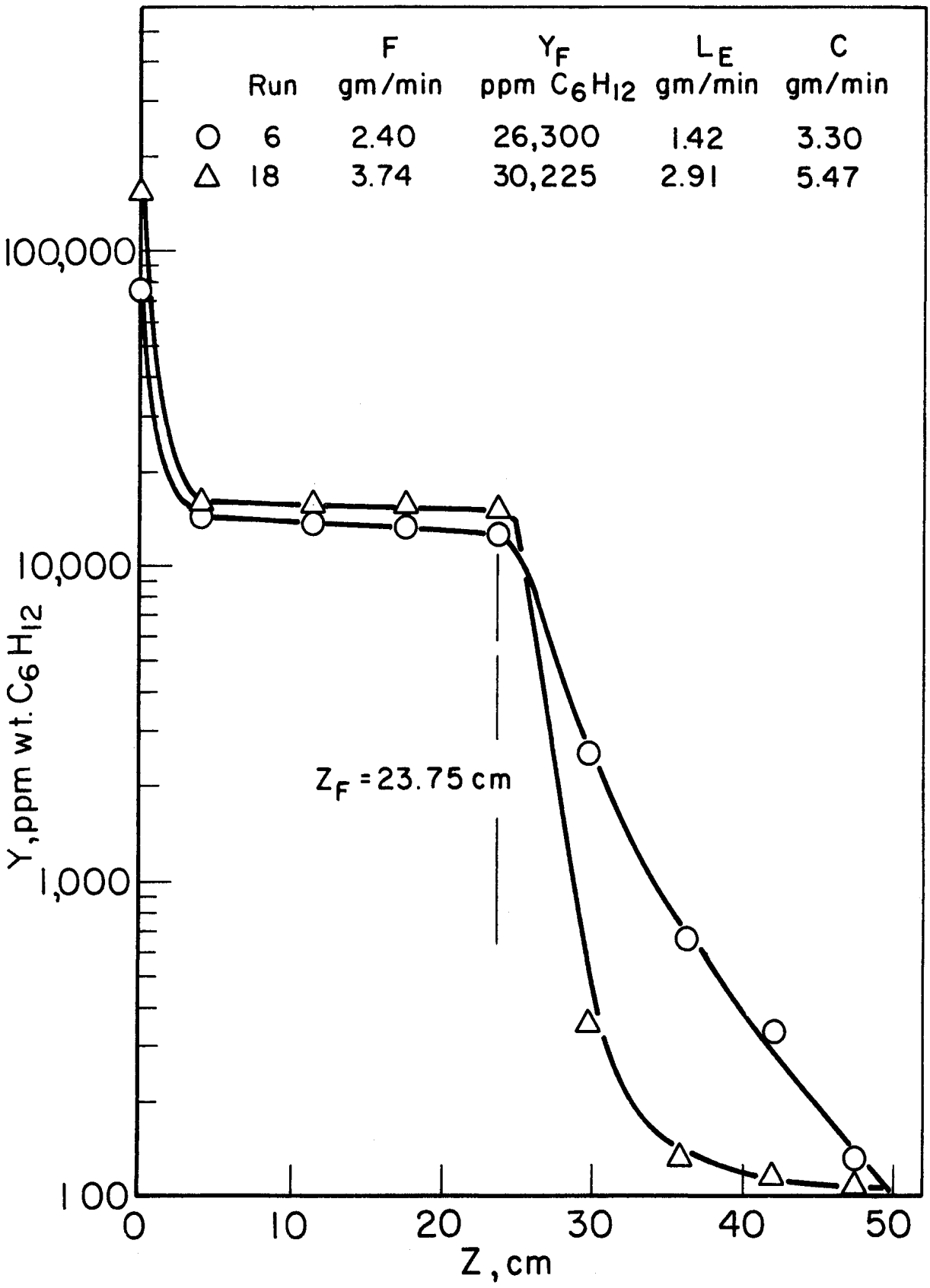

Figure 17. Enriching and stripping section composition profiles.

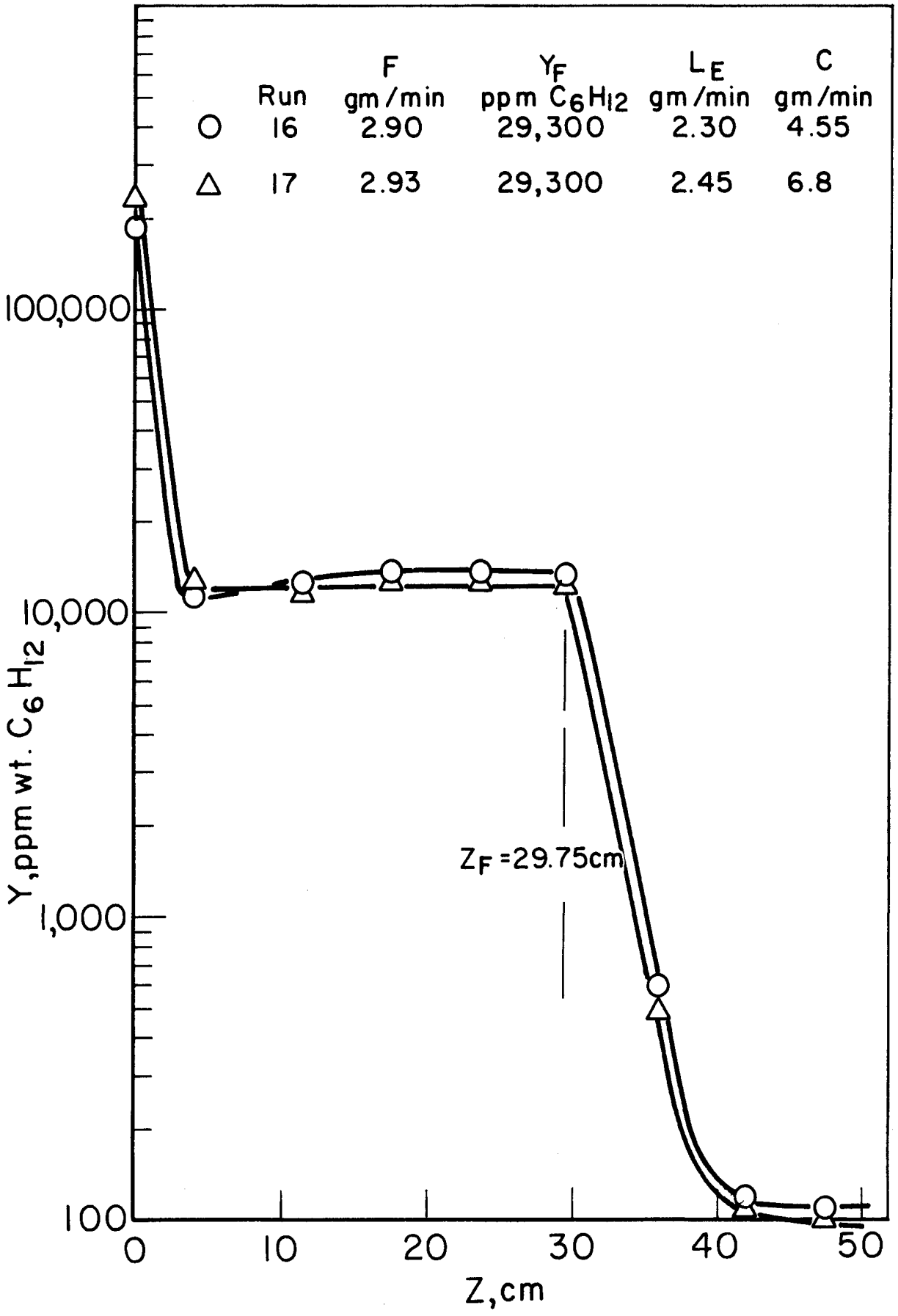

Figure 18. Enriching and stripping section composition profiles.

this experimental study.

The shape determining group for the stripping section, $\overline{Y}_P$, is the particular solution of the differential equation which describes the stripping section composition profile (Eq. (17)). The values of $\overline{Y}_P$ obtained from the stripping section composition profiles ($\overline{Y}_P$ is the composition where the profile becomes flat) are compared in Table II with those calculated from Eq. (69) which relates Y_P to F, C, L_S and Y_S.

TABLE II

COMPARISON OF CALCULATED AND EXPERIMENTAL VALUES OF THE SHAPE DETERMINING GROUP FOR THE STRIPPING SECTION

Run	$\overline{Y}_P$, from Eq. (69)	$\overline{Y}_P$, from Figs. 17 & 18	% error
6	14,750	13,200	11.7
16	16,500	13,300	24.1
17	11,800	12,200	3.3
18	17,940	15,000	19.6

In view of the experimental confirmation of the flat region in the stripping section profile, and the reasonable agreement of the experimental and calculated values of $\overline{Y}_P$, it is concluded that the model satisfactorily explains the shape of the stripping section profile.

Difficulty was encountered in selecting operating conditions that would produce a non-flat profile in the stripping section. The relation for $\overline{Y}_P$

(Eq. (68)) can be rearranged to yield the following equation which suggests operating conditions that might give a stripping section profile with an appreciable negative slope:

$$\overline{Y}_P/Y_S = L_S/(C+L_S) \qquad (71)$$

The slope of the profile should increase as the value of $\overline{Y}_P/Y_S$ decreases. Therefore in Runs 16, 17, 18 the column was operated with large crystal rates and small bottoms product rates. Figures 17 and 18 demonstrate, however, that the stripping section profiles for these runs remained flat. This can be explained by noting that the stripping section mass transfer factor probably decreases when the crystal rate is increased (this can be seen by examining Eq. (47b) for the case when the diffusional term is dominant). A decrease in the stripping section mass transfer factor corresponds to a more rapid exponential decay of the composition Y to Y_P thus cancelling the effect of the decreased value of $\overline{Y}_P/Y_S$.

The slight positive slope of the stripping section profile for Run 16 (Figure 18) is attributed to slow sampling of the composition profile for this run. The longer sampling time very likely allowed some of the crystals to melt and dilute the liquid that was withdrawn from the lower sample taps (the upper sample taps were sampled first).

3. Impurity Associated with the Crystal Phase

The mathematical model includes the effect of impurity transport by the crystal phase. It was argued that impurities could be entrapped in the crystal or on their irregular surface. The impurity associated with the crystal

phase, ϵ, is assumed to be independent of position in the column. This assumption is tested in this section with ϵ values calculated from the experimental data.

The impurity composition in the crystal phase, ϵ, can be calculated from the values of Y_P obtained from the composition profile data. Rearrangement of the expression which relates Y_P to ϵ, C, and L_E (Eq. (7)) yields:

$$\epsilon = \frac{Y_P(C-L_E)+L_EY_E}{C} \qquad (72)$$

The values of ϵ calculated from Eq. (72) are tabulated in Table X of Appendix C. It is emphasized that these values were calculated from experimental values of Y_P, C, and L_E. In no case was the crystal composition, ϵ, measured directly.

Gates[15] suggested that ϵ should increase when the mother liquor composition in the freezing section increases. Other parameters such as the agitation level are not considered because the spiral oscillation and rotation rates were held constant in this study. The mother liquor composition in the freezing section is assumed to be equal to the bottoms composition, Y_S. This is equivalent to assuming that the freezing section is perfectly mixed. Figure 19 illustrates that ϵ does increase with Y_S. The $\epsilon(Y_S)$ dependence is linear. A least squares fit of the values of ϵ and Y_S gives the following relation:

$$\epsilon = 0.00142\ Y_S \qquad (73)$$

Figure 19 reveals considerable scatter of the values of ϵ calculated from Eq. (72) from the line predicted by Eq. (73). It is noted, however, that both ϵ and Y_S varied fifty-fold. Therefore the dependence described by Eq. (73) is considered to be significant. The coefficient of determination, which is interpreted

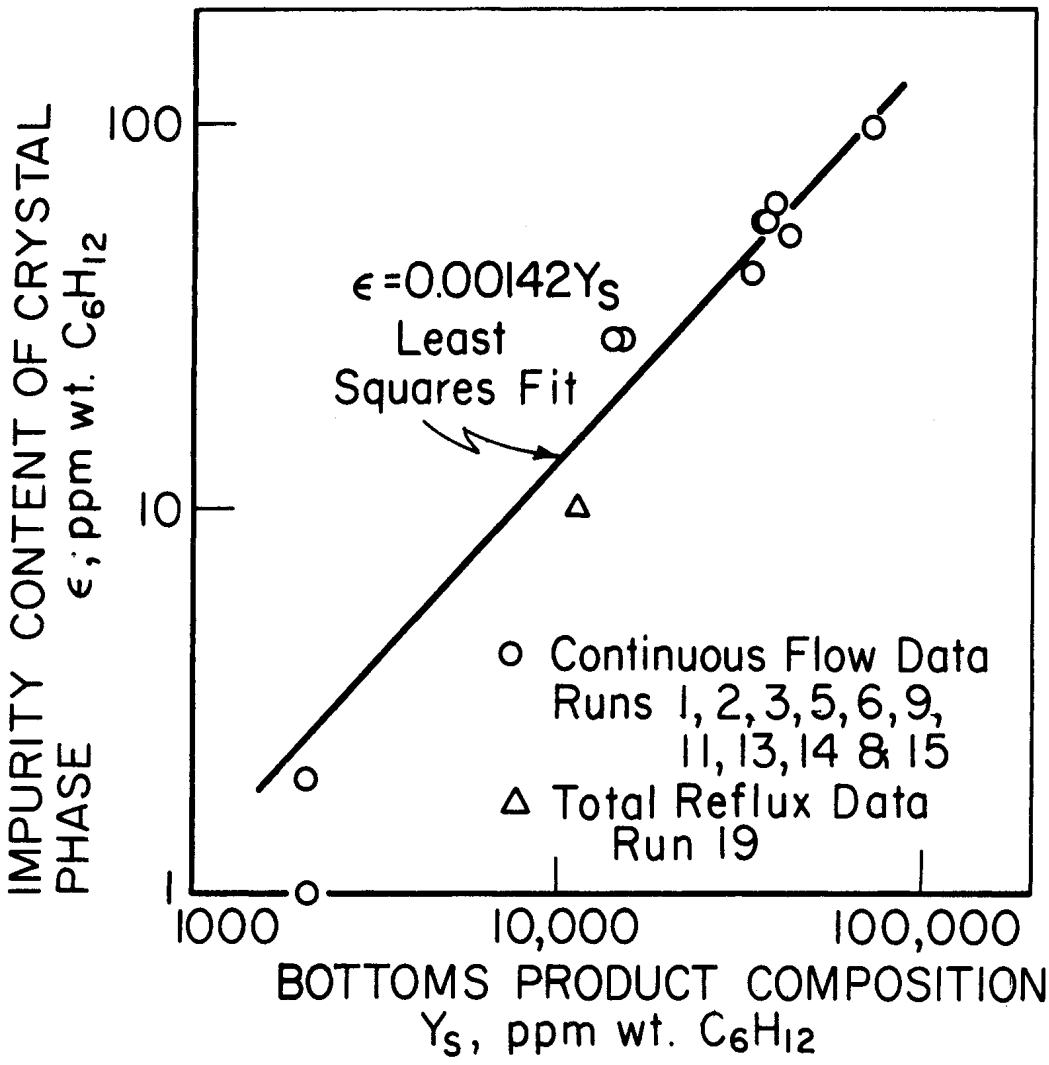

Figure 19. Correlation of crystal phase impurity composition with the bottoms product composition.

as the fraction of the systematic variation of ϵ that is explained by Eq. (73), is 0.986. Correlating expressions which assumed that ϵ was proportional to $Y_S^{0.9}$, $Y_S^{1.1}$, etc. did not give significantly better correlations. The data of Run 7 was excluded from the final correlation because the value of ϵ contradicted the trend that ϵ increases when Y_S increases (see Table X). The data from Runs 16, 17, 18 are excluded from the correlation due to the minimal number of point compositions in the enriching section profile which could be used to determine Y_P (or equivalently ϵ).

The linear $\epsilon(Y_S)$ dependence has been found by other investigators. Moulton and Hendrickson[23] found a linear dependence of the crystal phase composition on the mother liquor composition for the crystallization of ice from sea water. A linear dependence is consistent with the occurrence of volumetric liquid inclusions, but it does not rule out the possibility of slight solid solubility in the ppm range.

The validity of the assumption that ϵ is independent of position in the purification section is implied by the correlation of ϵ with Y_S. The expression used to calculate ϵ from Y_P (Eq. (72)) is based on this assumption. The three enriching section composition profile shapes presented in Figure 14 are further indications of the validity of the constant ϵ hypothesis.

The fact that ϵ decreases with Y_S leads to an interesting consequence. For a given feed or charge composition, ϵ would be largest when the column is operated at total reflux, because Y_S is largest due to the concentration of impurities in the freezing section. When the column is operated continuously the impurity level in the freezing section is reduced due to the removal of

impurities in the bottoms stream. Thus it is possible to produce purer materials with continuous draw-off of product (when R_E is sufficiently small) than can be produced with total reflux operation. This effect is illustrated by the following experimental results: at a feed composition of 28,000 ppm wt C_6H_{12}, $R_E = 0.354$, and $z_F = 4.0$ cm (Run 2); the overhead product composition, Y_E, was 57 ppm wt C_6H_{12}; the ultimate purity that could be achieved with total reflux operation is approximately 100 ppm wt C_6H_{12} (see Appendix E).

The $\epsilon(Y_S)$ dependence also implies a restriction on the ultimate purity that can be achieved with a continuous flow column crystallizer for a particular feed composition. The simplified form of the terminal stream balance, Eq. (67) is employed. The minimum value of Y_S occurs when the stripping section is flushed with feed material or when the enriching section is operated at conditions approaching total reflux, i.e., $\frac{F}{L_S} \cong 1$. Equation (67) therefore suggests that $(Y_S)_{min} = Y_F$. Therefore the equation below gives the minimum level of impurity associated with the crystal phase that can be attained.

$$\epsilon_{min} = 0.00142\ Y_F \qquad (74)$$

The ultimate purity that can be achieved in a column crystallizer, ϵ_{min}, would occur when the washing of the adhering liquid is complete.

4. Effect of Feed Composition

Three feed compositions were used in this investigation: 1500, 10,000, and 28,000 ppm C_6H_{12}. The experiments show that the feed composition has the following two effects:

- Increasing Y_F increases Y_S and in turn ϵ as suggested by Eqs. (69) and (72).
- The impurity composition in other streams are related to Y_F by material balance considerations.

The separation factor ψ_E is independent of feed composition. This condition was implied in Chapter III by the assumption that the transport properties are constant. Figure 20 shows that for comparable operating conditions, with the exception of the feed composition, the composition profiles are parallel. This is equivalent to ψ_E being the same for both feed compositions.

Composition profiles for the lowest feed composition that was used (1500 ppm C_6H_{12}) are given in Figure 21. The feed stock for these runs was Phillips pure grade benzene. It can be seen that very pure materials were obtained. The production of ultrapure benzene is discussed in more detail in Chapter VI.

5. Column Calculations with Experimentally Determined Parameters

A further test of the model is accomplished by comparing experimental profiles with those calculated using experimental values of the mass transfer factor, ψ_E, and crystal phase composition, ϵ.

The iterative calculation procedure described in Chapter III has been used to calculate the terminal compositions and composition profiles for the experimental runs. The appropriate operating parameters, $\mathcal{L}$, z_F, F, Y_F, L_S and C were specified for each run. In addition experimental values of the enriching section mass transfer factor, ψ_E, and the crystal composition, ϵ, were used in the calculations. Experimental values of the stripping section mass trans-

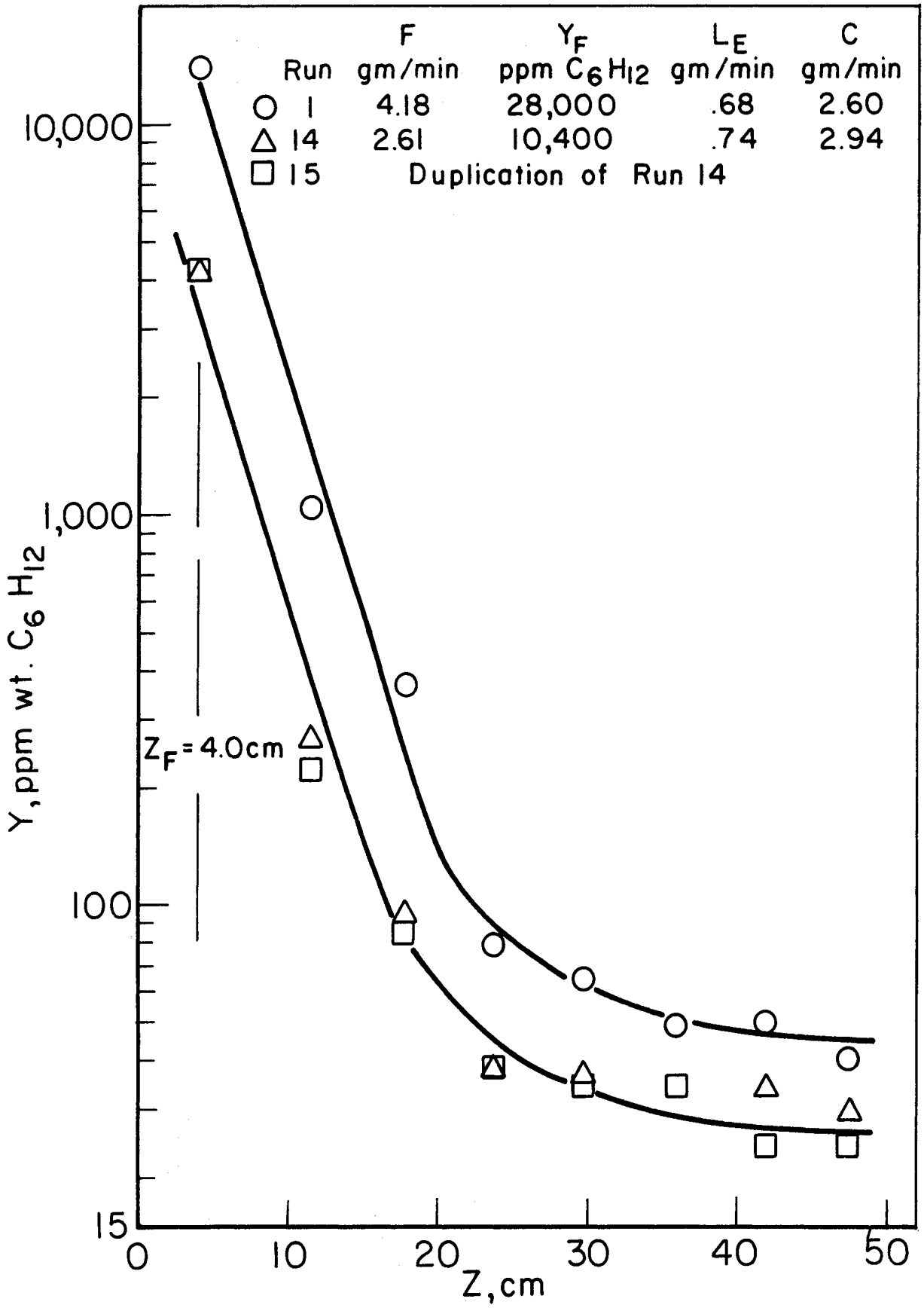

Figure 20. Influence of feed composition on the impurity level in the enriching section.

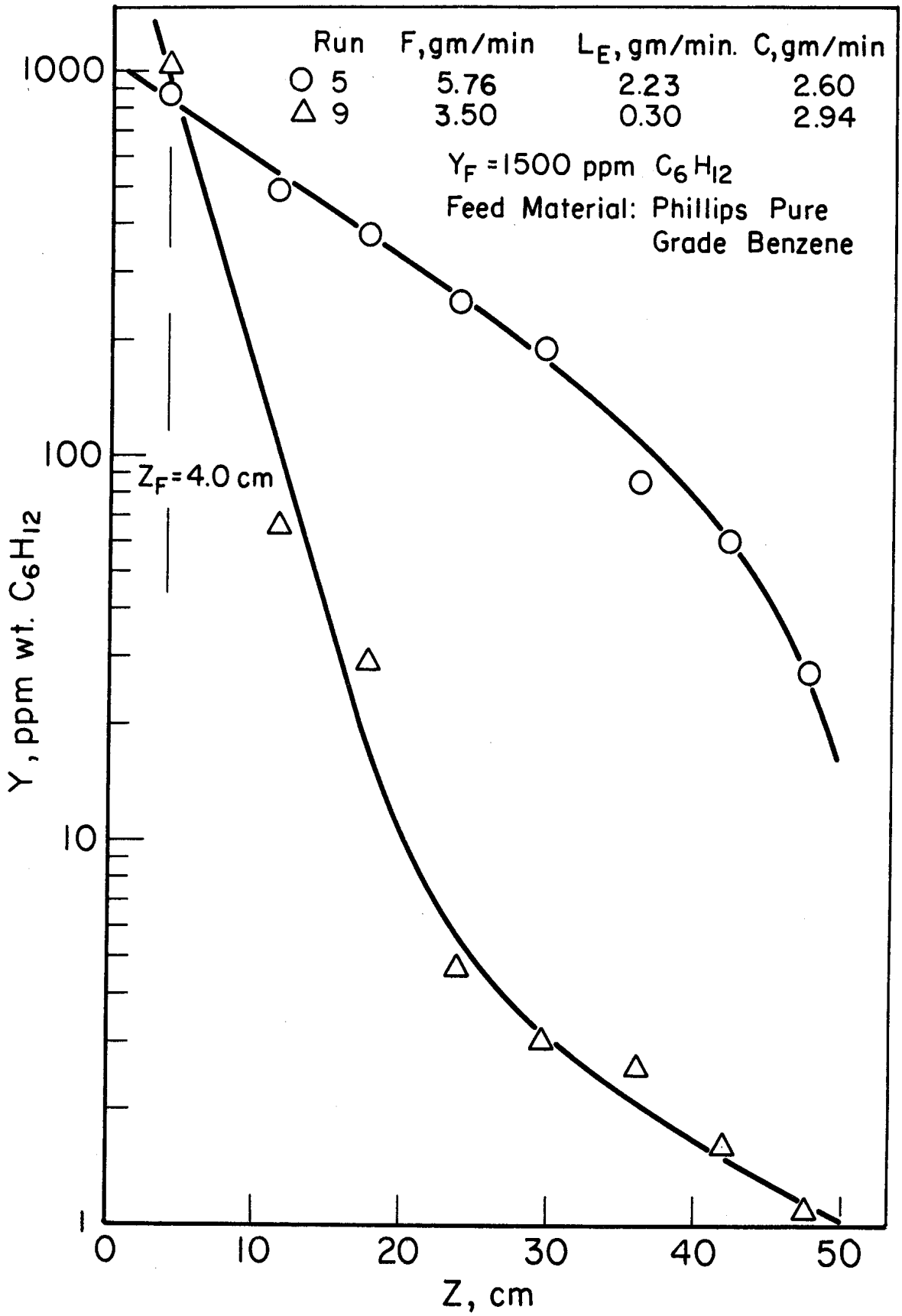

Figure 21. Enriching section composition profiles for the purification of Phillips pure grade benzene.

fer factors could not be obtained because the composition profiles in this section were essentially flat, i.e., the slope could not be measured. Therefore the values of ψ_S were calculated from ψ_E. It is assumed that the results of the transport equation approach are applicable in order to relate ψ_S to ψ_E, i.e., $\psi_E = \psi_E'$ and $\psi_S = \psi_S'$. The following relation that was developed in Chapter III is employed:

$$\psi_S' = \psi_E' \frac{(C-L_E)}{(C+L_S)} \tag{70}$$

The calculations were facilitated by the computer program described in Appendix D.

Figure 22 compares the calculated profiles with two sets of experimental data. It is concluded that the mathematical model satisfactorily explains the form of the experimental data. The calculations also reflect the internal consistency of the flow rate, profile, and terminal composition data. It is emphasized that these calculations are not completely predictive, because experimental values were used for ψ_E and ϵ which are strictly dependent variables once $\mathcal{L}$, z_F, F, Y_F, L_S, and C are specified.

Table III compares the experimental values of the terminal compositions Y_E and Y_S with the values calculated by the above procedure. The reasonable agreement again illustrates the consistency of the data. Further, it experimentally confirms the validity of the end conditions that were specified in Chapter III, i.e.,

$$z = \mathcal{L}, \quad Y = Y_E \tag{62}$$

$$z = 0, \quad Y = Y_S \tag{65}$$

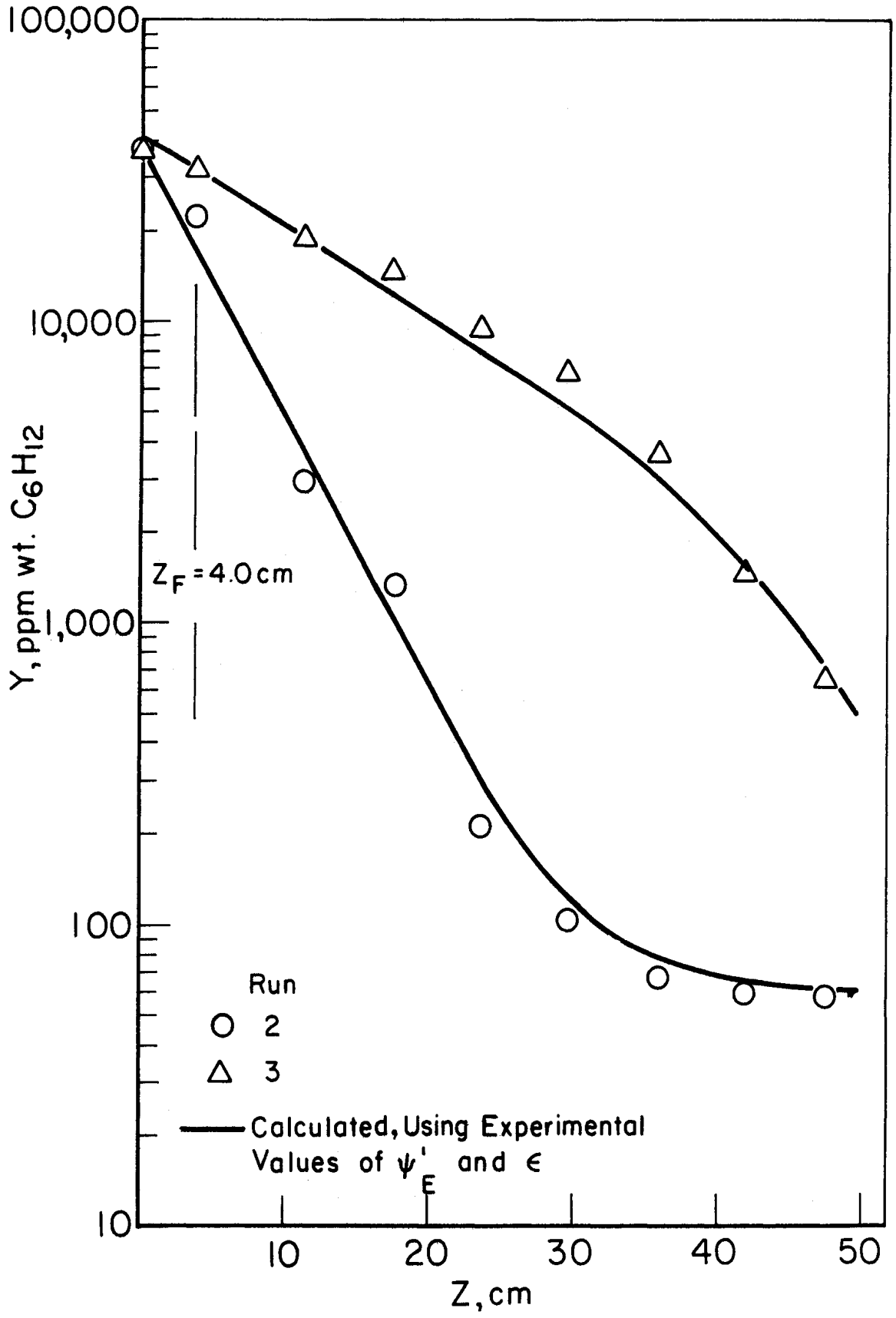

Figure 22. Comparison of experimental and calculated composition profiles.

TABLE III

COMPARISON OF EXPERIMENTAL AND CALCULATED VALUES OF THE TERMINAL COMPOSITIONS

Run	Y_E, Experimental	Y_E, Calculated	Y_S, Experimental	Y_S, Calculated
	ppm wt C_6H_{12}			
2	60	57	37,000	37,800
3	370	440	37,000	56,200
5	16	21	2,090	2,460
6	101	111	72,000	64,300
7	300	403	43,400	41,800
9	1	1	2,140	1,640
11	62	69	39,600	39,000
13	55	58	41,200	41,400
14	29	28	14,200	14,500
15	29	28	14,300	14,000
16	65	80	186,000	165,000
17	84	84	225,000	180,000
18	107	105	153,000	136,000

These conditions were used in the column calculations discussed above.

6. Mass Transfer Factors

The only difference between the two forms of the model developed in Chapter III is the expressions that represent the mass transfer factors (see Eqs. (41b), (42b), (46b), and (47b)). The purpose of this section is to correlate the experimental mass transfer factors with an appropriate mathematical expression developed earlier.

It was shown earlier that the mass transfer factors which result from the transport equation approach can be related to the more complicated expressions which result from the original form of the model that includes the axial diffusion term in the free liquid material balance. The mass transfer factors derived by the two approaches differ by a factor $\theta(X)$ as shown in Eqs. (53) and (54). The experimental mass transfer factors will be correlated by assuming that $\theta(X) \cong 1$. Using this approximation, the mass transfer factors developed by the two methods become identical, i.e., $\psi_E = \psi_E'$ and $\psi_S = \psi_S'$. Thus the simpler expressions, ψ', can be used. If a satisfactory correlation of the data is obtained by this method, no attempt will be made to fit the data with the more complicated expressions for ψ (Eqs. (41b) and (42b)).

Experimental values of ψ_E' and ψ_O' can be obtained by measuring the slope of the modified composition profiles, e.g., the slope of $\ln(Y-Y_P)$ vs z is the negative reciprocal of ψ_E' (see Eq. (39)). Total reflux mass transfer factors, ψ_O', are available from Albertins' data.[1] Only experimental values of ψ_E' are available for the continuous draw-off case. The stripping section mass trans-

fer factor ψ_S' could not be determined due to the flat region that occurred in the experimental profiles. Hence only experimental values of ψ_E' and ψ_O' are correlated.

It is important to reemphasize the assumption that the parameters $D\eta$, Ka, etc., are assumed to be constant for fixed spiral agitation conditions. This assumption implies that the mass transfer factor data for different feed compositions, feed positions, terminal stream flow rates and internal crystal rates can be correlated by single values of $D\eta$, Ka, etc., for either total reflux or continuous flow operation. Consequently the expression that relates ψ_E' to C and L_E (Eq. (46b)) can be transformed to Eq. (75a) which suggests that a multiple linear regression analysis of the experimental data will yield the correlation constants:

$$\psi_E' = b_1X_1 + b_2X_2 + b_3X_3 \tag{75a}$$

where,

$$b_1 = D\rho A\eta \tag{75b}$$

$$b_2 = \alpha(\alpha+1)/KaA\rho \tag{75c}$$

$$b_3 = -\alpha/KaA\rho \tag{75d}$$

$$X_1 = 1/(C-L_E) \tag{75e}$$

$$X_2 = C^2/(C-L_E) \tag{75f}$$

$$X_3 = CL_E/(C-L_E) \tag{75g}$$

Note that the expression for ψ_O' for total reflux operation is a special case of the above equations, that is, when $L_E = 0$ the total reflux separation factor becomes:

$$\psi_0' = b_1 X_1 + b_2 X_2 \tag{76}$$

It is emphasized that the constants b_1, b_2, and b_3 have physical significance. They are determined by the physical parameters of the system (see Eqs. (75b), (75c) and (75d)).

Albertins'[1] total reflux data ψ_0' vs C are tabulated in Appendix E. These data were obtained with the same spiral rotation speed, oscillation frequency and amplitude as employed in the present study. A regression analysis of his data employing Eq. (76) yields the following expression:

$$\psi_0' = 6.862/C + 0.9096\ C \tag{77}$$

where C and ψ_0' are expressed in gm/min and cm, respectively. Gates[13] obtained the same constants by correlating Albertins' data with the following expression:

$$\psi_0' C = b_1 + b_2\ C^2 \tag{78}$$

Utilizing Eqs. (75b) and (75c) the following relations are evident:

$$D\rho A\eta = 6.862 \text{ gm-cm/min} \tag{79}$$

$$\alpha(\alpha+1)/KaA\rho = 0.9096 \text{ cm-min/gm} \tag{80}$$

Equation (77) predicts the experimental values with a maximum deviation of 5.5%. The accuracy of the correlation is considered to be excellent and implies that using ψ_0' rather than ψ_0 (or equivalently taking $\theta(X_0)$ to be one) is consistent with the data.

A regression analysis of the ψ_E' data obtained in this investigation resulted in the following expression:

$$\psi'_E = \frac{6.538}{(C-L_E)} + \frac{0.4102\ C^2}{(C-L_E)} - \frac{0.4185\ CL_E}{(C-L_E)} \qquad (81)$$

The experimental values of ψ'_E are given in Table X. The data of Runs 9 and 10a were excluded from the correlation due to uncertainties in the experimental values of the crystal and overhead product rates C and L_E. Runs 16, 17, and 18 were deleted due to the minimal number of data points that were obtained in the enriching section profile. In these runs a larger number of the sample taps were below the feed point.

The calculated values of the mass transfer factors are in reasonable agreement with the experimental values. Figure 23 compares the experimental

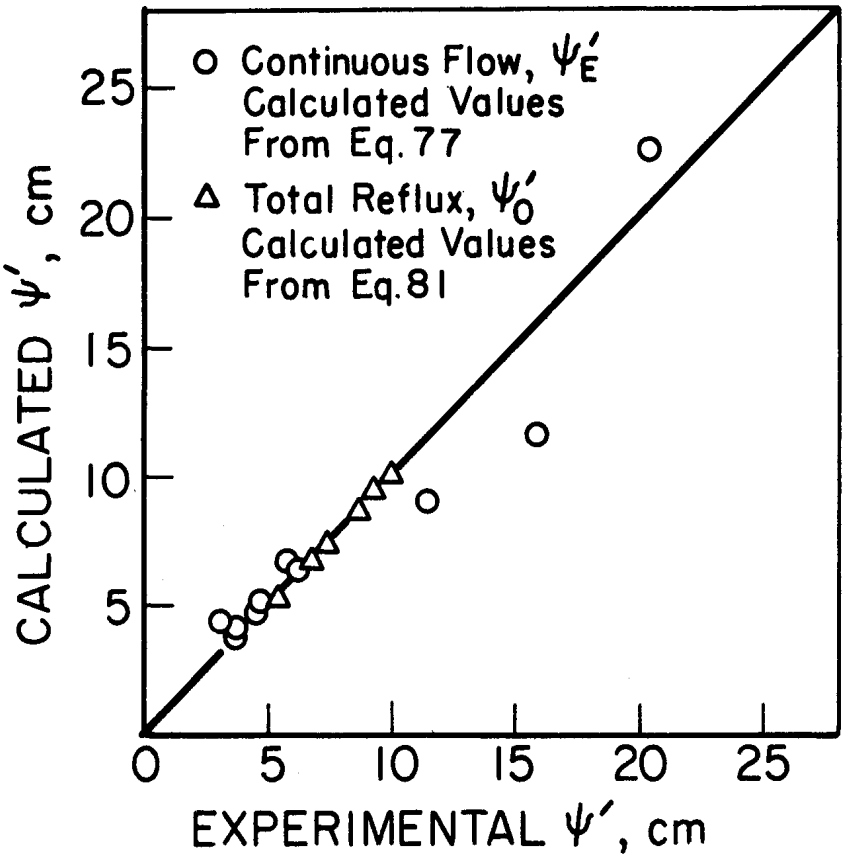

Figure 23. Comparison of calculated and experimental values of the mass transfer factor.

and calculated values. As mentioned earlier the maximum error between the

predicted and experimental values for the total reflux case was 5.5%. The errors were larger for the continuous flow case. The average error between the predicted and experimental values of the enriching section mass transfer factors was 17%. The uncertainity in the experimental values of ψ_E' used in the correlation was 12%.

The correlation results indicate that axial diffusion is the dominant effect in determining the mass transfer factor. The relative contribution of the mass transfer terms was determined for each run by calculating the magnitude of all three terms with Eq. (81). The average contribution of the second two terms in Eq. (81) to ψ_E' was 18%. The maximum contribution of the mass transfer terms was 29% in the case of Run 1.

Table IV compares the values of the constants obtained from the contin-

TABLE IV

COMPARISON OF THE MASS TRANSFER AND DIFFUSION GROUPS OBTAINED FROM TOTAL REFLUX AND CONTINUOUS FLOW DATA

Group	Total Reflux Data of Albertins	Continuous Flow Data of this Study
$b_1 = D\rho A\eta$, $\frac{gm\text{-}cm}{min}$	6.862 ± .1134	6.538 ± 1.936
$b_2 = \alpha(\alpha+1)/KaA\rho$, $\frac{cm\text{-}min}{gm}$	0.9096± .0770	0.4102± 0.4439
$b_3 = -\alpha/KaA\rho$, $\frac{cm\text{-}min}{gm}$	----	-0.4185± 0.4192

uous draw-off and total reflux data. In both cases the diffusional term $D\rho A\eta$

is dominant and the agreement between the values obtained from the two sets of data is satisfactory. Also the mass transfer terms obtained from the continuous flow data b_2 and b_3 have the signs that are suggested by the theory (see Eqs. (75c) and (75d)). These constants, however, differ markedly. It is also noted that the standard errors of b_2 and b_3 given in Table IV for the continuous draw-off case are large. These errors coupled with the dominance of the diffusional term illustrate the insensitivity of the continuous flow data to the mass transfer terms b_2 and b_3. This insensitivity of the continuous flow data relative to the total reflux data can be explained by rearranging the expression for ψ_E' (Eq. (46b)) and comparing it with the corresponding relation for ψ_0'.

$$\psi_E' = \frac{1}{C-L_E}\left\{D\rho A\eta + \frac{\alpha}{KaA\rho}\left[(\alpha+1)C^2-CL_E\right]\right\} \tag{82}$$

$$\psi_0' = \frac{1}{C}\left[D\rho A\eta + \frac{\alpha(\alpha+1)C^2}{KaA\rho}\right] \tag{83}$$

It can now be seen that the dependence of ψ_E' on the overhead product rate, L_E, dampens the sensitivity of the continuous flow data to the mass transfer effect. Therefore it is evident that the total reflux data provides a more severe test than continuous flow data of the relative importance of the diffusional and mass transfer terms.

It must be remembered that the mass transfer factor data have been correlated using the expressions that result from the transport equation approach, that is, $\theta(X_0)$ and $\theta(X_E)$ were assumed to be one. A direct check of this hypothesis would require a calculation of X_0 and X_E from the constants obtained

from the above correlations. Comparison of the defining relation for X_E (Eq. (51), X_0 is a special case of this equation for $R_E = 0$) with the definitions of b_1, b_2, and b_3 (Eqs. (75b), (75c), and (75d)) reveals that α must be separated from the constants in order to calculate X_E or X_0, i.e., α must be known individually. The adhering liquid-crystal rate ratio, α, cannot be obtained from the total reflux data. It is grouped with the parameters $KaA\rho$ as shown in Eq. (80). In principle α can be obtained from the correlation constants obtained from the continuous flow data, i.e., combination of Eqs. (75c) and (75d) yields:

$$\alpha = -\left(\frac{b_2}{b_3} + 1\right) \tag{84}$$

Unfortunately the standard errors of b_2 and b_3 given in Table IV do not permit the application of this relation. Therefore α cannot be obtained from either the total reflux or continuous flow data. Consequently X_E or X_0 cannot be calculated or equivalently the validity of the approximation $\theta(X) = 1$ cannot be directly determined.

The justification for using the mass transfer factors obtained by the transport equation approach is the excellent correlation of the total reflux data mentioned above. The approximation, $\theta(X) = 1$, should be even more accurate for the enriching section, because $X_E < X_0$. In view of the above considerations it is concluded that the model summarized in Eqs. (46) and (47) provides a satisfactory representation of the experimental data. Henceforth in this dissertation all discussions that refer to the "model" will be in reference to the expressions that result from the transport equation approach.

7. Predictive Column Calculations

The model is subjected to its severest test in this section. The correlations developed in the earlier section of this chapter are used in conjunction with the model to perform column calculations. The results are compared with experimental data.

The composition profiles and terminal compositions are calculated by the iterative procedure presented in Chapter III by specifying only the column operating conditions: $\mathcal{L}$, z_F, F, Y_F, L_S and C. The mass transfer factors and the crystal compositions can be calculated from the correlations developed earlier. The enriching section mass transfer factor is related to the flow rates by Eq. (81).

$$\psi'_E = \frac{6.538}{(C-L_E)} + \frac{0.4102\ C^2}{(C-L_E)} - \frac{0.4185\ CL_E}{(C-L_E)} \qquad (81)$$

The stripping section mass transfer factor is calculated using the same constants in conjunction with Eq. (47b) as shown in Eq. (86).

$$\psi'_S = \frac{6.538}{(C+L_S)} + \frac{0.4102\ C^2}{(C+L_S)} + \frac{0.4185\ CL_S}{(C+L_S)} \qquad (85)$$

Finally, the impurity composition of the crystals ϵ is given by Eq. (73).

$$\epsilon = 0.00142\ Y_S \qquad (72)$$

It is emphasized that these relations are peculiar to the benzene-cyclohexane systems and the spiral agitation conditions employed in this study.

Figure 24 compares experimental data with composition profiles calculated

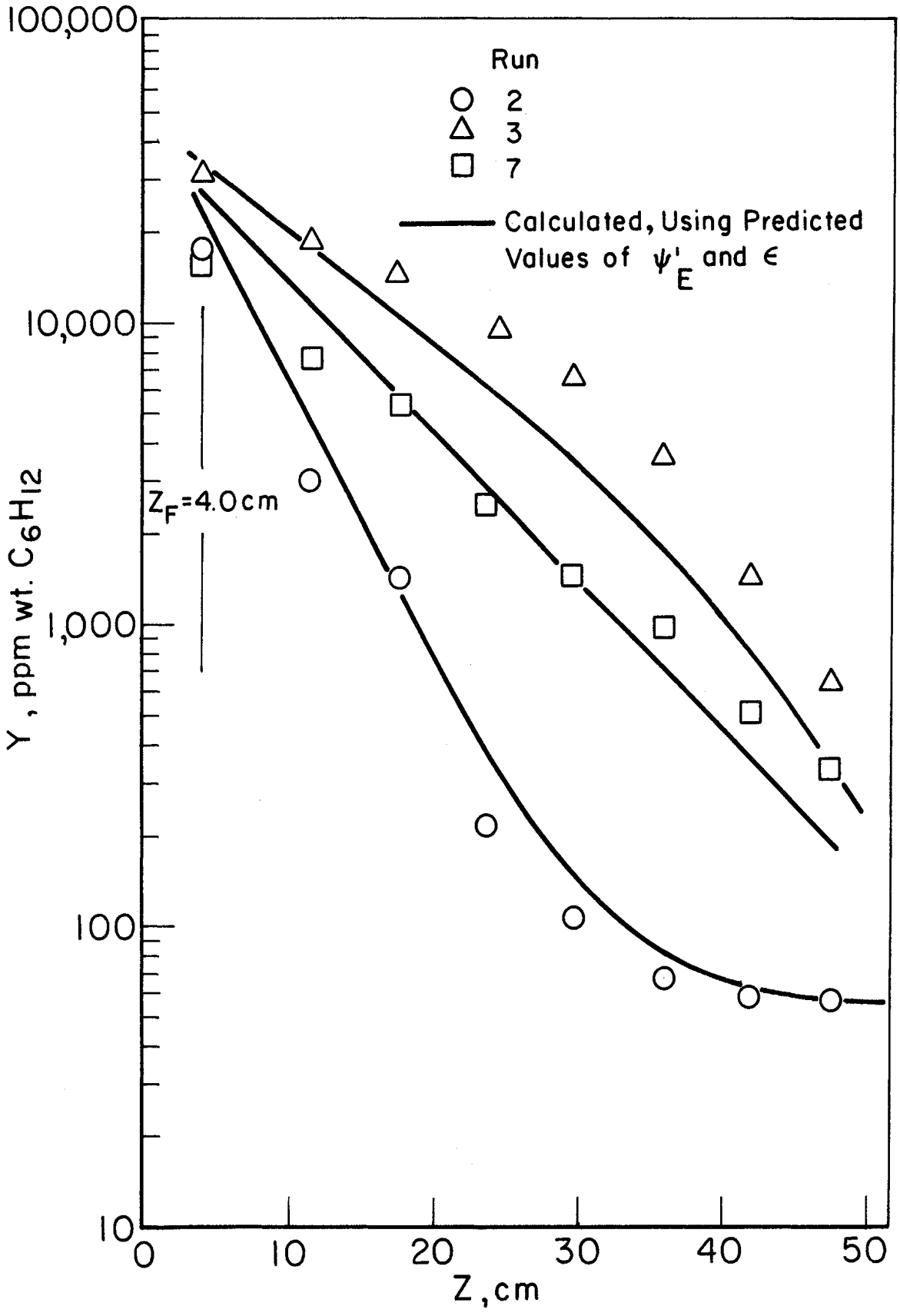

Figure 24. Comparison of experimental and calculated composition profiles.

by this method. The deviation between the calculated and experimental values of the point compositions for Run 3 (one of the worst cases) are as large as 200%. Errors of this magnitude can be explained by errors in the predicted values of ψ_E'. It was mentioned above that the values of ψ_E' predicted by Eq. (81) show an average error from the experimental values of 17%. It is further noted that the calculated values of ψ_E' enter the calculation in an exponential term (see Eq. (46)) which magnifies the error and thus results in the discrepancy between calculated and experimental values of the point compositions.

While the point compositions calculated from the model are in considerable error the predictive calculations do qualitatively predict the influence of variables.

8. Effect of the Enriching Section Product-Crystal Rate Ratio, R_E

As pointed out in Chapter III the separation that is achieved in a column crystallizer decreases with increasing R_E. Experimental data are presented in this section which illustrate this effect. The operation of the enriching section with cocurrent flow is also discussed.

The effect of R_E is illustrated by Runs 2, 3 and 7 shown earlier on Figure 14. The relative position of the enriching section composition profiles indicate that increasing R_E decreases the separation. The enriching section product composition, Y_E, for Run 2 was 60 ppm wt C_6H_{12} for a value of R_E of 0.354. The corresponding product composition for Run 3, where R_E was 0.782, was 370 ppm wt C_6H_{12}. The bottoms product rate was approximately the same for each run (see Table IX of Appendix C). The increase of Y_E with R_E, which is

exponential when $Y_E > \epsilon$, occurs due to the exponential dependence of the free liquid composition on the enriching section mass transfer factor. The column calculations presented in the previous section demonstrate that the model predicts the influence of R_E.

When R_E is further increased the separation continues to decrease as shown in Figure 25. In Run 10A R_E is 0.99. The enriching section profile is observed to have a small slope which corresponds to a large value of ψ_E'. In the limit when R_E is one, the composition profile in the enriching section is described by Eq. (59) which predicts a linear relationship between Y and z. The mass transfer factor increases sharply as R_E approaches one. The individual flow rates L_E and C are only known within 10%, consequently the true value of R_E is between 0.8 and 1.2. The sensitivity of ψ_E' to R_E can be demonstrated for the crystal rate employed in Run 10A by calculating values of ψ_E' for $R_E = 0.8$ and 0.99. Equation (81) which relates ψ_E' to C and L_E gives $\psi_E' = 11.0$ cm for $R_E = 0.8$ and $\psi_E' = 197.0$ cm for $R_E = 0.99$. In view of this range of possible enriching mass transfer factors there is no justification to assume that $R_E = 1.0$ for Run 10A in order to test Eq. (59).

When R_E is greater than one, the flow in the enriching section can be cocurrent depending on the magnitude of the adhering liquid rate (see Eqs. (60) and (61)). Run 10b was obtained with $R_E = 1.69$ and a feed composition of 26,400 ppm wt C_6H_{12}. The overhead product composition Y_E was 12,400 ppm wt C_6H_{12}. The corresponding value calculated from the model using the end condition for cocurrent operation given by Eq. (63) was 11,870 ppm.

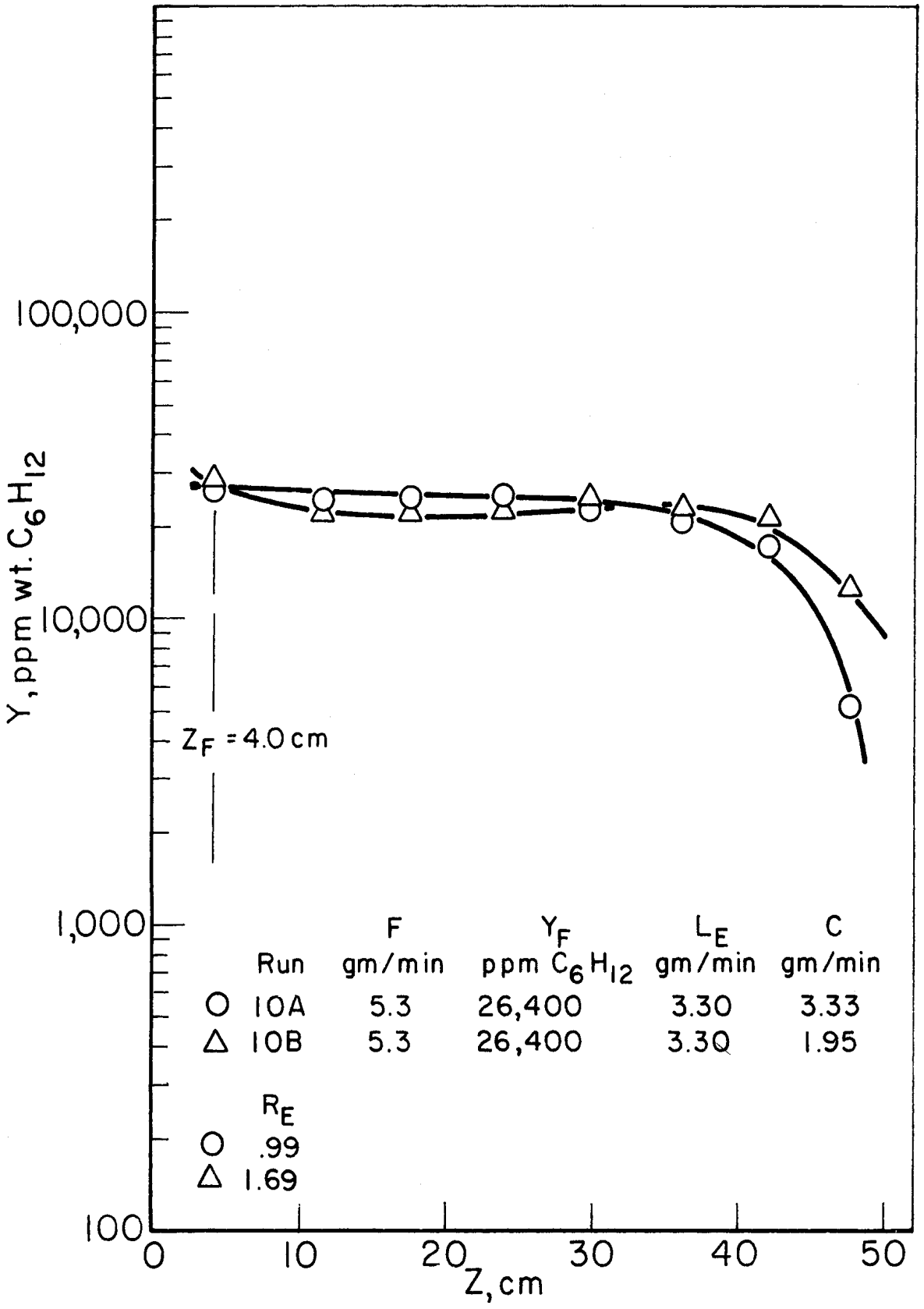

Figure 25. Enriching section composition profiles for large values of enriching section product-crystal rate ratio.

The overhead product purity obtained for cocurrent operation of the enriching section is compatible with the purity obtained by dilution of the portion of the feed that rises through the enriching section with the crystals from the melting section. This can be illustrated by a simple calculation. In Run 10b 5.3 gm/min of 26,400 ppm C_6H_{12} feed was fed to the column, but due to the fact that L_E was greater than C, 1.35 gm/min of feed passed cocurrently up the column with 1.95 gm/min of crystals. These streams were combined in the melting section to give an overhead product rate of 3.3 gm/min. Now if it is assumed that the portion of the feed and the crystals are transported through the enriching section without interacting, i.e., with no separation in this section, the overhead product composition Y_E can be calculated by considering only the dilution effect of melting the pure crystals in the melting section. Such a calculation gives Y_E = 10,800 ppm wt C_6H_{12}.

The experimental results and calculations for Run 10b are summarized as follows:

- The experimental enriching section product composition is 12,400 ppm wt C_6H_{12}.
- The value of Y_E calculated with the model using the end condition for cocurrent flow is 11,870 ppm wt C_6H_{12}.
- The value of Y_E calculated considering only the dilution in the melting section is 10,800 ppm wt C_6H_{12}.

The purity that was obtained in Run 10b can be explained by the dilution effect alone. Consequently, it is apparent that the purification section of the column crystallizer does not contribute to the separation when the enriching

section is operated with cocurrent flow. Thus this mode of operation is not of further interest and the cocurrent enriching section model is not discussed further.

B. LIMITS OF OPERATION

The limits of operation of the center-fed column crystallizer are considered in this section. The internal crystal rate, and the ratio of overhead product rate to crystal rate are discussed relative to the operability of the column.

1. Crystal Rate

The capacity of a column crystallizer is determined by the maximum crystal rate that can be achieved. The experimental results discussed below show that the column plugs and becomes inoperable at a crystal rate higher than 6.95 gm/min. At this crystal rate cavities started to form in the freezing section indicating the onset of plugging. When the crystal rate was increased beyond 6.95 gm/min the column plugged. Albertins[1] found that with total reflux operation the same column plugged at a crystal rate of 5.4 gm/min. According to Albertins[3] the spiral may have been binding slightly with the glass wall in the lower region of the column. Other than this effect which may have limited the crystal rate which he obtained, no attempt is made to explain the differences in the observed plugging crystal rates.

The experimental results deviated from the mathematical model when the plugging crystal rate was approached. Figure 26 shows an enriching section composition profile for a crystal rate of 6.95 gm/min. It can be seen that

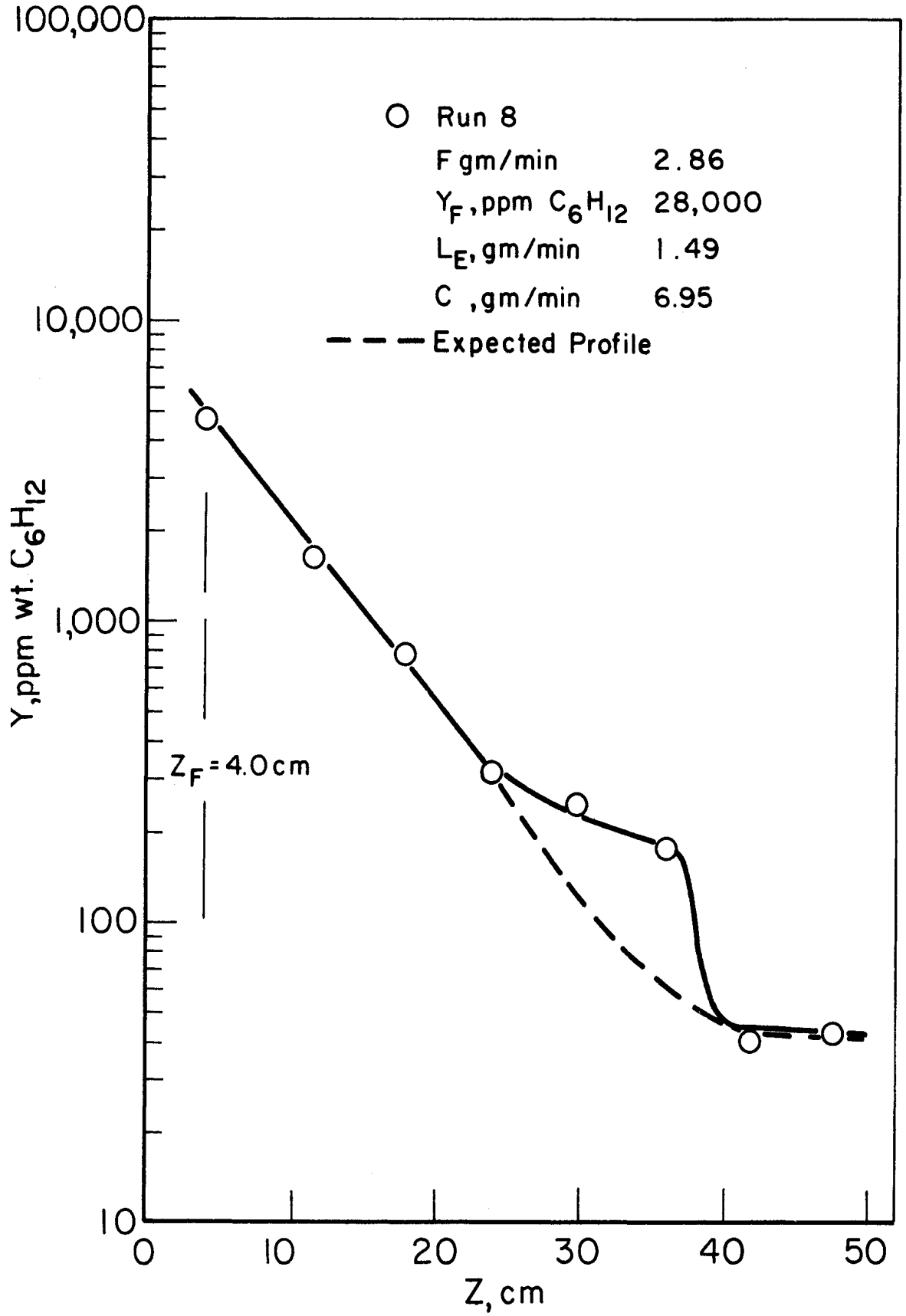

Figure 26. Enriching section composition profile obtained at the onset of crystal plugging.

the profile deviates from any of the three characteristic profile shapes discussed earlier. The dashed line indicates the profile shape that would be expected for the value $R_E = 0.21$ which was used in this run. At crystal rates below the plugging level no such deviation was observed, for example, in Run 17 (Figure 18) when the crystal rate was 6.8 gm/min the enriching section profile was consistent with the model.

2. Overhead Product-Crystal Rate Ratio, R_E

The column was found to be operable for all the values of R_E that were used (R_E was varied from 0.1 to 1.69). This range of R_E embraces both countercurrent and cocurrent operation of the enriching section. There were no observable differences in the nature of the fluidized crystal liquid slurry in the purification section over the range of R_E studied.

C. ERROR ANALYSIS

The results of an error analysis of the various experimental parameters that were determined in this study are presented below:

- The point compositions can be in error as much as 8%. This includes errors in the analytical method (3%) and the effect of back diffusion while the profile is being sampled (5%).[1] The maximum uncertainity in the position of the syringe tip during sampling was 0.5 cm. This could occur if the hypodermic needle were deflected by the spiral.
- The terminal stream flow rates (F, L_E, and L_S) are known within ± 10%. The magnitude of this error was obtained by repeated measurement of the flow rates during each run.

The terminal stream material balance, Eq. (64), closes within ± 10%. This was established by comparing calculated and experimental values of the feed composition.

. The internal crystal rate in the purification section is known within 15%. This error is based on a consideration of refreezing of crystals due to the axial temperature gradient, errors in reading the voltmeter which was used to determine the power input to the melting section (this was the basis for determining the crystal rate), and the heat gain to the purification section from the surroundings.

. The mass transfer factors, ψ_E', are obtained from the negative reciprocal of the slopes of the enriching section composition profiles. Multiple values of ψ_E' were calculated for Run 2 by using all possible combinations of the experimental point compositions to calculate the slopes. The values of ψ_E' were found to flu +12% around the mean value.

The procedure used to estimate the error associated with measuring the internal crystal rates requires clarification. The estimate was made for a crystal rate of 2.6 gm/min. The percentage error that results increases as the magnitude of the crystal rate decreases. Only four of the experimental runs employed crystal rates below this level. Possible refreezing on the crystals due to the axial temperature drop in the purification section (4.9°C) was estimated as 6% of the 2.6 gm/min crystal rate. The error in reading the voltmeter could have been as much as 0.5 volt; this corresponds to a ± 3% of the crystal rate. The heat gain of the purification section was determined by Albertins[1] for total reflux operation. He found that the heat gain in the

purification section corresponded to a decrease in the crystal rate of 0.48 gm/min. This provides a conservative estimate for continuous flow operation because the temperature difference with the surroundings is larger for total reflux operation. For a crystal rate of 2.6 gm/min this heat gain would decrease the crystal rate 18%. The errors due to refreezing and heat gain tend to cancel one another. Therefore the net uncertainity in the measured crystal rate is 15%.

D. CONCLUSIONS

On the basis of the comparisons in earlier sections of this chapter of the experimental data with the mathematical model it is concluded that the form of the model developed by the transport equation approach (Eqs. (46) and (47)) is consistent with the experimental data. It provides a satisfactory explanation of the influence of the variables that were studied in this investigation. The model breaks down as the plugging crystal rate is approached.

The concept that the level of impurity in the crystals is independent of position in the purification section was subjected to more tests than could be applied with total reflux. The variable profile shapes that occur in the enriching section, the $\epsilon(Y_S)$ dependence, and the fact that purer material can be obtained with continuous draw-off (for small values of R_E) than with total reflux operation all support the constant ϵ hypothesis.

Finally the internal flow rates were assumed to be constant in the mathematical analysis. The crystal rate was only measured at one position (the melting section), i.e., the validity of the assumption of constant flow rates

was not verified by direct experiments. The error analysis presented above which considers the heat effects in the purification section shows that the crystal should not vary more than 15%. This in conjunction with the linearity of the modified enriching section composition profiles (Figure 15) justifies the assumption of constant internal crystal rate, i.e., the constant slope, $-1/\psi_E'$, implies that the crystal rate is constant. Both Albertins[2] and Gates[14] found that their data for total reflux operation were consistent with this assumption.

CHAPTER VI

DISCUSSION OF CONTINUOUS FLOW COLUMN CRYSTALLIZATION

This chapter discusses continuous flow column crystallization in view of the theoretical and experimental results that were compared in the previous chapter. The mathematical model is used to predict the influence of some of the variables in ranges that were not evaluated experimentally. Also the application of continuous flow column crystallization to the production of ultrapure benzene is discussed.

All of the calculations presented in this chapter are based on the model derived from the transport equation approach (Eqs. (46) and (47)). The mass transfer factors ψ_E' and ψ_S' are calculated using the correlations given by Eqs. (81) and (85). The impurity level in the crystal phase, ϵ, is represented by Eq. (73). All column calculations were performed using the iterative procedure described in Chapter III which is implemented by the computer program given in Appendix D.

A. PARAMETER STUDIES

The influence of the feed position, feed rate, enriching section product-crystal rate ratio and product recovery are discussed in this section. No attempt is made to exhaust all the possible combinations of the parameters. The intent is to illustrate the effect of these variables rather than map the entire region of interest.

1. Feed Position

The separation that is achieved in a column is a function of the feed position. It was demonstrated both theoretically and experimentally in Chapters IV and V that a flat portion can exist in the stripping section composition profile (see Figures 17 and 18). A flat region of this type corresponds to inefficient utilization of the purification section. The flat region of the profile can be eliminated by decreasing the length of the stripping section.

Figure 27 illustrates the effect of feed position on the enriching section product composition for fixed feed composition, Y_F, crystal rate, C, and terminal stream flow rate, F, L_E, and L_S. There is a feed position which corresponds to a maximum product purity. The plot of the composition of the free liquid at the feed point, Y_ϕ, vs z_F shown on the same figure illustrates that the maximum separation that is achieved occurs when there is a feed match, i.e., $Y_\phi = Y_F$.

2. Enriching Section Product-Crystal Rate Ratio, R_E

Figure 28 illustrates that the product purity reaches a limiting value as R_E is decreased. When R_E is decreased to a value where $Y_E = \epsilon$ (complete washing), a further decrease does not effect the product purity. Decreasing R_E beyond this point decreases the mass transfer factor, ψ_E', but does not necessarily increase the enriching section product purity. As mentioned in Chapter III the washing process does not reduce the level of impurity associated with crystal phase. Consequently in applications where maximum purity is

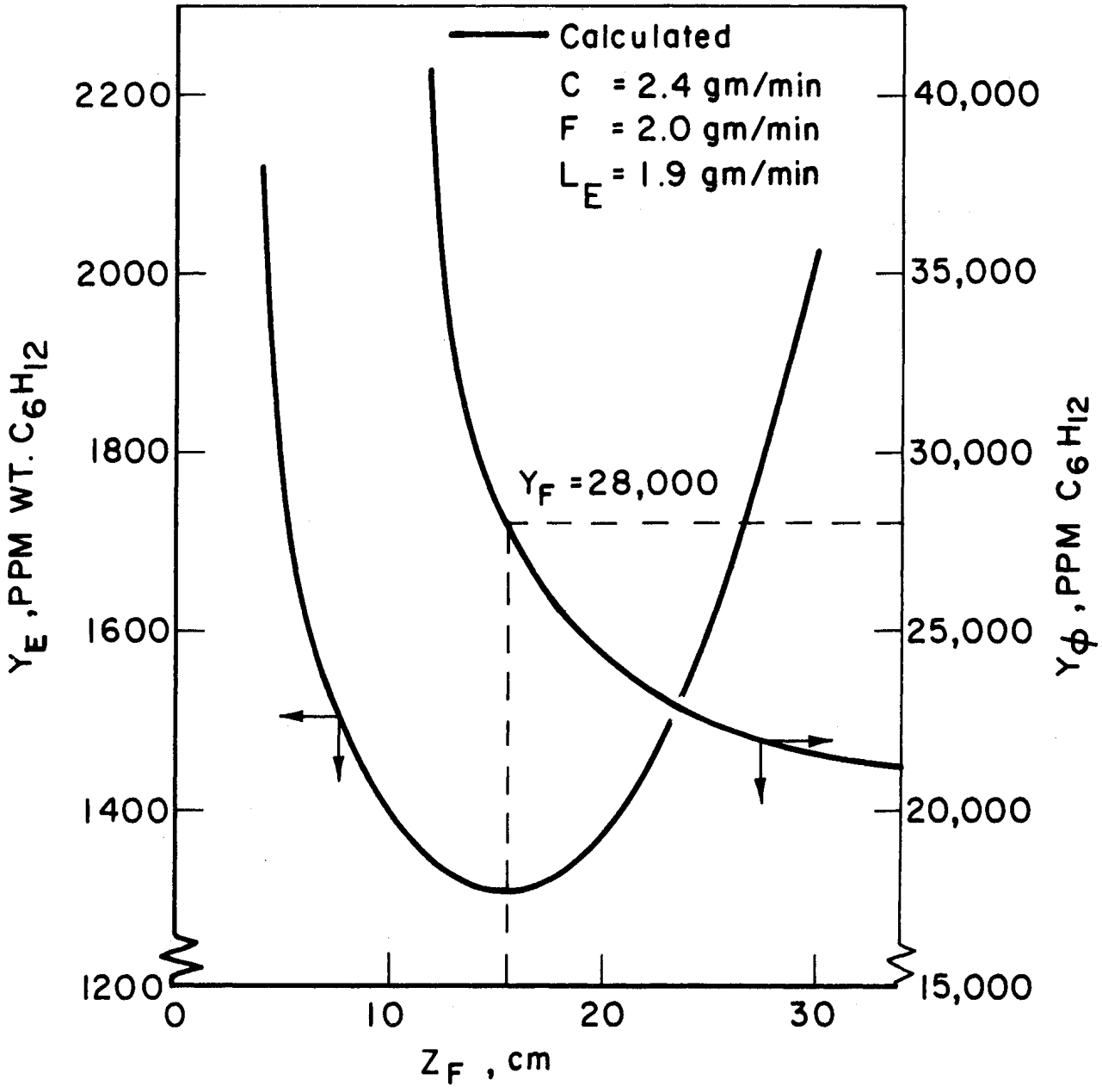

Figure 27. Influence of feed position on the enriching section product composition.

desired, R_E should be chosen so that Y_E is just equal to ϵ, i.e., so there is not a flat region in the enriching section composition profile.

Figure 28 also illustrates that the product purity decreases as the

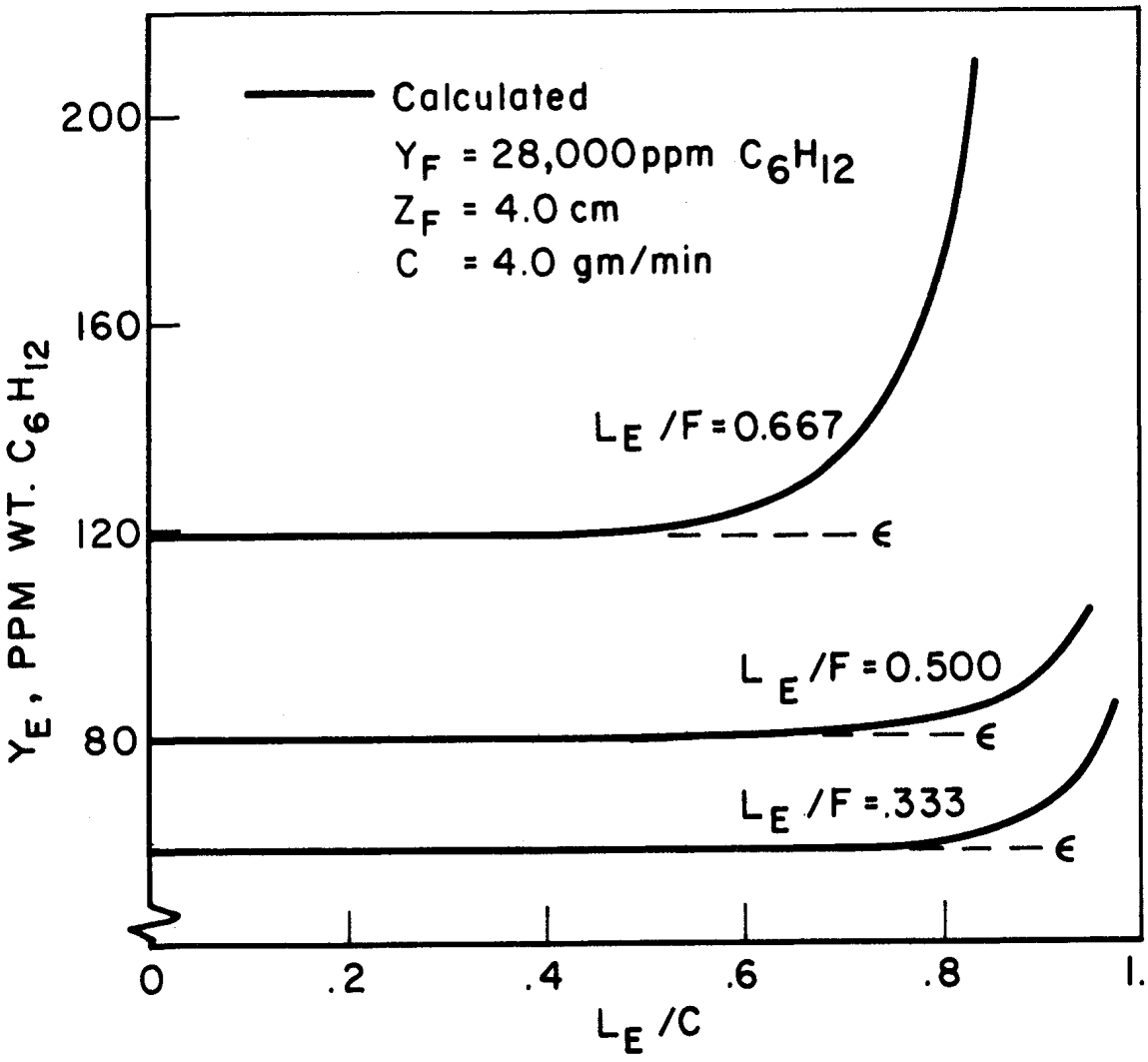

Figure 28. The effect of the enriching section product-crystal rate ratio and product recovery on the enriching section product purity.

recovery, L_E/F, is increased. The crystal phase composition, ϵ, increases when the recovery is increased. This can be explained by Eq. (67) in Chapter III which shows that for a given feed composition Y_S is determined by the value of F/L_S which is uniquely determined by the value of L_E/F. Also, it was shown in Chapter V that ϵ is determined by Y_S (see Eq. (73)). Note that the maximum

value of R_E which corresponds to $Y_E = \epsilon$ (the break point in the curves on Figure 28) increases as the recovery is decreased.

3. The Relation Between Continuous and Total Reflux Operation

The expressions for the enriching and stipping section composition profiles each reduce to the expression for the composition profile for total reflux operation when R_E and R_S are zero and Y_ϕ is replaced by the free liquid composition at $z = 0$, Y_0. Figure 29 shows the effect of the feed rate on the

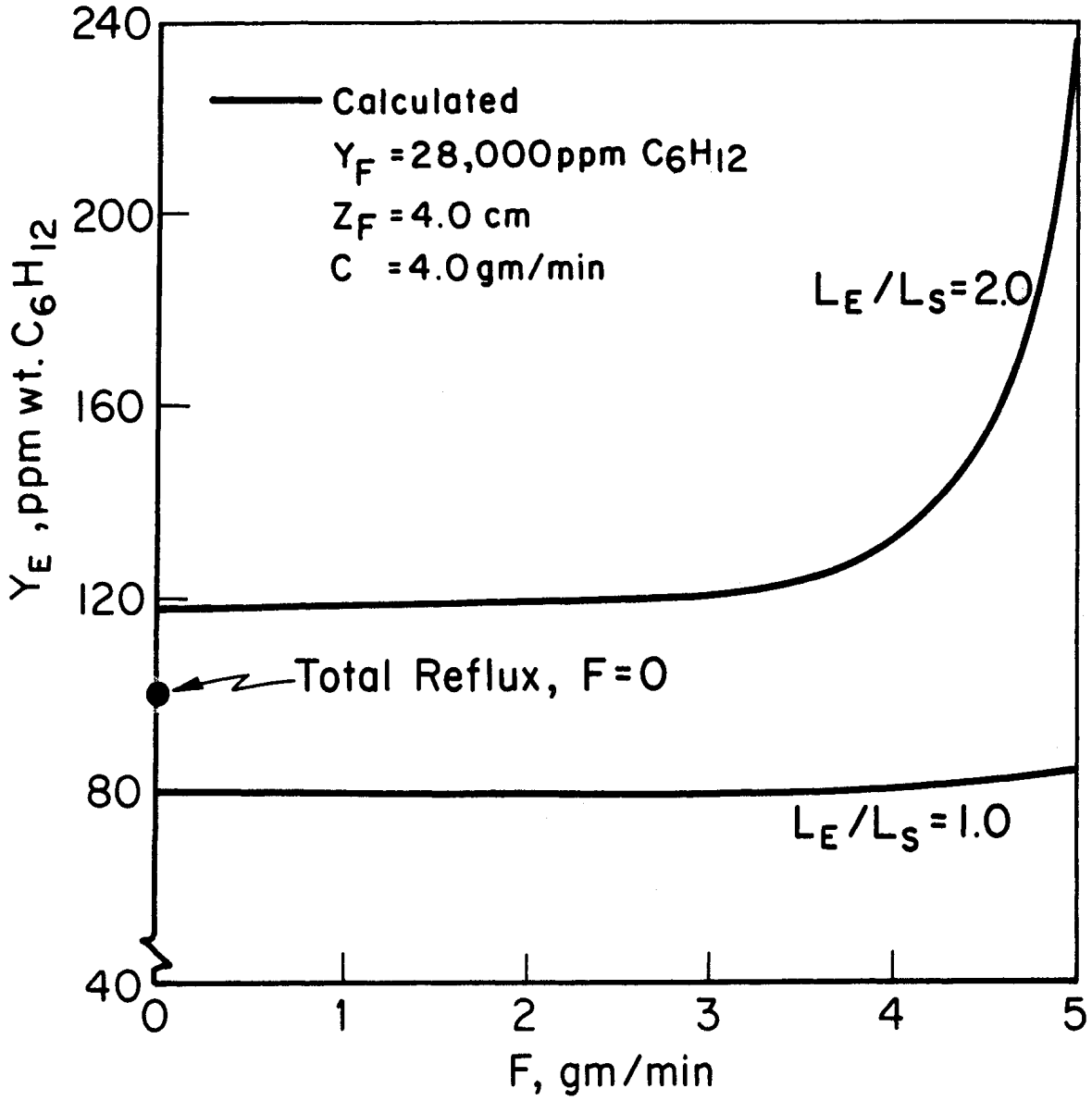

Figure 29. Comparison of the purity achieved with continuous flow and total reflux operation.

enriching section product composition. Total reflux operation corresponds to $F = 0$. The continuous flow calculations ($F \neq 0$), however, do not predict the correct pure end composition for total reflux operation when F is made arbitrarily small. This occurs because the end conditions (see Eqs. (62) and (65)) for continuous flow operation do not apply for the total reflux case. The corresponding relation for total reflux is an initial condition, i.e., the total mass of impurity initially charged to the column must be equal to the sum of the masses of impurity in the melting section, purification section, and freezing section at steady state.

B. PRODUCTION OF ULTRAPURE BENZENE

It has been demonstrated in the previous chapter that it is possible to greatly reduce the cyclohexane content of benzene by column crystallization. Figure 21 illustrates that the cyclohexane content of Phillips pure grade benzene can be reduced three orders of magnitude.

There are many other impurities besides cyclohexane in Phillips pure grade benzene (see Table I). These impurities are identified on the chromatogram presented in Figure 30. The chromatogram of the overhead product for Run 9, also given in Figure 30, illustrates that all of these impurities were removed to a level where they could not be detected by the gas chromatograph. The lower limit of detection of the chromatograph used for this analysis, which was equipped with a non-polar Squalane packing, was less than 10 ppm for each of the impurities. The cyclohexane content of the Run 9 overhead product was approximately 1 ppm as determined by a chromatograph equipped with a polar

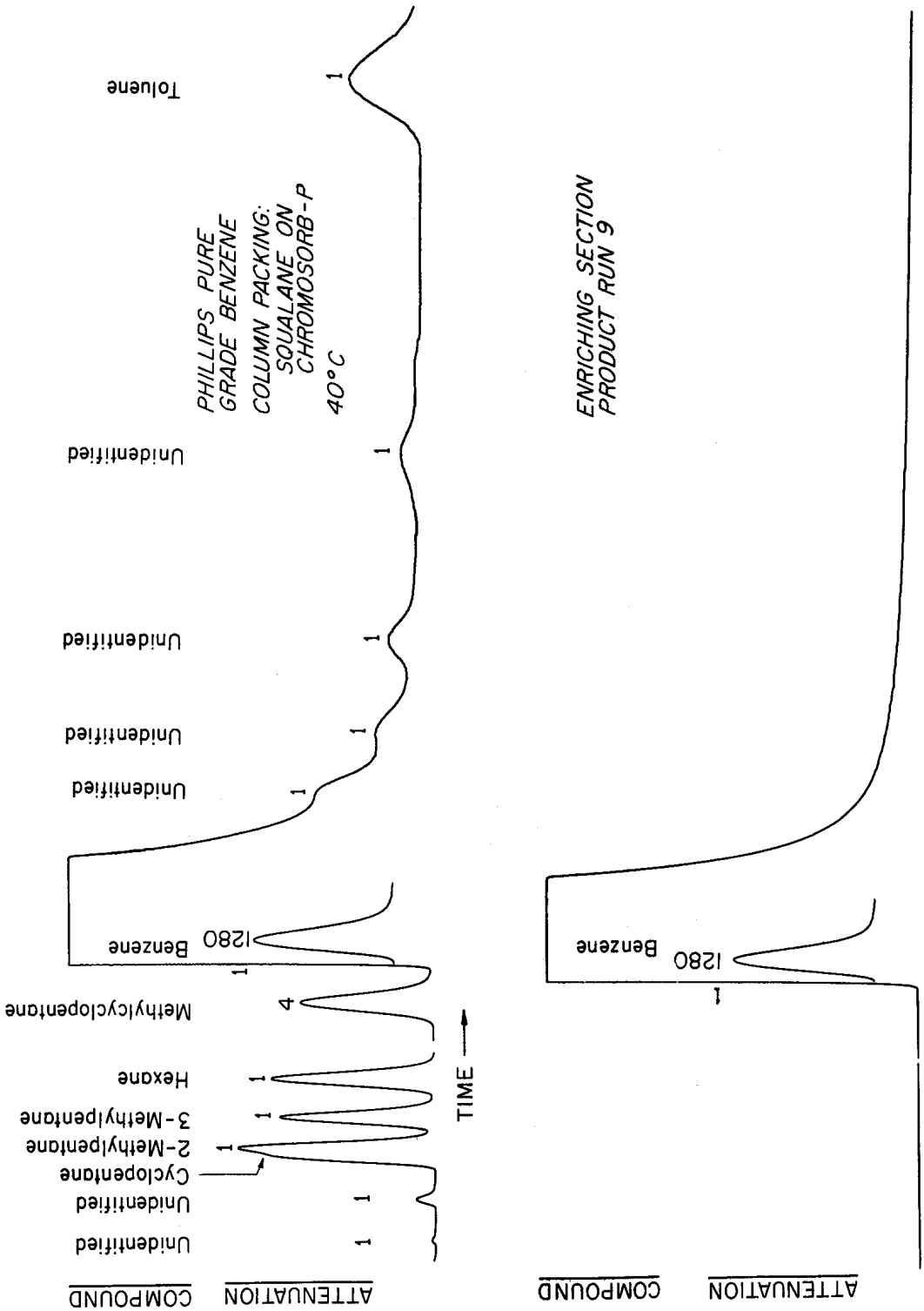

Figure 30. Chromatograms which confirm the purification of Phillips pure grade benzene by column crystallization.

Carbowax packing.

It is apparent that column crystallization provides an effective means of reducing the impurity content of benzene. The benzene product purities obtained by column crystallization are comparable to those of zone refined benzene, e.g., zone refined benzene is commercially available[18] containing ten, one hundred, and ten thousand ppm impurities. Column crystallization, however, provides a means of producing much larger quantities of very pure materials than can be obtained by zone refining techniques. The remainder of this chapter is devoted to discussion of operating conditions and methods that could be used to produce ultrapure benzene.

1. Multiple Pass Operation

There is a limit to the purity that can be achieved in a column crystallizer with one pass operation. As discussed in Chapter V the minimum level of any impurity that can be obtained for a given feed composition is ϵ_{min}. The relation for ϵ_{min} (Eq. (74)) indicates that the minimum impurity level is determined by the feed composition, Y_F. With multipass operation the feed composition to the second and any subsequent passes is reduced, i.e., the pure product from the first pass becomes the feed to the second pass, etc. Therefore theoretically there is no limit to the purity that can be obtained by multiple pass operation. The same effect could be achieved for large scale applications by staging column crystallizers in series with the product from one column becoming the feed for the next.

Another advantage of multiple pass over single pass operation is the fact that higher production rates can be achieved if sufficiently large quan-

tities of product are required. This results from operating the first pass and second pass at higher overhead product rates than could be achieved with single pass operation.

2. Design Example

An example is presented to illustrate the conditions under which there is a production time advantage of two pass over one pass operation. The discussion concerns the determination of operating conditions that will minimize the operating time of the existing laboratory column (described in Chapter IV) to produce benzene containing 3 ppm wt C_6H_{12} from Phillips pure grade benzene. This purity was chosen because it can be attained by either single or two pass operation.

The problem of determining the operating conditions was constrained so that only the overhead product rate from the first pass and the quantity of final 3 ppm wt C_6H_{12} product could be varied independently. The feed and crystal rates were set at 5 gm/min for each pass. The cyclohexane content of the feed to the first pass was 1500 ppm wt.

Column calculations were performed for the first pass for a variety of overhead product rates. Similar calculations were done for the second pass for several feed compositions obtained from the first pass. The results of these calculations were used to determine the time required to produce various quantities of 3 ppm product by both one pass and two pass operation. The calculation of time required included consideration of start up time (5 hr for each pass), and steady state running time for both passes. Figure 31

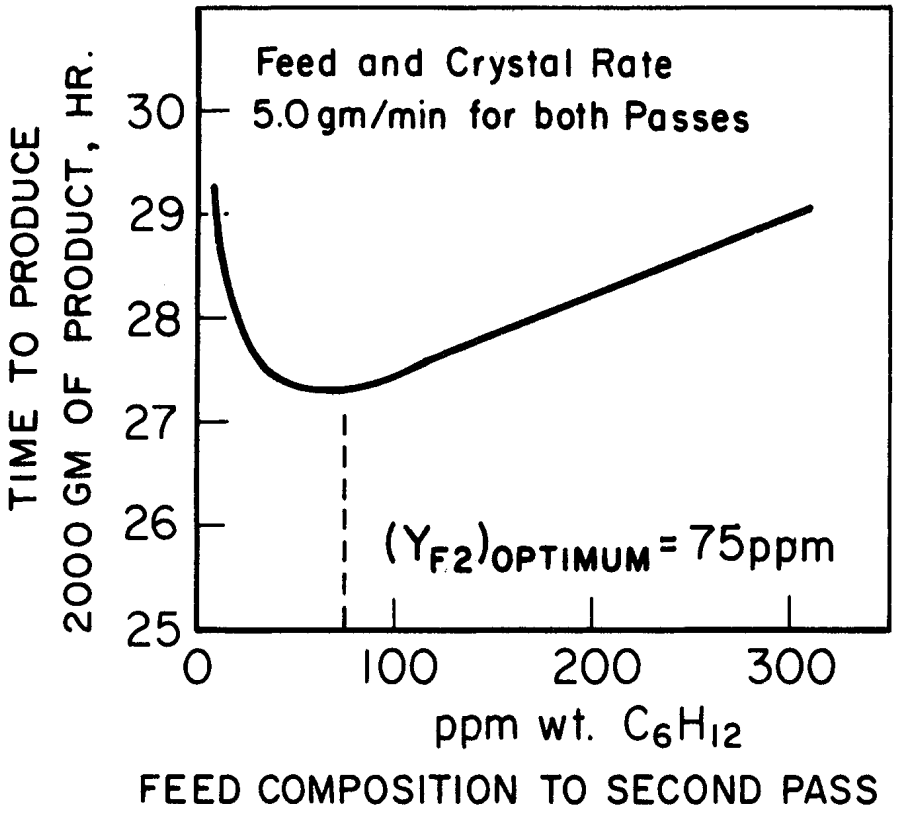

Figure 31. Effect of the second pass feed composition on the time required to produce 2,000 gm of 3 ppm product.

illustrates the effect of the feed composition to the second pass on the processing time for the production of 2000 gm of 3 ppm product. The optimum (minimum production time) second pass feed composition was 75 ppm which corresponds to a first pass enriching section product rate of 4.6 gm/min. Figure 32 compares one pass and two pass operation. It can be seen that two pass operation becomes advantageous when more than 2000 gm of 3 ppm product are required. The curve for two pass operation in Figure 32 represents the time required for producing the various quantities of product with the optimum second pass feed composition for each product weight shown.

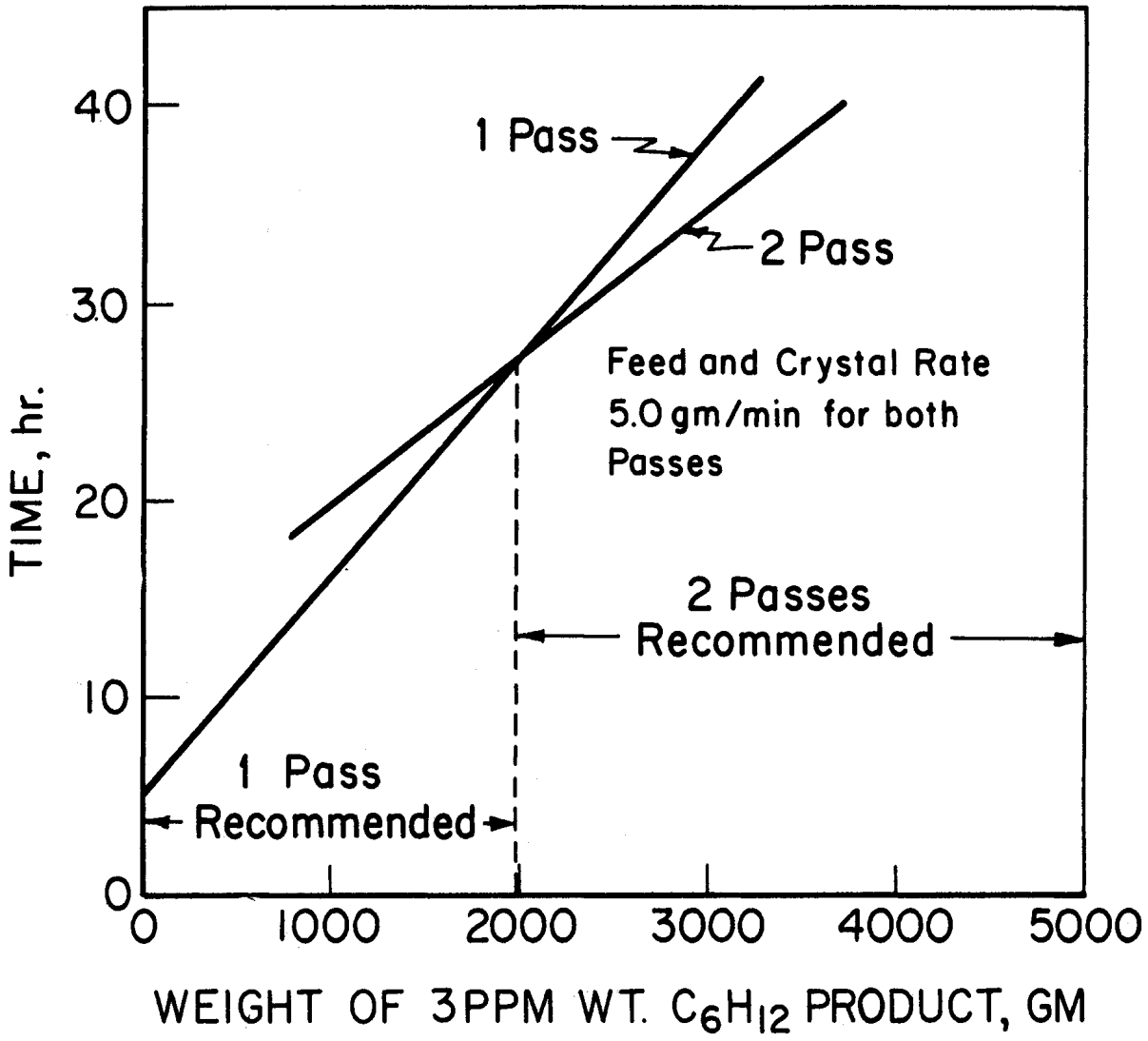

Figure 32. Comparison of one pass and two pass operation.

CHAPTER VII

SUMMARY AND CONCLUSIONS

A theoretical and experimental investigation of the component separation of a system of the simple eutectic type by column crystallization illustrated the effects of the variables associated with continuous flow operation. Terminal composition and axial composition profile data were obtained to study the column performance.

The effects of the variables associated with the continuous flow problem are satisfactorily explained by a mathematical model which includes consideration of mass transfer by axial dispersion of impurity in the free liquid, mass transfer of impurity from the adhering liquid to free liquid, and the presence of impurity associated with the crystal phase which is assumed to be constant throughout the purification section. The model was derived using the transport equation assumption which greatly simplified the final form of the expressions for the mass transfer factors (parameters which are an inverse measure of the separation power of the column).

The model satisfactorily explains the shape of the experimental composition profiles in both the enriching and stripping sections. The variable profile shape in the enriching section and the correlation of the impurity composition of the crystal phase, ϵ, with the stripping section product composition, Y_S, are further justifications beyond Albertins'[2] investigation for total reflux operation that ϵ is independent of position in the purification section. The $\epsilon(Y_S)$ dependence implies that purer material can be obtained with continuous

flow than with total reflux operation (at low values of R_E).

The interpretation of the mass transfer factors obtained from both continuous flow and total reflux data show that axial dispersion is the dominant mechanism determining the extent of separation, but that mass transfer between the adhering and free liquids is significant. The average values of the diffusional terms $D\rho A\eta$ obtained from the continuous data flow of this study and total reflux data of Albertins are in excellent agreement. The values of the mass transfer terms, $\alpha(\alpha+1)/KaA\rho$, obtained from these two data sources differ by a factor of two (see Table IV). The deviation is explained by the relative insensitivity of the enriching section mass transfer factors to the mass transfer terms, i.e., the melting section product rate L_E reduces the contribution of the mass transfer terms as shown by Eqs. (82) and (83).

The computer program developed for column calculations can be used to predict the influence of variables associated with continuous flow operation. The agreement between calculated and experimental compositions is excellent when experimental values of the mass transfer factors are used. When values of the mass transfer factors are calculated using the values of the diffusional and mass transfer groups ($D\rho A\eta$, $\alpha(\alpha+1)/KaA\rho$, and $\alpha/KaA\rho$) obtained from the correlation of ψ_E' with C and L_E given by Eq. (81), there is considerable discrepancy between the calculated and experimental composition. In Run 3, for example, some of the calculated point compositions were 200% less than the experimental values. This occurs due to the exponential nature of the model, i.e., its sensitivity to relatively small errors in the predicted values of the mass transfer factors. The model does a reasonable job of predicting

point compositions in view of the tremendous separations that are achieved; the cyclohexane composition of the free liquid was typically decreased one to three orders of magnitude in the enriching section.

Both countercurrent and cocurrent operation of the enriching section were investigated both experimentally and theoretically. Countercurrent operation is the conventional case in which reflux is provided to wash impurities from the adhering liquid. The calculated and experimental results obtained for the cocurrent case indicate that the separation which is achieved can be explained by the dilution effect of melting the crystals in the melting section. Therefore it is apparent that the purification section does not contribute to the separation when the enriching section is operated cocurrently.

The experimental data demonstrate the capability of producing ultrapure benzene. The column crystallizer removed all of the impurities in Phillips pure grade benzene to a level comparable to cyclohexane. The separation that is achieved is very sensitive to the enriching section product-crystal rate ratio, R_E. There is no advantage, however, in operating a column with R_E less than that value corresponding to $Y_E = \epsilon$ (see Figure 28). The ultimate purity that can be achieved is limited by impurities associated with the crystal phase. Calculations show that the separation is maximized when the feed position is such that there is a feed match. In most cases with relative dilute feeds such as used in this study the feed match will occur at a feed position close to the freezing section.

The capacity of the center-fed column is limited by the maximum internal crystal rate that can be achieved. The column plugged and became inoperable

when the crystal rate was greater than 6.95 gm/min. The mathematical model breaks down when the plugging crystal rate is approached.

CHAPTER VIII

RECOMMENDATIONS FOR FUTURE INVESTIGATION

The results of this investigation as well as previous studies[2,14] suggest several topics that may be profitable for future investigation.

The experimental data of this and Albertins' investigation indicate that the impurity associated with the crystal phase can limit the separation obtained in a column crystallizer. While there is considerable evidence that the crystal phase composition is not affected by the washing that occurs in the purification section, experimental data do not exist that permit a positive identification of the mechanism by which the impurity becomes associated with the crystal phase. It is of interest to know whether the phenomena is caused by volumetric inclusion of impurity or by a slight solid solubility in the ppm C_6H_{12} range. One method of experimentally distinguishing between the two effects would be to determine the composition profile of two impurities (a second impurity such as methylcyclopentane could be added to the feed). ϵ could then be calculated for each impurity from the composition profiles. Both impurities should be present in the feed at the 30,000 ppm level to permit convenient analysis of the profile samples with a gas chromatograph. It has been shown that the impurity composition of the crystal phase, ϵ, for cyclohexane is proportional to the cyclohexane composition of the stripping section product (see Eq. (73)). If the impurities in the crystals are due to volumetric inclusion then the proportionality constant in Eq. (73) should be the same for each impurity. If the proportionality constant for cyclohexane

is significantly larger than that for methylcyclopentane, the occurrence of solid solubility is likely, i.e., one would expect cyclohexane to have a higher solid solubility than methylcyclopentane.

Locating the freezing section at the top rather than at the bottom of the column should have two desirable effects for systems where the specific gravity of the crystals exceeds that of the liquid (this is the case for cyclohexane-benzene). First, the crystal flux that can be achieved is increased due to the effect of gravity, e.g., the Benzole Producers[16] achieved higher fluxes for the C_6H_{12}-C_6H_6 system with the freezing section at the top of the column than were obtained in this investigation. Second, increasing the crystal flux also tends to minimize the effect of axial dispersion which opposes the separation. A limited experimental investigation utilizing a column with the freezing section at the top should be performed to determine whether the effects of the variables are the same as those demonstrated by the results of this study. The key to comparing the experimental data from each configuration is the assumption that the hydrodynamics of the crystal-liquid movement are similar in both cases which must of course be determined experimentally.

Before commercial scale column crystallizers could be designed confidently, the effect of column size on the diffusional and mass transfer parameters (D, η, K, and a) must be determined. Also any volumetric inclusion that occurs is certainly a function of the configuration of the freezing section. These problems suggest a scale-up study.

It was shown in Chapter V that it is necessary to know the ratio of the adhering liquid to crystal rate, α, to obtain a direct verification of the validity of the assumption that $\theta(X) \cong 1$ (see Eqs. (51) and (53)) which would directly prove that the transport equation approach applies. It was pointed out also that α could not be calculated with any confidence from the correlation coefficients obtained from the enriching section mass transfer factors. Therefore the only approach would be to determine α experimentally. This is indeed a difficult problem and no approaches are obvious to the author.

The mathematical model developed for cocurrent operation of the enriching section included an assumed boundary condition, $dY/dz = 0$ at $z = \mathcal{L}$, which was based on the concept that little separation occurs in the enriching section with cocurrent operation. The model predicts results that agree with experimental data. There is little incentive from a practical point of view to develop a more rigorous boundary condition because the enriching section would seldom be operated cocurrently. The question then is largely an academic one; can a rigorous boundary condition for the cocurrent case be obtained from strictly diffusional considerations?

APPENDIX A

METHODS OF ANALYSIS

1. DETERMINATION OF CYCLOHEXANE BENZENE COMPOSITIONS

An F and M Research Gas Chromatograph, Model 5750, was used to determine the cyclohexane-benzene compositions of the composition profile and terminal stream samples that were withdrawn from the column. The instrument was equipped with a flame ionization detector. Benzene and cyclohexane were separated with a column packed with a 10% solution of Carbowax 20M on a 40/45 mesh Chromosorb support phase. The column was constructed from 1/8 in. stainless steel tubing six feet in length. The carrier gas was Matheson prepurified nitrogen. Matheson dry air and prepurified hydrogen were used to support and maintain the flame.

The operating conditions for the chromatograph are presented below:

injection port temperature ..... 110°C

column temperature..... 82°C

detector temperature..... 220°C

carrier gas rate (nitrogen)..... 30 ml/min

air rate..... 600 ml/min

hydrogen rate..... 40 ml/min

The chromatograph heaters and carrier gas were turned on at least three hours prior to the analysis. The flame was turned on one hour in advance of the analysis.

A Hamilton syringe, type 701, was used to introduce 0.6 μml of liquid

sample into the injection port. The chromatogram was recorded with a Brown (Model 153X12-X-30) recorder which has a range of 0-2 millivolts and a response of one second full scale. A typical benzene-cyclohexane chromatogram is shown in Figure 33.

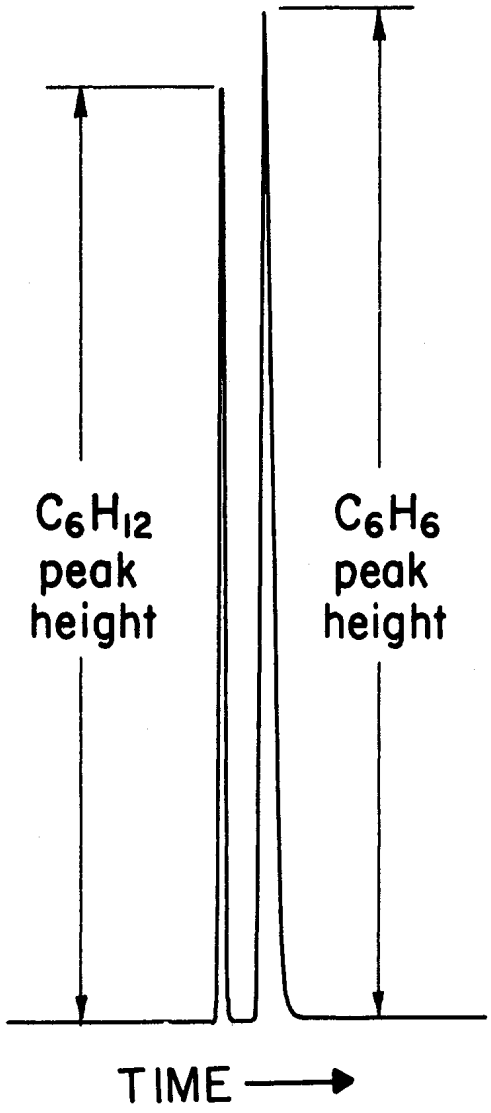

Figure 33. Typical cyclohexane-benzene chromatogram.

The chromatograph was calibrated using standard samples that were prepared by weighing and successive dilution. The response of the flame detector to cyclohexane and benzene is a function of the hydrogen, air, and carrier gas rates; the shape of the flame; and the injection port, column, and detector

temperatures. Consequently the response factor was calculated from Eq. (86) with the peak height data from the chromatograms of the standard samples each time unknown samples were analyzed.

$$F = \frac{(10^6 \text{ parts } C_6H_6)\ (C_6H_{12} \text{ peak height})\ (C_6H_{12} \text{ attenuation})}{(\text{parts } C_6H_{12})\ (C_6H_6 \text{ peak height})\ (C_6H_6 \text{ attenuation})} \qquad (86)$$

Table V gives the response factors calculated from Eq. (86) for the standard

TABLE V

RESPONSE OF THE FLAME DETECTOR TO BENZENE-CYCLOHEXANE MIXTURES

Ratio of C_6H_{12}/C_6H_6, ppm	Response Factor, F
162	1.97
1,459	1.94
6,997	2.02
30,900	1.96
55,858	2.00

samples. The fact that the response factors are constant ± 3% illustrates that the response of the detector was linear. The reproducibility of the response factors indicates that the compositions of the unknown samples can be calculated from Eq. (86) within ± 3%. These results are comparable to those obtained by Albertins[1] for cyclohexane-benzene with the same chromatograph. The analytical method for cyclohexane was confirmed independently by Professor E. A. Boettner of the Public Health School of The University of Michigan by

both gas chromatographic and mass spectrographic techniques.

2. ANALYSIS OF IMPURITIES IN PHILLIPS PURE GRADE BENZENE

As mentioned in Chapter VI there are several impurities in Phillips pure grade benzene besides cyclohexane. An analysis of this material is given in Table I and a chromatogram is shown in Figure 30. These impurities were identified and their compositions determined because the Phillips pure grade benzene was the starting material for preparing the feed stocks used in this investigation.

Professor Boettner and his staff isolated most of the individual impurities with a gas chromatograph (Beckman GC-2A) equipped with a stream splitter upstream of the detector. The column was packed with Squalane on Chromosorb-P. Approximately 80% of each impurity exiting the column was diverted to a cold trap. The impurities that were collected in this manner were identified by comparing their mass spectra with the mass spectra of known compounds. An Associated Electrical Industries, Ltd. (Type MS10) mass spectrometer was used. Calibration standards were prepared for the impurities that were identified and the composition of the impurities in the Phillips pure grade benzene were determined with the same chromatograph that was used to isolate the impurities. The results of this analysis are summarized in Table I of Chapter IV. The compositions of the impurities for the compounds that were not identified were obtained from the peak area ratios.

APPENDIX B

CALIBRATIONS

Pertinent calibrations are summarized in this section. The sample tap and thermocouple positions are also presented. Other column dimensions are given in Chapter IV.

The feed pump described in Chapter IV was calibrated by determining the flow rate-stroke length curve. Figure 34 illustrates that the flow rate

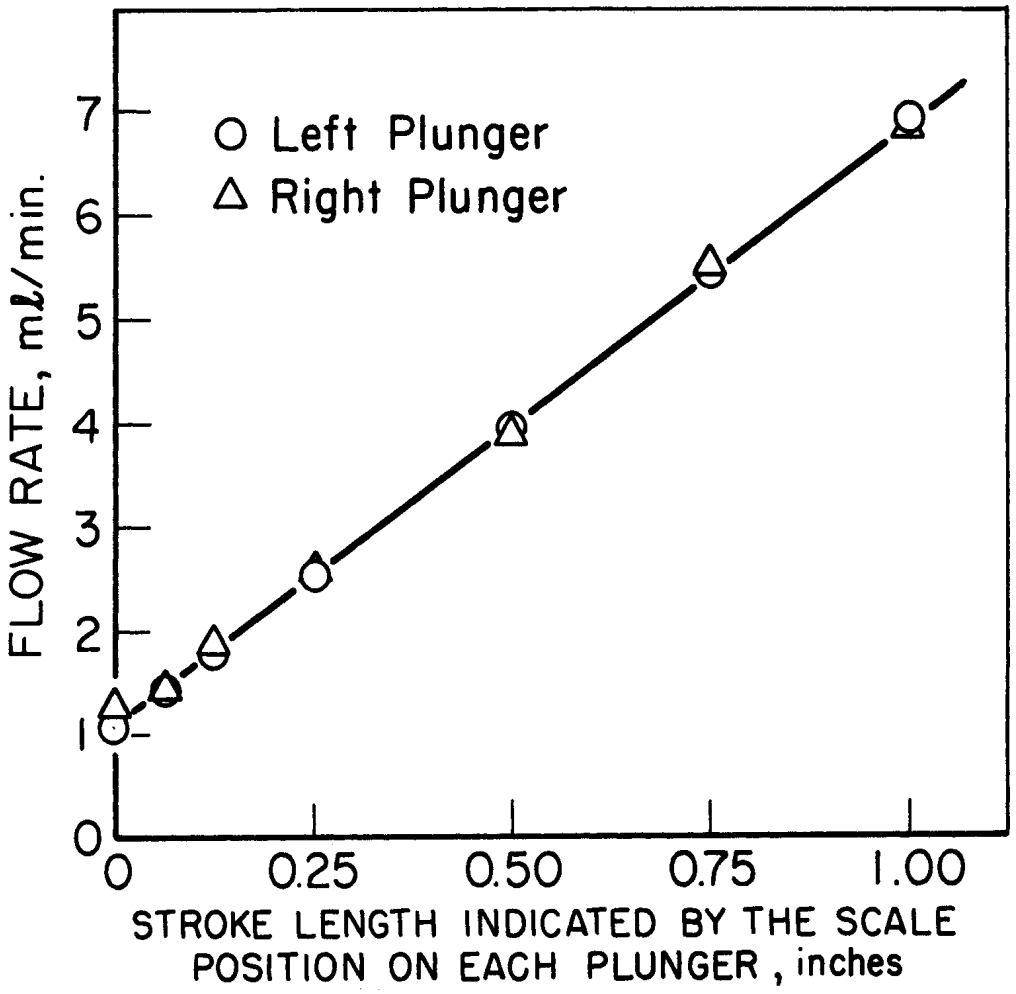

Figure 34. Calibration curve for the feed and bottoms pumps.

stroke length response is linear. A scale which was machined on each plunger by the manufacturer was used as an indication of stroke length. The zero

position on the scales did not correspond to a zero stroke length, consequently, Figure 34 does not have a zero intercept. This curve was used to choose the stroke length for various flow rates, but the actual flow rates reported in Appendix C were obtained by collecting and weighing products during the course of each experiment.

The voltmeter used to measure the power input to the internal melting section heater was calibrated against a standard voltmeter (± 0.1% accuracy) at the Electrical Measurements Laboratory of The University of Michigan. Table VI illustrates that the YEW voltmeter used in this study is within ± 0.3% of the standard voltmeter.

TABLE VI

VOLTMETER CALIBRATION

YEW Voltmeter, volts	Standard Voltmeter, volts
10.0	10.00
20.0	20.04
30.0	30.08
40.0	40.08
50.0	50.05
70.0	69.99

The locations of the sample taps and thermocouples in the column are given in Tables VII and VIII. The sample tap positions shown in Table VII are the

TABLE VII

LOCATIONS OF THE SAMPLE TAPS IN THE PURIFICATION SECTION

Sample tap number	Location in the purification section, cm above the freezing section
1	47.5
2	42.0
3	36.0
4	29.75
5	23.75
6	17.75
7	11.5
8	4.0

TABLE VIII

LOCATIONS OF THE THERMOCOUPLES IN THE COLUMN

Thermocouple number	Location in the purification section, cm above the freezing section
1	47.5
2	37.5
3	27.5
4	17.5
5	7.5
6	inside the freezing section
7	refrigerant in the jacket about the freezing section

values of the positions in the purification section that correspond to the sample tap numbers given in Table IX of Appendix C. These sample tap and thermocouple positions are the same as those used by Albertins.[1] These measurements were checked at the beginning of this investigation.

APPENDIX C

EXPERIMENTAL DATA AND CALCULATED PARAMETERS

The experimental data obtained in this investigation are summarized in Table IX. The steady state terminal stream and internal crystal mass flow rates, terminal stream compositions, and free liquid composition profile are presented for each experimental run. The purification section temperature profile was not measured for each run, but is shown for those runs where it was obtained.

The parameters that were calculated from the free liquid composition profile data are given in Table X. The shape determining group for the enriching section profile, Y_P, was chosen so the modified composition profile, $\ln(Y-Y_P)$ vs z would be linear. The impurity associated with the crystal phase, ϵ, was calculated from the experimental values of Y_P and their defining relation (Eq. (72)). The shape determining group for the stripping section profile ($\bar{Y}_P$) is the value of the free liquid composition in the flat region of the profile ($\bar{Y}_P$ was obtained only for the runs where $z_F > 4.0$ cm). The enriching section mass transfer factor, ψ_E, is the negative reciprocal of the slope of the modified enriching section composition profile. The procedures used to calculate Y_P, ϵ, $\bar{Y}_P$ and ψ_E were described in Chapter V.

TABLE IX

EXPERIMENTAL DATA

	Run Number									
	1	2	3 (2)	5 (3)	5B	6	7	8 (4)	9	10A
Operating Conditions										
Feed Position	4.0	4.0	4.0	4.0	4.0	23.75	4.0	4.0	4.0	4.0
Feed Temperature, °C	6.0	6.0	5.5	7.5	7.5	5.0	5.0	5.0	7.5	5.0
L_E gm/min	0.68	1.04	2.30	2.23	1.19	1.42	0.68	1.49	0.3	3.30
L_S gm/min	3.50	2.98	3.00	3.53	3.53	0.98	1.30	1.37	3.2	2.00
C, gm/min	2.60	2.94	2.94	2.60	2.94	3.30	1.46	6.95	2.94	3.33
Terminal Compositions, ppm wt C_6H_{12}										
Y_F	28000	28000	32000	1500	1500	26300	28000	28000	1500	26400
Y_E	(1)	60	370	16	4	101	300	40	1	4800
Y_S	33900	37000	37000	2090	2540	72000	43400	44200	2140	74800
Composition Profile, ppm wt C_6H_{12}										
Sample Tap Number										
1	40	56	635	28	-	131	333	42	1.1	5060
2	50	58	1452	61	-	338	500	39	1.6	17200
3	49	66	3520	87	-	660	962	177	2.6	20400
4	64	101	6700	191	-	2550	1577	246	3.0	18100
5	79	212	9320	256	-	12840	2480	318	4.7	25400
6	365	1310	14780	385	-	13100	5120	785	29	24600
7	1006	2940	18800	496	-	13700	7620	1635	66	24400
8	14100	17500	31300	891	-	14400	15110	4780	1030	26100
Temperature Profile, °C										
Thermocouple Number										
1	5.4	5.5	5.5	-	-	5.5	5.5	-	-	-
2	5.5	5.5	5.4	-	-	5.4	5.5	-	-	-
3	5.5	5.5	5.1	-	-	5.2	5.5	-	-	-
4	5.5	5.4	4.8	-	-	4.9	5.3	-	-	-
5	5.0	4.9	4.3	-	-	4.9	4.6	-	-	-
6	3.8	3.4	2.1	-	-	2.2	2.8	-	-	-
7	-1.1	-2.1	-3.7	-	-	-2.9	-0.7	-	-	-

TABLE IX (Concluded)

	Run Number								
	10B	11	13 (5)	14	15	16	17	18	19(6)
Operating Conditions									
Feed Position, cm	4.0	4.0	4.0	4.0	4.0	29.75	29.75	23.75	-
Feed Temperature, °C	5.2	5.2	5.0	5.0	5.5	6.0	5.9	5.9	-
L_E, gm/min	3.30	0.80	0.80	0.74	0.67	2.30	2.45	2.91	-
L_S, gm/min	2.00	1.94	2.03	1.87	1.93	0.60	0.48	0.83	-
C, gm/min	1.95	1.94	1.99	2.94	2.87	4.55	6.8	5.47	1.72
Terminal Compositions, ppm wt C_6H_{12}									
Y_F	26400	28000	29700	10400	10400	29300	29300	30225	1500
Y_E	12400	62	55	29	29	65	84	107	-
Y_S	52700	39600	41700	14209	14300	186000	225000	152600	-
Composition Profile, ppm wt C_6H_{12} Sample Tap Number									
1	12680	70	62	29	24	109	100	105	-
2	21200	85	73	34	24	115	112	117	17
3	22200	121	114	-	34	590	486	130	23
4	24700	232	188	36	34	13280	12190	352	34
5	22800	416	674	38	38	13270	12600	15100	102
6	22500	1880	1856	93	84	13850	12380	15800	152
7	22200	3600	4340	262	220	12210	12100	15400	314
8	28100	16500	18470	4140	4140	11460	12800	15300	3360
Temperature Profile, °C Thermocouple Number									
1	-	-	5.5	5.5	-	5.5	-	5.5	-
2	-	-	5.5	5.5	-	5.3	-	5.2	-
3	-	-	5.5	5.5	-	4.0	-	4.9	-
4	-	-	5.1	5.5	-	3.9	-	4.3	-
5	-	-	4.7	5.4	-	3.9	-	4.3	-
6	-	-	3.4	4.6	-	-2.5	-	-0.2	-
7	-	-	-0.3	-0.2	-	-10.5	-	-9.6	-

Notes for Table IX

(1) The gap above the melting section was not completely flushed for this run. The enriching section product composition was 282 ppm wt C_6H_{12}.

(2) Run 4 is not shown. The purpose of this run was to check the overall balance. A description of this experiment appears in Chapter IV.

(3) There were two Runs 5 (5A and 5B). Run 5A is denoted as Run 5 throughout the dissertation. The Run 5B composition profile data are not shown because the septum in the No. 4 sample tap failed while the profile was being sampled, i.e., the column contents drained from the column.

(4) Cavities were observed in the freezing section. When the crystal rate was increased above 6.95 gm/min the column became plugged and was inoperable.

(5) Run 12 is not shown because the benzene on the tube side of the feed cooler was frozen solid before the column reached steady state.

(6) This total reflux run was performed to obtain a value of ϵ for a moderate value of the mother liquor composition in the freezing section. The value of ϵ and the mother liquor composition are 10 and 11,700 ppm wt C_6H_{12} respectively.

TABLE X

PARAMETERS CALCULATED FROM THE COMPOSITION PROFILES

Run	Y_P	ϵ	$\overline{Y}_P$	ψ_E, cm (1)
	ppm wt C_6H_{12}			
1	40	40 (1)	-	3.22
2	54	57	-	4.42
3	-1070	57	-	15.82
5	- 82	2	-	20.41
6	100	100	13,200	4.62
7	0	140	-	11.56
9	0.9	0.9	-	6.47
11	61	63	-	5.53
13	50	52	-	5.81
14	27	28	-	3.53
15	27	28	-	3.53
16	108	86	13,300	1.94
17	90	88	12,200	1.80
18	90	105	15,000	1.46

(1)The value of ϵ for Run 1 was taken as the value of Yp because the enriching section composition profile became flat at 40 ppm wt C_6H_{12}. See note (1) of Table IX.

APPENDIX D

COMPUTER PROGRAM FOR COLUMN CALCULATIONS

A Fortran IV program was written to implement the iterative procedure for column calculations summarized in Chapter III. The computer symbols are defined in Table XI. The program listing is presented in Table XII, and typical computer output for one column calculation is shown in Table XIII.

Two options are available with respect to data input. Simplified input-output are used; the namelists FIXED and VARY include all of the required input data (see statements 5 and 6 of the program listing). Statements 23 and 24 allow the predicted values of the mass transfer factors to be used in the column calculations, i.e., they override the mass transfer factors that are specified as data. If it is desired to specify the mass transfer factors directly (for example, when experimental data are available) statements 23 and 24 must be deleted. Similarly if it is desired to specify the impurity composition of the crystal phase rather than calculating it, statements 30 and 38 must be deleted.

TABLE XI

DEFINITIONS OF COMPUTER SYMBOLS

Program Symbol	Thesis Symbol	Description
		Physical Parameters
A	$-Y_P$	defined by Eq. (7)
B	$\overline{Y}_P$	defined by Eq. (18)
C	C	crystal rate, gm/min
F	F	feed rate, gm/min
HE	ψ'_E	enriching section mass transfer factor, cm
HS	ψ'_S	stripping section mass transfer factor, cm
L	$\mathscr{L}$	length of purification section, cm
LE	L_E	enriching section product rate, gm/min
LS	L_S	stripping section product rate, gm/min
RUN	-	run number
X	ϵ	composition of crystal phase, ppm wt C_6H_{12}
Y	Y	free liquid composition, ppm wt C_6H_{12}
YFEED	Y_F	feed composition, ppm wt C_6H_{12}
YO	Y_E	enriching section product composition, ppm wt C_6H_{12}
YPHI	Y_ϕ	free liquid composition at the feed point, ppm wt C_6H_{12}
YS	Y_S	stripping section product composition, ppm wt C_6H_{12}
Z	z	position above freezing section, cm
ZFEED	z_F	feed position, cm

TABLE XI (Concluded)

Program Symbol	Description
	Artifical Parameters Associated with Numerical Calculation
A1	defined by statement 21
A2	defined by statement 22
A3	defined by statement 31
B1	defined by statement 25
B2	defined by statement 26
C1	defined by statement 45
DERIV	slope of Y_ϕ vs Y_0 response; it is used to calculate incremented value of Y_0, defined by statement 63
EPS1	convergence criterion for Y_ϕ
I	subscript associated with position in stripping section, z(I)
ITER	counter for iterations
ITMAX	maximum number of iterations
J	subscript associated with position in enriching section, z(J)
PHI	subscript used to specify feed position
STEP	initial incrementation of YE
TEST 1	defined by statement 36
TEST 2	defined by statement 44
YE	initial assumption for YO
YFEW	free liquid composition at feed point calculated from stripping section model
YFOLD	free liquid composition at feed point calculated from enriching section model

TABLE XII

PROGRAM LISTING

```
FORTRAN IV G COMPILER        PROFILE

0001                INTEGER PHI,RUN
0002                REAL LS,LE,L
0003                DIMENSION Z(8),Y(8)
0004                DATA Z /4.,11.5,17.75,23.75,29.75,36.,42.,47.5 /
0005                NAMELIST/FIXED/L,YE, EPS1, STEP, ITMAX
0006                  NAMELIST/VARY/RUN,PHI,YFEED,HE,HS,X,C,F,LS
0007          61    FORMAT(' ITMAX ITERATIONS, NO CONVERGENCE ')
0008            62  FORMAT(' OPERATING CONDITIONS ')
0009            63  FORMAT(' COLUMN PARAMETERS AND TERMINAL COMPOSITIONS ')
0010            64  FORMAT(' COMPOSITION PROFILE Y(8)...Y(1) ')
0011                NAMELIST/OUTA/C1,TEST1,TEST2,DERIV,YFEW,YFOLD
0012                NAMELIST/OUTB/RUN
0013                NAMELIST/OUTC/L,ZFEED,YFEED,C,F,LE,LS
0014                NAMELIST/OUTD/HE,HS,X,YO,YPHI,YS
0015                NAMELIST/OUTE/Y
0016                READ (5,FIXED)
0017          101   ITER=0
0018                READ (5,VARY,END=998)
0019                ZFEED=Z(PHI)
0020                         LE = F -LS
0021                          A1 = C- LE
0022                        A2 = C + LS
0023                 HE=(6.538/(C-LE))+(0.4102*C*C/(C-LE))-(0.4185*C*LE/(C-LE))
0024                  HS=(6.538/(C+LS))+(0.4102*C*C/(C+LS))+(.4185*C*LS/(C+LS))
0025                           B1 = (L- ZFEED)/HE
0026                       B2 =ZFEED/HS
0027          102           YO = YE + STEP + .0001
0028                       ITER = ITER + 1
0029                          YS = (F*YFEED - LE*YE)/LS
0030                 X = .00142*YS
0031                        A3= C*X
0032                        A = (LE*YE -A3)/A1
0033                         B = (LS*YS + A3)/A2
0034                YFOLD= (YE+A)/EXP(-B1) -A
0035                YFEW=(YS-B)*EXP(-B2) +B
0036                        TEST1 = YFOLD -YFEW
0037                        YS = (F*YFEED - LE*YO)/LS
0038                 X = .00142*YS
0039                        A3= C*X
0040                        A = (LE*YO -A3)/A1
0041                        B = (LS*YS + A3)/A2
0042                YFOLD=(YC+A)/EXP(-B1)-A
0043                YFEW=(YS-B)*EXP(-B2) + B
0044                        TEST2 = YFOLD -YFEW
0045                         C1 = TEST2/YFOLD
0046                IF (ABS(C1) .LT. EPS1) GO TO 106
0047                IF (ITER .LT. ITMAX) GO TO 105
0048                WRITE (6,61)
0049                        YPHI = (YFOLD +YFEW)/2.
0050                DO 103 I = 1,PHI
0051          103   Y(I)=B+(YS-B)*EXP(-Z(I)/HS)
0052                DO 104 J = I,8
0053          104   Y(J)= -A+(YPHI+A)*EXP(-(Z(J)-ZFEED)/HE)
0054                WRITE(6,OUTA)
0055                WRITE(6,OUTB)
```

TABLE XII (Concluded)

```
0056                WRITE (6,62)
0057                WRITE(6,CUTC)
0058                WRITE(6,63)
0059                WRITE(6,OUTD)
0060                WRITE(6,64)
0061                WRITE(6,OUTE)
0062                GO TO 101
0063          105           DERIV = (TEST2 -TEST1)/(YO -YE)
0064                        YE = YO -TEST2/DERIV
0065                      STEP =STEP/2.
0066                GO TO 102
0067           106          YPHI = (YFOLD +YFEW)/2.
0068                DO 107 I = 1,PHI
0069          107   Y(I)=B+(YS-B)*EXP(-Z(I)/HS)
0070                DO 108 J = I,8
0071          108   Y(J)= -A+(YPHI+A)*EXP(-(Z(J)-ZFEED)/HE)
0072                WRITE(6,CUTB)
0073                WRITE (6,62)
0074                WRITE(6,CUTC)
0075                WRITE(6,63)
0076                WRITE(6,CUTD)
0077                WRITE(6,64)
0078                WRITE(6,CUTE)
0079                GO TO 101
0080          998   CONTINUE
0081                END
```

TABLE XIII

TYPICAL OUTPUT

```
EXECUTION BEGINS
&OUTB
RUN=          2
&END
OPERATING CONDITIONS
&OUTC
L=  50.000000     ,ZFEED=  4.0000000     ,YFEED=  28000.000     ,C=  2.9399996     ,F=  4.0199995     ,LE=  1.0400000     ,LS=
   2.9799995
&END
COLUMN PARAMETERS AND TERMINAL COMPOSITIONS
&OUTD
HE=  4.6336813     ,HS=  2.3226614     ,X=  53.609009     ,YO=  54.314026     ,YPHI=  22386.832     ,YS=  37752.836
&END
COMPOSITION PROFILE Y(8)...Y(1)
&OUTE
Y=  22386.828     ,  4479.2812     ,  1201.9907     ,  367.90991     ,  139.42664     ,  75.596939     ,  59.352051     55.093323
&END
IHC002I STOP      0  ***** RESTART AT LOCATION  103C3C
EXECUTION TERMINATED
```

APPENDIX E

TOTAL REFLUX DATA

Some of Albertins' experimental and calculated data were included in the previous chapters of this thesis. These data are tabulated here for the convenience of the reader. The details of Albertins' investigation are available in his thesis.[1] All of the data reported below is for the benzene-cyclohexane system and spiral agitation conditions of 59 rpm, 290 osc/min, and 1 mm amplitude. These conditions are the same as those used in the continuous flow study of this thesis.

1. IMPURITY ASSOCIATED WITH THE CRYSTAL PHASE

Albertins determined ϵ from the total reflux composition profile data. The values of ϵ were chosen such that the modified composition profiles for total reflux operation, $\ln(Y-Y_P)$ vs z, would be linear. Y_P is equal to ϵ for total reflux operation. Table XIV illustrates that the pure end composition

TABLE XIV

ULTIMATE PURITY THAT CAN BE OBTAINED BY COLUMN CRYSTALLIZATION OF A 30,000 PPM CYCLOHEXANE-BENZENE MIXTURE WITH TOTAL REFLUX OPERATION

Crystal Rate, gm/min	Pure End Composition, ppm wt C_6H_{12}
1.99	98
2.65	101
3.92	106
4.35	103

(equivalently ϵ) is independent of crystal rate at large values of the crystal rate. A composition of ~ 100 ppm C_6H_{12} corresponds to the ultimate purity that can be achieved by total reflux column crystallization of a 30,000 ppm C_6H_{12} charge. The charge composition was reported as the nominal value (±5%). Consequently these total reflux data were obtained for a charge composition that is comparable to the feed composition of 28,000 ppm for Run 2 of this study.

2. TOTAL REFLUX MASS TRANSFER FACTOR, ψ_0

Albertins calculated the total reflux mass transfer factors from his modified composition profile data. These values are tabulated in Table XV. They were used in Chapter V to obtain the ψ_0' vs C correlation (Eq. (77)).

TABLE XV

TOTAL REFLUX MASS TRANSFER FACTORS

Crystal Rate, gm/min	ψ_0, cm
0.73	10.00
0.79	9.28
0.90	8.65
1.02	7.71
1.20	6.88
1.95	5.00
2.54	5.12

APPENDIX F

CALCULATION OF THE CHARACTERISTIC ROOTS OF EQUATION (13)

The values of the characteristic roots r_1 and r_2 of Eq. (13) which correspond to the minimum ratio of r_2/r_1 were used in Chapter III to show that the term $C_2\ e^{r_2 z}$ in the expression for the free liquid composition profile (Eq. (12)) could be neglected relative to $C_1\ e^{r_1 z}$. The case corresponding to the minimum value of r_2/r_1 was used because it is the most conservative, i.e., the contribution of $C_2\ e^{r_2 z}$ is maximized relative to $C_1\ e^{r_1 z}$. This occurs when Q_2/Q_1^2 is a maximum with respect to crystal rate and for total reflux operation, $R_E = 0$. For total reflux the relation for $(Q_2/Q_1^2)_{max}$ (Eq. (25)) becomes:

$$(Q_2/Q_1^2)_{max} = \frac{1}{4(\alpha+1)} \tag{87}$$

The value of Q_1 which corresponds to $(Q_2/Q_1^2)_{max}$ is given by Eq. (88).

$$(Q_1)_{min} = 2\left[\frac{KaA\rho}{D\rho A\eta}\left(\frac{\alpha+1}{\alpha}\right)\right]^{1/2} \tag{88}$$

This expression can be simplified further by introducing the correlation constants b_1 and b_2 obtained from the total reflux mass transfer factor data.

$$(Q_1)_{min} = 2\left[\frac{(\alpha+1)^2}{b_1 b_2}\right]^{1/2} \tag{89}$$

The characteristic roots for these values of Q_1 and Q_2/Q_1^2 become:

$$r_1 = \frac{(Q_1)_{min}}{2}\left[-1+(1-4(Q_2/Q_1^2)_{max})^{1/2}\right] \quad (90)$$

$$r_2 = \frac{(Q_1)_{min}}{2}\left[-1-(1-4(Q_2/Q_1^2)_{max})^{1/2}\right] \quad (91)$$

The values of b_1 and b_2 are 6.862 gm-cm/min and 0.9096 cm-min/gm, respectively (see Table IV). The value of α was assumed to be 0.2 for these calculations. The values of $(Q_1)_{min}$ and $(Q_2/Q_1^2)_{max}$ can be calculated from Eqs. (87) and (89).

$$(Q_1)_{min} = 0.961 \text{ cm}^{-1}$$

$$(Q_2/Q_1^2)_{max} = 0.833, \text{ dimensionless}$$

The roots r_2 and r_1 are now calculated from Eqs. (90) and (91):

$$\underline{r_1 = 0.284 \text{ cm}^{-1}}$$

$$\underline{r_2 = 0.676 \text{ cm}^{-1}}$$

BIBLIOGRAPHY

1. Albertins, R., Ph.D. Dissertation, The University of Michigan, 1967.

2. Albertins, R., and J. E. Powers, accepted for publication in A.I.Ch.E.J.

3. Albertins, R., Sinclair Research Co., Harvey, Illinois, Personal Communication, 1968.

4. Albertins, R., W. C. Gates, and J. E. Powers, in Fractional Solidification Vol. I (M. Zief and W. R. Wilcox, eds.) Marcel Dekker, Inc., New York (1967) pp. 343-367.

5. Anikin, A. G., Dokl. Akad. Nauk SSSR, 151 (5), 1139 (1963).

6. Arnold, P. M., U. S. Patent 2,540,977 (1951).

7. Breiter, J., Ph.D. Dissertation, Ruprecht-Karl-Universität, Heidelberg, Germany, 1967.

8. Cohen, K. J., Chem. Phys., 8, 588 (1940).

9. Danyi, M. D., C. M. 690 Report, The University of Michigan, 1968.

10. Danyi, M. D., J. D. Henry, and J. E. Powers, in Fractional Solidification Vol. II (M. Zief, ed.) Marcel Dekker, Inc., New York (to be published in 1969).

11. Findlay, R. A., U. S. Patent 2,683, 178 (1954).

12. Furry, W. H., R. C. Jones, and L. Onsager, Phys. Rev., 55, 1083 (1939).

13. Gates, W. C., Ph.D. Dissertation, The University of Michigan, 1967.

14. Gates, W. C., and J. E. Powers, presented at the Symposium on Crystallization from the Melt, Preprint 37F, Second Joint A.I.Ch.E.-I.I.Q.P.R. Meeting, Tampa, Florida, 1968.

15. Gates, W. C., Texaco, Inc., Beacon, New York, Personal Communication, 1968.

16. Girling, G. W., and A. D. McPhee, Benzole Producers Ltd., Research Report 66-4, Watford, Herts, Britain, 1966.

17. Girling, G. W., A. D. McPhee, and M. H. Radley, Benzole Producers Ltd., Research Report 67-3, Watford, Herts, Britain, 1967.

BIBLIOGRAPHY (Concluded)

18. Hinton, J., Price List 37, James Hinton Co., Valpariso, Florida (1967).

19. McKay, D. L., U. S. Patent 2,823,242 (1958).

20. McKay, D. L., C. H. Dale, and D. C. Tabler, presented at 59th National Meeting of the A.I.Ch.E., Preprint 8E, Columbus, Ohio (1966).

21. McKay, D. L., and H. W. Goard, CEP, 61 (11), 94 (1965).

22. McKay, D. L., G. H. Dale, and J. A. Weedman, IEC, 52 (3), 197 (1960).

23. Moulton, R. W., and H. M. Hendrickson, Office of Saline Water, R and D Progress Report No. 10, U. S. Department of Interior (1956) p. 114.

24. Newton Chambers Ltd., Sheffield, Britain, Chem. Eng., 75 (16), 64 (1968).

25. Palermo, J. A., IEC, 58 (11), 67 (1966).

26. Player, M. R., Submitted to IEC, Manuscript No. 8-180 (1968).

27. Powers, J. E., in Symposium über Zonenschmelzen und Kolonnenkristallisiern (H. Schildknecht, ed.) Kernforschungszentrum, Karlshrue, 57 (1963).

28. Schildknecht, H., Anal. Chem., 181, 254 (1961).

29. Schildknecht, H., and K. Mass, Die Wärme, 69 (4), 121 (1963).

30. Sherwood, T. K., and P.L.T. Brian, Office of Saline Water, R and D Progress Report No. 96, U. S. Department of Interior (1964) pp. 7-16.

31. Speciality Design Co., Box 276, Ann Arbor, Michigan.

32. Thomas, R. W., U. S. Patent 2,854,494 (1958).

33. Timmermans, J., Physico-Chemical Constants of Binary Systems in Concentrated Solutions Vol. I, Interscience Publishers, Inc., New York (1959) p. 107.

34. Weedman, J. A., U. S. Patent 2,747,001 (1956).

35. Yagi, S., H. Inove, and H. Sakamoto, Kagaku Kogaku, 27 (6), 415 (1963).